CATALYST DEVELOPMENT FOR HYDROCARBON PRODUCTION BY CARBON MONOXIDE HYDROGENATION

by

Murat Erol

B. S. in Ch.E., Middle East Technical University, 2009

Submitted to the Institute for Graduate Studies in
Science and Engineering in partial fulfillment of
the requirements for the degree of
Master of Science

Graduate Program in Chemical Engineering

Boğaziçi University

2011

CATALYST DEVELOPMENT FOR HYDROCARBON PRODUCTION
BY CARBON MONOXIDE HYDROGENATION

APPROVED BY:

Prof. Zeynep İlsen Önsan .....…….....
(Thesis Supervisor)

Assoc. Prof. Ahmet Kerim Avcı .....…….....

Prof. Ayşe Nilgün Akın .....…….....

DATE OF APPROVAL: 15.06.2011

to my family

ACKNOWLEDGEMENTS

Firstly, I would like to express my truthful gratitude to my thesis supervisor, Prof. Zeynep İlsen Önsan, for her continuous encouragement, clear-sighted suggestions and self-confidence. I am grateful to her for her patience and was very lucky to work with a kind and optimistic advisor. It was a privilege for me to work with Prof. Zeynep İlsen Önsan.

I would like to acknowledge Assoc. Prof. Ahmet Kerim Avcı for providing valuable technical vision and for his help all the time, and to Prof. Ayşe Nilgün Akın for reading and commenting on my thesis. I am thankful to Prof. Ahmet Erhan Aksoylu and Prof. Ramazan Yıldırım for their valuable comments during my experimental work. I wish to express my great appreciation to Assoc. Prof. Ayşe Neren Ökte for her invaluable support and patience in surface characterization measurements despite her busy program.

I am indebted to Eyüp Şimşek for sharing his technical experience, his kindness and patience during my experimental studies. I wish a successful academic career for him. I am grateful to Burcu Selen Çağlayan, Feyza Gökaliler, Tuğba Davran, Mustafa Karakaya for their support and comments. Special thanks go to Nilay, Merve, Vasfiye, Ali, Caner, Aybüke, Selcen, Burcu, Okan, Bahar, Gülsüm, İrfan, Kerem, Aslıgül, Simay, Ünal, Çağlar, Duygu, Şefik, Sıla for their friendship and joyful help. Heartfelt thanks go to Bilgi Dedeoğlu, Nurettin Bektaş, Yakup Bal for their technical assistance, to Melike Gürbüz and Kamuran Çevre for their friendship and kindness.

I am also very grateful to a special person in my life, Aysun İpek Paksoy, for her encouragement, motivation and technical comments in the writing of my thesis.

Last but not least, I would like to thank my family for their support, motivation and trust throughout my entire education.

Financial support for this work was provided by the Boğaziçi University Research Fund project BAP-09HA506D.

ABSTRACT

CATALYST DEVELOPMENT FOR HYDROCARBON PRODUCTION BY CARBON MONOXIDE HYDROGENATION

The aim of this work was the development and testing of supported rhodium catalysts for hydrocarbon production by CO hydrogenation. Four different catalysts were prepared by sequential or co-impregnation to incipient wetness of δ-Al_2O_3 and SiO_2 supports, namely 2wt%Rh/δ-Al_2O_3 and 1.5wt%Rh/SiO_2 in addition to La and V promoted catalysts, 1.5wt%Rh-2.6wt%La/SiO_2 and 1.5wt%Rh-2.6wt%La/1.5wt%V/SiO_2. Experimental plan included a parametric study of reaction temperature and contact time (W/F_{CO}) as well as effects of support material and promoters on CO conversion. The reaction system used in the experiments consisted of mass flow controllers for gases, a down-flow micro-reactor located in a temperature-controlled furnace, traps, heated stainless steel connecting lines and two on-line gas chromatographs for feed and product analysis. Parametric studies were first conducted on 2wt%Rh/δ-Al_2O_3 and 1.5wt%Rh/SiO_2 using a fixed inlet composition of 10 mol% CO, 20 mol% H_2 and balance N_2 for W/F_{CO} ratios of 0.49-1.30 mg.min.μmol^{-1} at 270^{o}C and atmospheric pressure. Subsequent experiments were performed at 230-290^{o}C using various W/F_{CO} ratios in the same range over both non-promoted and singly or doubly-promoted Rh/SiO_2. Silica-supported catalyst samples were characterized by X-ray diffraction (XRD), surface area (BET) analysis, and environmental scanning electron microscopy (ESEM) with energy dispersive X-ray analysis (EDX) techniques. Increasing contact times, increasing reaction temperatures and addition of La or La-V promoters all improved catalytic activity (CO conversion) significantly. Among the catalyst samples tested for CO hydrogenation, doubly-promoted 1.5wt%Rh-2.6wt%La/1.5wt%V/SiO_2 catalyst yielded the highest CO conversion. Since reaction tests were conducted at atmospheric pressure, methane was the major product observed in all cases.

ÖZET

KARBON MONOKSİT HİDROJENASYONU İLE HİDROKARBON ÜRETİMİ İÇİN KATALİZÖR GELİŞTİRİLMESİ

Bu çalışmanın amacı karbon monoksit hidrojenasyonu yoluyla hidrokarbon üretimi için destekli rodyum katalizörlerinin geliştirilmesi ve denenmesi olarak belirlendi. δ-Al_2O_3 ve SiO_2 destek malzemeleri üzerinde ardışık veya birlikte emdirme yöntemi kullanılarak dört farklı katalizör örneği hazırlandı: 2wt%Rh/δ-Al_2O_3 ve 1.5wt%Rh/SiO_2, ayrıca La ve V katkılı 1.5wt%Rh-2.6wt%La/SiO_2 ve 1.5wt%Rh-2.6wt%La/1.5wt%V/SiO_2. Deney planı çerçevesinde, sıcaklık ve reaktörde kalma süresinin (W/F_{CO}) yanısıra destek malzemesinin ve katkı maddelerinin CO dönüşmesine etkileri incelendi. Deneylerde, gazlar için kütle akış denetleyici sistemi, programlamalı sıcaklık denetimi bulunan fırın içine yerleştirilmiş aşağı-akışlı mikro-reaktör, su kapanı, ısıtılmış paslanmaz çelik bağlantı hatları ile girdi ve ürün analizi için gerekli iki gaz kromatografından oluşan bir reaksiyon sistemi kullanıldı. Parametrik çalışmalar önce 270^oC sıcaklıkta ve atmosfer basıncında, 2wt%Rh/δ-Al_2O_3 ve 1.5wt%Rh/SiO_2 katalizörleri üzerinde, sabit girdi bileşimi olarak mol bazında %10 CO, %20 H_2 ve fark N_2 kullanılarak reaktörde kalma süresi 0.49-1.30 mg.min.µmol^{-1} aralığında değiştirilerek gerçekleştirildi. İzleyen deneyler, aynı W/F_{CO} oranları ve 230-290^oC sıcaklık aralığı kullanılarak gerek katkısız, gerekse tek ve çift-katkılı Rh/SiO_2 katalizör örnekleri üzerinde yapıldı. SiO_2-destekli katalizör örnekleri X-ışını kırınımı (XRD), yüzey alanı (BET) analizi ve taramalı elektron mikroskopisi-enerji dağılımlı X-ışını spektroskopisi (ESEM-EDX) teknikleriyle incelendi. Artan reaktörde kalma sürelerinin ve artan reaksiyon sıcaklıklarının yanısıra La veya La-V katkı maddelerinin eklenmesinin de CO dönüşmesini olumlu yönde etkilediği gözlendi. CO hidrojenasyonu için hazırlanan katalizörler arasında 1.5wt%Rh-2.6wt%La/1.5wt%V/SiO_2 katalizörünün en yüksek CO dönüşmelerini sağladığı ve deneylerin atmosfer basıncında yapılması nedeniyle, başlıca ürünün metan olduğu belirlendi.

TABLE OF CONTENTS

LIST OF FIGURES

LIST OF TABLES

LIST OF SYMBOLS

dp	Catalyst particle size
Ea	Activation Energy
F_{CO}	Carbon monoxide flow rate
ID	Internal diameter
MW	Molecular weight
T	Temperature
Wcat	Weight of catalyst

LIST OF ABBREVIATIONS

ATR	Autothermal Reforming
BET	Branauer Emmett Teller
BOS	Birleşik Oksijen Sanayi
EDX	Energy dispersive X-Ray
GC	Gas chromatography
HPLC	High performance liquid chromatography
POX	Partial oxidation
SEM	Scanning electron microscopy
SR	Steam reforming
TCD	Thermal conductivity detector
TPR	Temperature programmed reduction
XRD	X-ray diffraction

1. INTRODUCTION

Coal and natural gas can utilized as possible feedstock of the chemical industry and the transportation fuels market. As for the energy industry, the conversion of natural gas to hydrocarbons is currently one of the most promising topics due to economic utilization of remote natural gas reserves to environmentally clean fuels, specialty chemicals and waxes. Alternatively, coal or heavy residues can be used on sites where these are available at low costs (Van der Laan, 1999).

Fischer-Tropsch synthesis (FTS) is possibly the most promising source of chemicals and fuels from a non-petroleum based supply such as natural gas and coal (Adesina, 1996). Ever since Fischer, Tropsch and co-workers developed FTS on cobalt and iron based catalysts, there has been great interest and dedication towards the commercialization of this synthesis technology (Fischer and Tropsch, 1923).

Fischer-Tropsch synthesis (FTS) provides a method for converting synthesis gas (syngas), obtained from the gasification of crude oil or alternative sources such as coal, natural gas or biomass, to liquid fuels suitable for use in standard motor vehicles. The economic viability of a commercial FT plant is highly dependent on the crude oil price, which has fluctuated considerably during the past few decades. Probably due to the risk of an ill-timed fall in crude oil prices, world-wide application of the technology has been hampered to some extent. However, due to the current high oil prices, there is renewed interest in coal and natural gas as alternative energy sources, and consequently the FT process is again receiving wide-spread attention (Botes, 2008).

In short, the FT reaction involves the hydrogenation of CO over a heterogeneous catalyst to an array of hydrocarbons. Even though a variety of metals are known to catalyze CO hydrogenation reactions in general and the FT reaction in particular, only catalysts based on iron or cobalt are of industrial significance for the FT synthesis (Schulz, 1999; Dry, 2004).

FT synthesis is distinguished from other CO hydrogenation reactions in that the product spectrum consists mainly of linear alkanes and alkenes (from methane to long chain waxes) with a carbon number distribution that is characteristic of a polymerization mechanism. Additional products formed include branched aliphatic compounds, alcohols, aldehydes, ketones, acids and, at sufficiently high operating temperatures, even aromatics (Anderson, 1981). It is not always clear which of these compounds are primary products of FT synthesis and which are formed afterward by secondary reactions. However, it is known that certain compounds (e.g. olefins and alcohols) undergo a range of secondary reactions, such as hydrogenation, double bond shift, chain branching, conversion to heavier compounds (Tau *et al*., 1991).

The objective of this study was the development and testing of supported rhodium catalysts for hydrocarbon production by CO hydrogenation, using an integrated reaction system suitable for studying this reaction. After modifying an existing reaction system for this purpose, Rh/δ-Al_2O_3 as well as non-promoted, singly and doubly promoted Rh/SiO_2 catalysts were prepared and tested to examine the effects of reaction parameters on carbon monoxide hydrogenation reaction. Four different catalysts were prepared by sequential or co-impregnation to incipient wetness of δ-Al_2O_3 and SiO_2 supports: 2wt%Rh/δ-Al_2O_3 and 1.5wt%Rh/SiO_2 in addition to La and V promoted catalysts, 1.5wt%Rh-2.6wt%La/SiO_2 and 1.5wt%Rh-2.6wt%La/1.5wt%V/SiO_2. The catalytic activity tests were conducted in a micro-reactor flow system run at atmospheric pressure at 230, 270 and 290°C. The effects of catalyst contact time (W/F_{CO}) and the addition of promoters to SiO_2-supports at different temperatures were tested.

Section 2 includes a literature survey on Fischer-Tropsch catalysts, supports and influence of total pressure, temperature, feed ratio and space velocity on the selectivity of the FTS reaction. Section 3 describes the experimental system and the procedures used in this study. The details of the reaction system and the results obtained in the experiments are presented and discussed in Section 4, while the conclusions and recommendations for future work are given in Section 5.

2. LITERATURE SURVEY

The reaction which entails the conversion of synthesis gas (H_2 and CO mixture) to liquid hydrocarbon fuels is known as Fischer-Tropsch synthesis (FTS). A block diagram of the overall Fischer-Tropsch process is presented in Figure 2.1. The commercial process consists of three fundamental sections, namely synthesis gas (syngas) production and purification, Fischer-Tropsch synthesis, and product up-grade (Van der Laan, 1999).

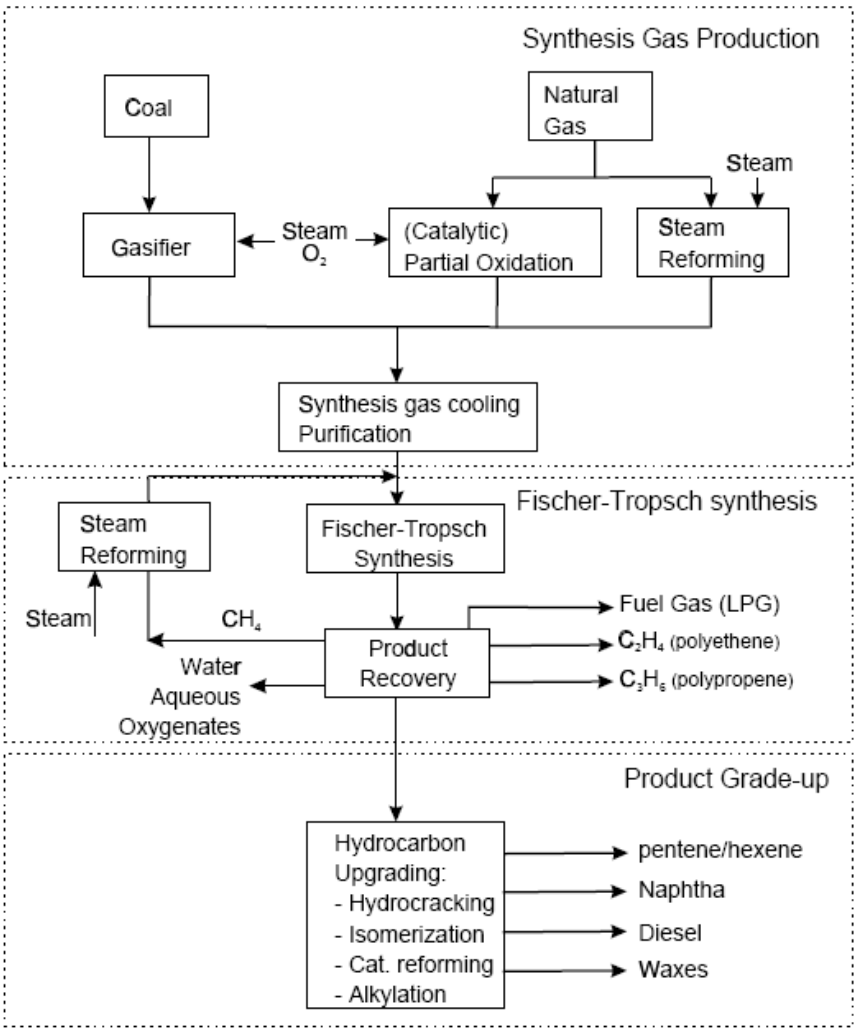

Figure 2.1. Overall process scheme of FTS (Van der Laan, 1999).

2.1. Synthesis Gas Production

Synthesis gas can be produced by steam reforming or (catalytic) partial oxidation of fossil fuels such as coal, natural gas, refinery residues, of biomass or industrial off-gases. The compositions of syngas obtained from various feedstocks and processes are listed in Table 2.1 (Cybulski *et al.*, 1993). Synthesis gas can be produced by reforming of natural gas with either steam or carbon dioxide, or by partial oxidation. The most important reactions are:

Steam reforming: $CH_4 + H_2O \leftrightarrow CO + 3H_2$ (2.1)

CO_2 reforming: $CH_4 + CO_2 \leftrightarrow 2CO + 2H_2$ (2.2)

Partial oxidation: $CH_4 + 1/2O_2 \leftrightarrow CO + 2H_2$ (2.3)

Water gas shift reaction: $CO + H_2O \leftrightarrow CO_2 + H_2$ (2.4)

Usually, a combination of synthesis gas production processes is used to generate syngas with a stoichiometric ratio of hydrogen and carbon monoxide. Synthesis gas produced in modern coal gasifiers (Shell/Koppers or Texaco gasifiers) and from heavy oil residues has a high CO content in comparison to synthesis gas from natural gas. In case of H_2/CO ratios less than 2, the composition of the feed mixture is not stoichiometric for the Fischer-Tropsch reactions given in Table 2.2, and the water gas shift reaction becomes crucial for setting the H_2/CO ratio to 2. Inexpensive iron catalysts, as compared to cobalt-based catalysts, can directly convert low H_2/CO ratio syngas into hydrocarbon products without an external shift reaction (Rao *et al*., 1992).

A comparison of the economical evaluations of steam reforming, CO_2 reforming, autothermal reforming, and combined reforming processes has indicated that combined reforming processes have the lowest production and investment costs at a H_2/CO ratio of 2 (Basini and Piovesan, 1998).

Table 2.1. Composition of syngas produced from different feedstocks by various processes (Van der Laan, 1999).

Feedstock	**Process**	**Component (vol%)**			
		H_2	**CO**	**CO_2**	**Other**
Natural gas, steam	SR	73.8	15.5	6.6	4.1
Natural gas, steam, CO_2	CO_2-SR	52.3	26.1	8.5	13.1
Natural gas, O_2, steam, CO_2	ATR	60.2	30.2	7.5	2
Coal/heavy oil, steam	Gasification	67.8	28.7	2.9	0.6
Coal, steam, oxygen	Texaco gasifier	35.1	51.8	10.6	2.5
Coal, steam, oxygen	Shell/Koppers gasifier	30.1	66.1	2.5	1.3
Coal, steam, oxygen	Lurgi gasifier	39.1	18.9	29.7	12.3

Table 2.2. Major overall reactions in the Fischer-Tropsch synthesis (Van der Laan, 1999).

Main reactions	
1. Paraffins	$(2n+1)H_2 + nCO \rightarrow C_nH_{2n+2} + nH_2O$
2. Olefins	$2nH_2 + nCO \rightarrow C_nH_{2n} + nH_2O$
3. Water gas shift reaction	$CO + H_2O \rightleftarrows CO_2 + H_2$
Side reactions	
4. Alcohols	$2nH_2 + nCO \rightarrow C_nH_{2n+2}O + (n-1)H_2O$
5. Boudouard reaction	$2CO \rightarrow C + CO_2$
Catalyst modifications	
6. Catalyst oxidation/reduction	a. $M_xO_y + yH_2 \rightleftarrows yH_2O + xM$
	b. $M_xO_y + yCO \rightleftarrows yCO_2 + xM$
7. Bulk carbide formation	$yC + xM \rightleftarrows M_xC_y$

2.2. Fischer-Tropsch Synthesis

Investigation of the conversion of synthesis gas to aliphatic hydrocarbons over metal catalysts by Franz Fischer and Hans Tropsch was conducted at the Kaiser-Wilhelm Institute for Coal Research in Mullheim in 1923 (Fischer and Tropsch, 1923). During their

studies they showed that CO hydrogenation over iron, cobalt or nickel catalysts with process conditions of 180-250°C and atmospheric pressure results in a product mixture of linear hydrocarbons. The Fischer-Tropsch product spectrum consists of a complex multicomponent mixture of linear and branched hydrocarbons and oxygenated products. Main products are linear paraffins and α-olefins (Van der Laan, 1999).

Apart from other CO hydrogenation reactions, the product spectrum of FT synthesis consists mainly of linear alkanes and alkenes (from methane to long chain waxes) with a carbon number distribution characteristic of a polymerization mechanism. Besides linear alkanes and alkenes, additional products such as branched aliphatic compounds, alcohols, aldehydes, ketones, acids and (at sufficiently high operating temperatures) even aromatics may form at the end of the reaction (Anderson, 1981). It is not always clear which of these compounds are primary products of FTS and which are formed subsequently by secondary reactions. On the other hand, it is known that certain compounds (e.g. olefins and alcohols) may further be exposed to a variety of secondary reactions, such as hydrogenation, double bond shift, chain branching and conversion to heavier compounds (Tau *et al*., 1991). Normally, water is discarded through the bulk of the oxygen from CO dissociation, but over certain catalysts a significant portion of the oxygen is also discarded as carbon dioxide. Carbon dioxide formation takes place especially over iron FT catalysts and is often visualized as an independent consecutive reaction, namely the water-gas-shift (WGS) reaction (Van der Laan and Beenackers, 1999). Stoichiometrically, the overall process can be represented as follows (Van der Laan, 1999):

$$\text{(FT)} \qquad CO + (1 + m/2n)H_2 \rightarrow 1/nC_nH_m + H_2O \quad \Delta H = -165 \text{ kJ/mol} \qquad (2.5)$$

$$\text{(WGS)} \qquad CO + H_2O \leftrightarrow CO_2 + H_2 \qquad \Delta H = -41.3 \text{ kJ/mol} \qquad (2.6)$$

Here *n* is the average carbon number and *m* is the average number of hydrogen atoms of the hydrocarbon products. Water is released as a primary product of the FT reaction, and CO_2 can be produced as a result of the WGS reaction. The WGS activity can be high over potassium promoted iron catalysts and is negligible over cobalt or ruthenium catalysts (Van der Laan, 1999).

2.2.1. Fischer-Tropsch Catalysts

The most widely used catalysts for CO hydrogenation are Group 8 to Group 10 elements, since they can dissociatively adsorb H_2 and carbon monoxide. Fe, Co, Ni and Ru are the primary FT catalysts; however Rh has been shown to have interesting properties in FTS and should probably be included in this list (Anderson, 1984). The relative prices of these metals are presented in Table 2.3. Ruthenium is known as the most active metal for FTS, and is followed by iron, nickel, and cobalt. It has been shown that the average molecular weight of the hydrocarbons produced by FTS decreases in the following sequence (Vannice, 1975):

$$Ru > Fe > Co > Rh > Ni > Ir > Pt > Pd$$

Table 2.3. Relative prices of metals (Rao *et al*., 1992).

Metal	**Price Ratio**
Iron	1
Cobalt	230
Nickel	250
Ruthenium	31.000
Rhodium	570.000

During typical FT operating conditions, Ni yields a large amount of methane, and during the reaction, nickel carbonyls are formed, resulting in loss of activity (Marura, 2002). Molybdenum and tungsten have also been used as FTS catalysts but they have shown rather low FTS activity, most probably due to oxidizing of these metals easily (Anderson, 1984; Dry, 1996).

In the beginning, FT catalysts were prepared by precipitation techniques. Novel catalyst preparation methods developed later include sintering and fusing metal oxides with desired promoters (Anderson, 1956). A novel K/Fe/β-Mo_2C catalyst prepared by a

temperature programmed reaction method gave high yields of alcohols; especially high C_2^+OH selectivity for mixed alcohols synthesis by CO hydrogenation (Xiang *et al*., 2007).

In another study, it was found that when cesium (Cs) was introduced into Cu/CeO_2 catalysts, the mass ratio of C_2^+OH to MeOH in the products was greatly enhanced from 0.13 to 0.71 although CO conversion decreased slightly. Introduction of Ni to $CsCu/CeO_2$, increased CO conversion from 22.2% to 37.6% and the mass ratio of C_2^+OH to MeOH in the products also increased from 0.71 to 0.85. Therefore, $CsNiCu/CeO_2$ was proposed as an excellent catalyst for the synthesis of mixed alcohols (Liu *et al*., 2010).

Tien-Thao and coworkers (2007) tested two $LaCo_{0.7}Cu_{0.3}O_3$ perovskite catalysts obtained by reactive grinding and by the citrate complex method. They stated that the catalytic activity and product distribution depend strongly on process variables, alkali promoter, preparation method, and catalyst morphology. While the ground perovskite was rather selective for the synthesis of higher alcohols, the citrate-derived precursor produced mainly methane and light hydrocarbons in addition to 10–15 wt. % of alcohols. The nanocrystalline perovskite precursor showed better catalytic performance compared to the citrate-derived sample in terms of both alcohol selectivity and productivity. The catalytic stability of the ground perovskite is dependent not only on the crystal domain size (or size of nanoparticles) and the amount of remnant sodium ions but also on the compactness of nanoparticles.

Furthermore, Mo–Co–K sulfide-based catalysts promoted by rare earth metal salts (La, Ce, and Y) that were prepared by an ultrasonic technology in a non-aqueous medium were studied. The catalytic performance for the selective synthesis of ethanol and mixed alcohols from syngas was evaluated and compared with that of the unpromoted catalyst Mo–Co–K. It was observed that the Mo–Co–K sulfide catalyst had a much lower CO conversion and ethanol distribution. In this work, the influence of the La/Mo molar ratio on CO conversion and ethanol yield was also determined to find that both CO conversion and ethanol distribution increase with the La/Mo molar ratio; however, very high La/Mo molar ratios eventually decreased CO conversion and ethanol distribution (Yong *et al*., 2007).

Catalytic performance of palladium catalysts prepared by a novel preparation method using water-in-oil micro-emulsion was compared with that of catalysts prepared by the conventional impregnation method. Preparation of Pd particles by the micro-emulsion technique showed narrower size distribution, and the average particle size was much smaller compared to preparation with impregnation method; the former exhibited a much higher activity for the hydrogenation of carbon monoxide than the catalysts prepared by impregnation (Kim *et al*., 1997).

2.2.1.1. Rhodium catalysts. Several recent studies were published about catalysts used for ethanol production via CO hydrogenation. In one of these studies, the reaction kinetics of ethanol synthesis by CO hydrogenation over SiO_2-supported Rh/Mn alloy catalysts was considered. It was found that Mn promoter can exist in a binary alloy with Rh and has a crucial role in reducing the CO insertion reaction (CO + CH_x (x = 1–3) barriers thus improving the selectivity toward ethanol and other C_2^+ oxygenates, although the barrier toward methane formation is not changed. Then, the effects of various promoters (M = Ir, Ga, V, Ti, Sc, Ca, and Li) on the CO insertion reaction over Rh/M alloy nanoparticles were investigated using DFT calculations. It was also found alloying the promoters with an electronegativity difference, Δx, between the promoter (M) and Rh equal to 0.7 is the most effective for reducing the barriers of CO insertion, which leads to a higher selectivity to ethanol (Mei *et al*., 2010).

In another study, the influences of support (silica or titania) and Fe promoter loading on the activity and selectivity of Rh-based catalysts for the direct synthesis of ethanol from syngas was explored. Although little ethanol was produced over 2 wt% Rh/SiO_2, a similar loading of Rh on titania was active for this reaction. Promotion of 2 wt% Rh/SiO_2 by 1 wt% Fe produced a catalyst that exhibited 22% selectivity to ethanol, with methane being the primary side-product. Addition of Fe to 2 wt% Rh/TiO_2 also improved the selectivity to ethanol with the highest value being 37% for a sample with 5 wt% Fe (Haider *et al*., 2010).

By employing modified SBA-15 molecular sieve as the support, iron-promoted Rh catalysts were investigated in the synthesis of ethanol from syngas through temperature programmed surface reaction (TPSR). Addition of promoter in certain range could partially block the rhodium surface, hence lowering the number of active sites and resulting in a

decrease in CO conversion. However, there is not a continuous decrease in the number of active sites responsible for methane production. There exists an optimum promoter loading at which the ability of Rh to dissociate CO molecules is a maximum (Chen *et al*., 2010).

CO hydrogenation to ethanol over 1.5wt%Rh/SiO_2 promoted with La and/or V oxides was taken up in another study. Combined La/V promotion reduced methane selectivity and increased C_2^+ oxygenates selectivity compared to the singly promoted catalysts by increasing the rate of CO insertion (Subramanian *et al*., 2010).

After H_2 reduction at 500ºC, FTS over an Rh vanadate ($RhVO_4$) catalyst supported on SiO_2 ($RhVO_4/SiO_2$) was studied, and the results of vanadia-promoted (V_2O_5-Rh/SiO_2) and unpromoted Rh/SiO_2 catalysts are compared. The $RhVO_4/SiO_2$ catalyst gave higher activity and selectivity to C_2 oxygenates than the unpromoted Rh/SiO_2 catalyst after the H_2 pretreatment. CO conversion over the $RhVO_4/SiO_2$ catalyst was much higher than that of V_2O_5-Rh/SiO_2, and the yield of C_2 oxygenates was enhanced. It was also found that the $RhVO_4/SiO_2$ catalyst can be regenerated by calcination or O_2 treatment at high temperature after the reaction (Ito *et al*., 1998).

FTS was explored over Rh polycrystalline foil and single crystal (111) catalysts at a pressure of 6 atm. At the beginning, clean Rh catalysts showed no structure sensitivity, and the primary product was methane (90 wt%) at an initial rate of 0.15 molecules $site^{-1}.sec^{-1}$ at 300°C, and no detectable amounts of oxygenated hydrocarbons formed. Preoxidation of Rh (800 Torr O_2, 600°C, 30 min) resulted in enhanced initial rates, a larger amount of higher molecular weight hydrocarbons in the product distribution, formation of methanol, ethanol and acetaldehyde, and also some structure sensitivity. Lowering the reaction temperature or H_2/CO ratio increased the C_2H_4 to C_2H_6 ratio and shifted the product distribution toward the higher molecular weight hydrocarbons. The addition of 1 mol% of CH_3OH, CH_3CH_2OH, or C_2H_4 to the H_2/CO reaction mixture slightly increased the fraction of higher molecular weight hydrocarbons (Castner *et al*., 1980).

Thin film catalysts, consisting of well-defined Rh particles in contact with promoting and supporting vanadium oxides were studied regarding to their structure and morphology, and they were exposed to oxidative and reductive pretreatments at high temperature and

then correlated in accordance with activity changes in CO hydrogenation. All systems showed a steady decrease of the catalytic activity with reduction temperature (373–823 K), which was in part because of vanadium oxide covering the free metal surface area and in part due to the formation of stable bulk alloy phases. Comparison of the results of electron microscopy indicated that the initial decrease in catalytic activity (between 373 and 473 K) was caused mainly by the decoration of Rh particles with reduced VO_x species. Dramatic decrease in catalytic activity after reduction above 573 K was due to the formation of distinct Rh–V alloys. A selectivity shift towards CH_4 at elevated reduction temperatures accompanied this activity loss (Jenewein *et al*., 2006).

Carbon nanotubes (CNTs)-promoted Rh-Ce-Mn/SiO_2 catalysts were prepared by impregnation, and the catalytic activity of Rh-Ce-Mn-CNTs/SiO_2 in CO hydrogenation to oxygenates was investigated. The results of XPS and XRD studies showed that the addition of CNTs improved the dispersion of Rh which resulted in an enrichment of active components on the catalyst surface. At the same time, introduction of CNTs increased the interaction between Rh and other components, and the amounts of strongly adsorbed H_2 or CO on the surface of the catalyst were significantly enhanced. CO hydrogenation activity of the Rh-Ce-Mn/SiO_2 catalyst was with the addition of CNTs. Under the specific reaction conditions with 10wt% CNTs content, CO conversion level was 11.86 % and the yield of oxygenates was 336.2 g/(kg·h) (Lihong *et al*., 2006).

2.2.1.2. Iron catalysts. Fe catalysts are used not only because of their low price compared to Co and Ru but also because they yield olefins when operated at elevated temperatures either in the low or the high alpha mode (Marura, 2002). Alkali-promoted iron catalysts have been used in the industrial operation for FTS for many years. These catalysts have high water gas shift tendency, high selectivity to olefins and stay stable when synthesis gas with a high H_2/CO ratio is converted (Jager and Espinoza, 1995; Kolbel and Ralek, 1980). Iron catalysts are very useful in applications to coal-derived gas since an iron catalyst has higher activity with low H_2/CO ratios (0.4–1.0), as compared to the cobalt-based catalyst (Hayakawa *et al*., 2007).

Iron-based catalysts are used in the LTFT for the production of wax. Addition of alkali metals has strong influence on the product selectivity of Fe catalysts. Especially

promotion with potassium has been found to enhance the wax and olefin selectivity and to diminish the methane production. Cu has been added to precipitated Fe catalysts in order to raise the rate of reduction and to lower the reduction temperature of Fe oxide to metal (Anderson *et al*., 1951)**.** The addition of SiO_2, Al_2O_3 and even Mn can be applied for structural promotion to enhance the olefin selectivity and to maintain high surface area and stability of the iron catalysts used in HTFT. Iron FT catalysts can lose activity because of sintering, fouling and chemical poisoning of the surface mainly by sulfur (Dry, 1983).

A series of La_2O_3-promoted precipitated iron catalysts (100Fe/2.8Si/*n*La, *n*=0, 0.5, 1, 2, and 4, atomic ratio) were prepared. It was established that the loading of a low amount of La_2O_3 (La/Fe<0.01) yields a significant decline in the particle size of Fe_2O_3, which enhances the specific surface area and metal dispersion of the catalysts. This also led to the formation of iron carbides, which gave high catalytic activity in FTS. With increasing La_2O_3 content (La/Fe>0.02), a high La_2O_3 coverage and formation of a $LaFeO_3$ compound decreased the formation of iron carbides, and the reaction performance decreased. The ideal La_2O_3 content was La/Fe=0.01. The addition of La_2O_3 increased the selectivity for methane and suppressed the formation of C_5^+ hydrocarbons (Lili *et al*., 2009).

Hydrocarbon product distributions of iron and physical mixtures of iron–zeolite catalyzed FTS have been studied. Existence of the zeolite enhanced secondary reactions that consist of cracking of heavier products and light olefins oligomerization. At high space velocity, product distribution of iron–zeolite catalyst was very similar to iron catalyst, because the role of the zeolite on overall reaction declined. Regarding product distribution, both iron and iron–zeolite catalysts showed that the average carbon number in product decreases with increasing reaction temperature and H_2/CO ratio (Pour *et al*., 2008).

A precipitated iron catalyst having sulfur was prepared by means of a novel method using a ferrous sulfate as precursor for CO hydrogenation. Catalyst deactivation rate was low, associated with an unexpectedly low CH_4 selectivity of 2.0–2.9 wt%. It was observed that a small amount of sulfur existing as sulfate may promote the catalyst by increasing activity and improving the heavier hydrocarbon selectivity (Wu *et al*., 2004).

The combination of iron-based FT catalysts with an HZSM-5 co-catalyst was studied at temperatures of 330 and 350 °C. The higher operating temperature adversely influenced the activity of the iron catalyst, since it caused a change in the Fischer–Tropsch product distribution towards lighter hydrocarbons at the expense of the desired product (gasoline). It was shown that the increased synthesis temperature does not have significant effect on the performance of an HZSM-5 zeolite with high aluminum content, but increases considerably the performance and useful lifetime of an HZSM-5 zeolite with low aluminum content (Botes, 2005).

2.2.1.3. Cobalt catalysts. Cobalt catalysts give the highest FTS yields, have the longest life-time and produce mostly linear alkanes (Chaumette *et al*., 1995). The drawbacks are high costs and low water gas shift activity.

The influence of methanol addition on the activity of Co/SiO_2 catalyst for CO hydrogenation was studied in a fixed-bed reactor at 210°C and 2.0 MPa. It was shown that introduction of methanol provided an increase in the selectivity of methane, water and CO_2 and a decrease in the activity of the catalyst (Zhoua *et al*., 2008). The influence of the introduction of ethanol (2% and 6%) during CO hydrogenation was investigated using a 10% Co/TiO_2 catalyst. The transformation of ethanol vapor (2 % and 6 % in nitrogen) over the Co/TiO_2 catalyst was also studied in the absence of the synthesis gas under FT reaction conditions. Ethanol was observed to be incorporated in the growing chain and was found to (i) increase the selectivity to light products, (ii) increase the olefin to paraffin ratio and (iii) considerably lower the catalyst activity. These effects were almost completely reversed when the ethanol in the feed was removed (Jalama *et al*., 2007).

The influences of the addition of Ag, Au, or Rh to a 15 wt% Co/SiO_2 catalyst on FTS were also studied. Both Au and Rh showed an enhancement effect on the FT performance, while the addition of Ag decreased the activity. The addition of a small amount of Rh (0.1–0.5 wt%) increased CO conversion by 50 % without affecting the selectivity. It was found that Rh catalyzed the reduction of cobalt oxides, but it did not change the number of surface cobalt atoms. It was proposed that the higher activity of Rh-promoted catalysts is due to the hydrogen spillover from Rh to Co during FTS (Yana *et al*., 2011).

FTS was studied on polycrystalline cobalt foils, and the influences of potassium and magnesium promoters have been explored. The selectivity towards methane decreased due to both promoters. However, the main effect with potassium was the suppression of carbon deposition at higher reaction temperatures (Lahtine and Somorjai, 1998).

A series of magnesia-modified alumina-supported cobalt catalysts were prepared and low amounts of magnesia showed improvement in the activity of cobalt catalysts for FTS but higher amounts of magnesia lowered the performance, and the methane and CO_2 selectivity increased for all the magnesia-modified catalysts; moreover, the olefin to paraffin ratio increased with an increase in magnesia content (Zhang *et al*., 2005).

The effect of La addition to Zr-Co/activated carbon (AC) catalysts on their FTS activity was also studied. The experimental results showed that CO conversion increased from 86.4 % to 92.3 %, and the selectivity to methane decreased from 14.2 % to 11.5% while C_5^+ selectivity increased from 71.0 % to 74.7 % when a low La loading (La= 0.2 wt%) was added to Zr-Co/AC. However, high loadings of La (La= 0.3−1.0 wt%) decreased catalyst activity as well as C_5^+ selectivity and increase CH_4 selectivity (Wang *et al*., 2008).

Effect of K promotion on the CO hydrogenation activity and selectivity of co-precipitated Co/Al_2O_3 was also studied, and K addition was found to lower total activity while enhancing C_2-C_4 olefins selectivity (Akın and Önsan, 2000).

Carbon monoxide hydrogenation reaction was conducted over Mn- and Zr-modified Co/SiO_2 catalysts. Co supported on SiO_2 with an average pore size of 10 nm exhibited high catalytic performance for FTS due to suitable Co particle sizes in the catalyst. Zr promoter improved the activity and Mn promoter improved the stability of Co/SiO_2 catalyst for FTS (Liu *et al*., 2009).

An extensive study of Co/Al_2O_3 Fischer–Tropsch synthesis catalysts promoted with different quantities of Group 11 metals (Cu, Ag, Au) is reported. With small promoter levels (0.83%Ag and 1.51%Au) and higher Ag levels (2.76%), important gains in Co active site densities were attained that led to improved CO conversion levels compared to the unpromoted catalyst. Furthermore, slight decreases in light product selectivity and

slight increases in C_5^+ selectivity were achieved. At high Au loading (5.05%), however, too much Au was loaded which, significantly increasing the fraction of Co reduced, blocked Co surface sites and resulted in decreased CO conversion rates. On the other hand, Cu made Co reduction easier; the increased fraction of reduced Co did not affect improved active site densities. It appears that a fraction of Cu tended to cover the edge of Co clusters, resulting in decreases in CO conversion rates and significant enhancement in light product selectivity (Jacobs *et al*., 2009).

Different amounts of cobalt, ruthenium and potassium addition on carbon nanotubes supported cobalt catalysts were characterized and tested for FTS. Up to 30 wt% Co, 1 wt% Ru and 0.0066 wt% K were added to the catalyst. Increasing the Co loading from 15 to 30 wt% increased CO conversion from 48 to 86% and the C_5^+ selectivity from 70 to 77%. Promotion by 0.5 wt%Ru increased the FTS rate of 15 wt% Co/CNT catalyst by a factor of 1.4 whereas introduction of 0.0066 wt% K decreased the FTS rate by a factor of 7.5. Both promoters enhanced the selectivity of FTS towards higher molecular weight hydrocarbons; however, the effect of Ru was less pronounced. Potassium increased the olefin to paraffin ratio from 0.73 to 3.5 and the C_5^+ selectivity from 70% to 87% (Trepanie *et al*., 2009).

2.2.1.4. Ruthenium catalysts. The fact that Ru is neither oxidized nor carburized during FT is crucial, so many workers have decided to study supported Ru catalysts (Van der Laan, 1999). Ru catalysts showed low selectivity towards methane and higher selectivity towards C_5^+ hydrocarbon products compared to other FT catalysts at atmospheric pressure and temperatures from 240°C to 280°C (Bahome, 2007).

It was found that increasing the pressure over the 0.5wt%Ru/Al_2O_3 catalyst increased the CO hydrogenation activity, and the selectivity towards heavier hydrocarbons whereas increasing the temperature enhanced catalytic performance but also shifted product distribution to methane. Ruthenium catalysts are most active in the pure metallic form and supports and/or promoters appear to have no beneficial effect (Everson and Mulder, 1993).

A series of TiO_2-supported Ru-Ni bimetallic catalysts, with total metal loading of ~4.5 wt% in each, were prepared to observe the effects of Ru loading and pretreatment procedures on CO hydrogenation activities of these catalysts and product selectivities. FTS

was studied over these catalysts in the 483–493 K temperature range, at a weight hourly space velocity of 1.5 h^{-1}, H_2/CO mole ratio of 2, and at atmospheric pressure. The catalyst containing 3.6 wt% Ni and 0.82 wt%Ru produced highest proportion of C_{5+} hydrocarbons (60 wt%). High olefin selectivities (40 wt% for $C2^{=}$ and 93 wt% for $C3^{=}$, respectively) were observed with catalysts containing only 5 wt% Ru (Das *et al*., 2004).

2.2.1.5. Nickel catalysts. Nickel has limited use in FTS since it is generally regarded as a methanation catalyst, and it was shown to be active for methanation in FTS when used either as alloy (Habazaki *et al*., 1998) or supported on silica (Louis *et al*., 1993). The earliest FTS reaction was carried out in 1902 when Sabatier and Sanderens became the first to report the hydrogenation of CO over a Ni catalyst to produce methane (Price, 1994).

In another study, a series of alumina supported Ni, Mo and Ni-Mo catalysts were prepared. The Ni and Mo contents of the catalysts were changed in the range of 0-15 wt%. The results of CO hydrogenation tests revealed that the specific activity of the active sites changes with Mo loading, Ni/Mo molar ratio and total metal loading. Addition of Mo as the second metal increases total hydrocarbon production as well as the C_2-C_4 hydrocarbons selectivity in the 498-573 K temperature range. Lower H_2/CO molar ratios increase C_2-C_4 selectivity, and this effect is enhanced with Mo addition especially to samples with higher Ni loading (Aksoylu and Önsan, 1998).

A series of γ-Al_2O_3 supported Ni, Ni–V, and Ni–V–K catalysts were prepared to observe the influences of V and K promotion on structural properties of Ni catalysts and their catalytic performance in FTS. The Ni content of the samples was fixed at 5 wt% while the V content was changed between 0.5 and 2 wt%. Finally, 0.5 wt% K was added to 5 wt% Ni–1 wt% V/Al_2O_3 for obtaining enhanced olefin selectivity. Experimental results revealed that total activity and C_2–C_4 hydrocarbons production were increased by V addition up to 1wt% while olefin selectivities showed a decreasing trend in the same range. The addition of K decreased the total hydrocarbons production of the catalyst, especially the production of paraffinic hydrocarbons and carbon dioxide that resulted in an increase in the ratio of C_2–C_3 olefins to paraffins (Karaselçuk *et al*., 2000).

2.2.2. Fischer-Tropsch Catalyst Supports

The principal function of the catalyst support in FT catalysts is to disperse the active metal and produce stable metal catalyst particles after reduction. The porous structure of the support can control the sizes of supported metal particles, and supported catalysts exhibit better characteristics than unsupported ones. Some of these characteristics include improved catalyst texture and porosity, controlled particle size, increased metal dispersion, reduction in formation of hardly reducible active metal oxides, facilitation of reducibility, and enhancement of mechanical properties as well as attrition resistance of active metals (Jongsomjit *et al*., 2005).

The effects of different supports used in FTS have been extensively studied and the support is an important component affecting the properties of the catalysts (Khodakov *et al*., 2002). Among the supports, Al_2O_3, SiO_2 and TiO_2 have been most often employed for FTS. This is due to the high surface areas that they possess. The pore structure of the support has a significant effect on the size, location, shape and appearance of the FT active metal catalysts. The catalytic activity of cobalt-based catalysts was studied as a function of support material, and it was concluded that there is declining trend in the following order: Co/TiO_2>Co/Al_2O_3>Co/SiO_2>100% Co>Co/MgO (Ruel and Bartholomew, 1984).

In another study, it was found that at pressures greater than 5 bars and at high CO conversions, the influence of the support on the selectivity to methane and C_5^+ formation could be insignificant (Iglesia *et al*., 1992). One of the greatest functions of the support is to dissipate the heat released by the reaction and thus reduce the temperature gradient in fixed-bed reactors.

The loading of low amounts of TiO_2 to silica-supported cobalt catalysts enhanced the dispersion of Co and the Co metallic surface area considerably, resulting in significant enhancement of FTS activity. The addition of TiO_2 adjusted the interaction between Co and the SiO_2 support quite well to realize the preferred dispersion and reduction degree of Co, leading to high catalytic activity in FTS (Hinchiranana *et al*., 2008).

A systematic study was conducted to observe the effects of Al_2O_3/SiO_2 ratio on reduction, carburization and catalytic behavior of iron based FTS catalysts promoted with potassium and copper. During reaction tests, it was found that a maximum in catalyst activity is provided at the Al_2O_3/SiO_2 weight ratio of 5/20. The selectivity to olefins showed a rapid decrease and the formations of methane and light hydrocarbons were promoted with increasing Al_2O_3/SiO_2 ratio. The oxygenate selectivity in total products was enhanced with increasing Al_2O_3/SiO_2 ratio (Wan *et al*., 2006).

The effect of adding SiO_2 to a precipitated iron-based FTS catalyst was investigated to compare the FTS performances of the catalysts with and without silica. The results indicated that SiO_2 decreases the FTS initial activity but improves the catalyst stability. Due to the lower surface basicity of the catalyst without SiO_2, the catalyst incorporated with SiO_2 had higher selectivity to light hydrocarbons and CH_4 and decreased selectivity to olefins and heavy hydrocarbons (Wan *et al*., 2006).

The effects of co-precipitated SiO_2 were investigated in Fe-based catalysts for FTS. The SiO_2-free catalyst had large pores (10–100 nm) and low specific surface area, whereas SiO_2-containing catalysts showed micro pores (<10 nm) and large specific surface areas. Co-precipitated silica increased the productivity of hydrocarbons in FTS, especially C_5^+ hydrocarbon selectivity. SiO_2-free and SiO_2-containing iron catalysts showed high activity and stability over 100 h time-on-stream tests, and displayed slight difference in product selectivity (olefin/paraffin ratio) at temperatures of 513–553 K (Hayakawa *et al*., 2007).

Carbon-based materials are advantageous over oxide supports since they do not react with the active metal to form inactive materials such as mixed oxides (aluminates, silicates or titanates) that are only reducible at high temperatures. The influence of metal catalyst addition and promoters on the activity and selectivity of CNT supported FTS catalysts was studied at 275°C, 8 bar, CO/H_2=1/2 and different flow rates. The FT catalysts supported on carbon nanotubes displayed high CO conversion and good stability with time on stream in the CO hydrogenation reaction. Iron catalysts displayed the lowest methane selectivity compared to Ru and Co catalysts (Bahome, 2007).

By using MCM-41 and SBA-15 as catalytic supports, the effects of promotion with Ru on the structure of Co catalysts and their performance in FTS were studied. It was investigated that monometallic cobalt catalysts supported by smaller pore mesoporous silicas (d_P=3–4 nm) had much lower activity in FTS than their larger pore counterparts (d_P=5–6 nm). Promotion with Ru of smaller pore Co catalysts led to a considerable increase in Fischer–Tropsch reaction rate, while the effect of Ru promotion was less significant in catalysts supported on larger pore silicas (Hong *et al*., 2009).

2.3. Influence of Process Conditions on the Selectivity

2.3.1. Total Pressure

Most studies show that the product selectivity shifts to heavier products and to more oxygenates with increasing total pressure (Dry, 1981). In a series of studies conducted on a 0.5%Ru/Al_2O_3 catalyst, it was established that increasing pressure increases activity of CO hydrogenation and selectivity towards heavier hydrocarbons (Everson and Mulder, 1993).

The influence of operating conditions on the activity of an Fe-Mn catalyst for FTS was investigated. Experiments were carried out under variation of temperature, pressure, inlet H_2/CO ratio and space velocity. The selectivity to low molecular weight hydrocarbons basically increased with the enhancement of reaction temperature, total pressure and inlet H_2/CO ratio, except for ethylene. Furthermore, the FTS reaction rate and the overall oxygenates formation rate increased with increasing reaction temperature, pressure, space velocity and H_2/CO ratio on the whole (Liu *et al*., 2007).

Hydrogenation of CO with an inlet reactant gases ratio of CO/H_2=1/3 on Raney ruthenium catalysts was carried out at 1.1 MPa and 2.1 MPa pressure. Hydrocarbons, whose distribution followed the Schulz-Flory pattern, were produced from CO-H_2, together with a trace amount of methanol. The activities for their production were much improved under high pressure, but the selectivity of methanol production decreased, probably due to the poisoning of active sites by water (Takeishia *et al*., 1998).

2.3.2. Temperature

The industrial reaction temperatures used in FTS varies between 200-350^{o}C. It is difficult to operate at high temperatures (e.g. above 350^{o}C) because most of the catalysts that are used degrade or deactivate at high temperatures. Cobalt for instance is known as a LTFT catalyst since it performs well at temperatures between 220-250^{o}C for production of long chain products mainly diesel and wax. If it is used at high temperatures, methane will be the abundant product. Iron, on the other hand, performs well at higher temperatures of 250-350^{o}C in the production of light products, gasoline and chemicals (Dry, 2004).

Higher reaction temperatures result in a shift towards products with lower carbon numbers on iron (Dictor and Bell, 1986), ruthenium and cobalt (Dry, 1981) catalysts. It was observed that the olefin to paraffin ratio on potassium-promoted precipitated iron catalysts increases with increasing temperature (Dictor and Bell, 1986; Anderson, 1956). However, a decrease in olefin selectivity with increasing temperature for un-alkalized iron oxide powders was also reported (Dictor and Bell, 1986).

2.3.3. Partial pressure of H_2 and CO

Increasing the H_2/CO ratios at reactor inlet results in lighter hydrocarbons and lower olefin content (Donnelly and Satterfield, 1989). For Co-based catalysts, a H_2/CO molar ratio of 2.15:1 is normally used for a H_2 to CO feed mixture, since the dominant reaction is FTS. The H_2/CO ratio in the syngas changes when iron is used, due to the WGS side reaction that takes place. For low-temperature FT (LTFT, 200-240^{o}C) process using iron, the H_2/CO ratio is typically 1.7:1, while for high-temperature FT (HTFT, 250-350^{o}C) it is 1.05:1, since WGS is rapid and CO_2 produced is allowed to be converted into FT products via the reverse WGS followed by the FT reaction (Dry, 2002).

FTS was investigated over Co/γ-Al_2O_3 and Co–Re/γ-Al_2O_3 using feed with H_2/CO molar ratios of 2.1, 1.5 and 1.0, simulating synthesis gas derived from biomass. With lower H_2/CO ratios in the feed, CO conversion and CH_4 selectivity decreased, while the C_5^+ selectivity and olefin/paraffin ratio for C_2–C_4 increased a little. For both catalysts, the drop in the production rate of hydrocarbons when shifting from an inlet ratio of 2.1 to 1.5 was

crucial mainly because the H_2/CO usage ratio did not follow the change in the inlet ratio. The hydrocarbon selectivities were rather similar for inlet H_2/CO ratios of 2.1 and 1.5, but they were significantly shifted from those for an inlet ratio of 1.0 (Tristantini *et al*., 2007).

The effect of co-feeding CO_2 on the catalytic properties of Fe–Mn catalyst during FTS was investigated by changing CO_2 partial pressure in the feed gas. It was observed that co-feeding CO_2 to syngas did not lower the activity of the catalyst; on the contrary, it caused a sharp increase in the activity and an increase in methane selectivity over the catalyst after removal of CO_2 from the feed gas. The addition of CO_2 led to an increase in olefin/paraffin ratios of low carbon hydrocarbons and a slight decrease in C_{19}^{+} selectivity. It also slightly decreased CO_2 formation rate on the catalyst by increasing the rate of reverse water–gas shift (RWGS) reaction and pushing the reaction towards equilibrium, and did not significantly influence the hydrocarbon formation rate. However, the co-feeding CO_2 can remarkably increase the water formation rate and the overall oxygenate formation rate under these reaction conditions (Liua *et al*., 2008).

2.3.4. Space Velocity

The influence of space velocity of syngas on FTS selectivity has been determined**.** Enhancement of the olefin to paraffin ratio with increasing space velocity (thus a decrease in CO conversion) was observed on a poly-crystalline cobalt foil (Kuipers *et al*., 1996).

Changing the space velocity had no effect on the molecular weight of hydrocarbons (Bukur *et al*., 1990), whereas in another study an increase was observed in the average molecular weight of the products at decreasing space velocity (Iglesia *et al*., 1991). The selectivity to methane and olefins decreased with a decrease in space velocity, while the selectivity towards paraffins remained unchanged.

The possibilities for selectivity control in FTS by selection of process conditions and modification of catalyst formulations are summarized in Table 2.4 (Röper, 1983), and the simple stepwise growth process for the formation of FT products is illustrated in Figure 2.2 as described by Dry (2002).

Table 2.4. Selectivity control in FTS by process conditions and catalyst modifications (Röper, 1983).

Parameter	Chain length	Chain branching	Olefin select.	Alcohol select.	Carbon deposition	Methane select.
Temperature	↓	↑	*	↓	↑	↑
Pressure	↑	↓	*	↑	*	↓
H_2/CO	↓	↑	↓	↓	↓	↑
Conversion	*	*	↓	↓	↑	↑
Space velocity	*	*	↑	↑	*	↓
Alkali content iron catalyst	↑	↓	↑	↑	↑	↓

Increase with increasing parameter: ↑
Decrease with increasing parameter: ↓
Complex relation: *

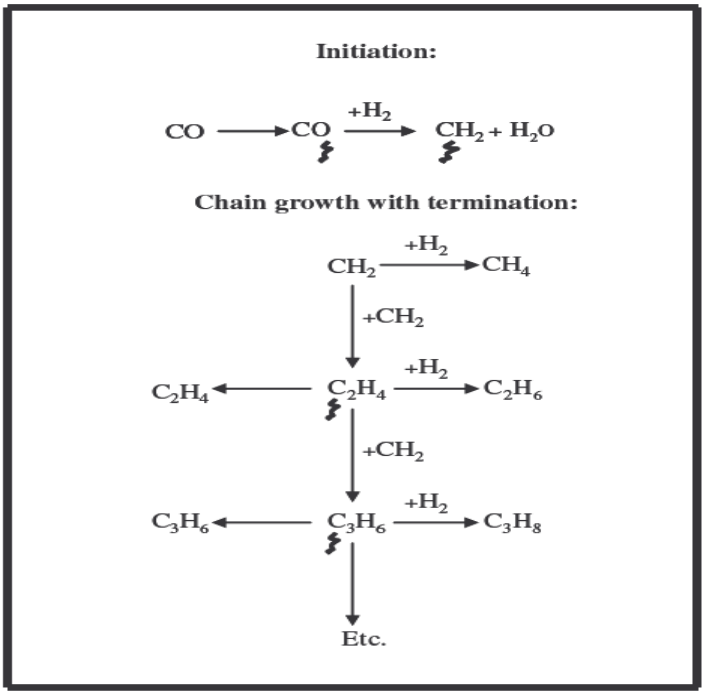

Figure 2.2. Simple stepwise growth process for FT products (ξ= surface) (Dry, 2002).

The stepwise growth process occurs at the surface of the catalyst, and when CO is hydrogenated, CH_2 units are formed which are taken as the "monomers" in a stepwise oligomerization process. These adsorbed units can either be desorbed or be hydrogenated further to form primary FT products, or another monomer unit can add to the chain to continue the chain growth. This process can take place at each stage of growth. Principally, two termination reactions are possible, namely α-hydrogenation, yielding a paraffin, or β-dehydrogenation, producing α-olefin as primary products.

2.4. Product Upgrading and Separation

Conventional refinery processes can be used for the upgrading of Fischer-Tropsch liquid and wax products. Wax hydrocracking, distillate hydrotreating, catalytic reforming, naphta hydrotreating, alkylation and isomerization are some of possible processes for FT products (Choi *et al*., 1997). Fuels produced by FTS are of a high quality because of very low aromaticity and zero sulfur content. The product stream consists of various fuel types: LPG, gasoline, diesel fuel, and jet fuel. The definitions and conventions for the composition and names of the different fuel types that are obtained from crude oil refinery processes are given in Table 2.5 (Van der Laan, 1999).

Table 2.5. Conventions of fuel names and composition (Kroschwitz and Howe-Grant, 1996).

Name	Synonyms	Components
Fuel gas		C_1-C_2
LPG		C_3-C_4
Gasoline		C_5-C_{12}
Naphta		C_8-C_{12}
Kerosene	Jet Fuel	C_{11}-C_{13}
Diesel	Fuel oil	C_{13}-C_{17}
Middle Distillates	Light gas oil	C_{10}-C_{20}
Soft wax		C_{19}-C_{23}
Medium wax		C_{24}-C_{35}
Hard wax		C_{35}+

3. EXPERIMENTAL WORK

3.1. Materials

3.1.1. Chemicals

All the chemicals used in catalyst preparation are listed in Table 3.1.

Table 3.1. Chemicals used in catalyst preparation.

Chemicals	**Formula**	**Grade**	**Source**	**Molecular Weight ($g.mol^{-1}$)**
Rhodium (III) nitrate solution, 10% (wt/wt)	$Rh(NO_3)_3$ hydrate	Extra Pure	Sigma-Aldrich	288.92
Lanthanum nitrate-6-hydrate	$La(NO_3)_3 \cdot 6H_2O$	Extra Pure	Riedel-de Haen	433.01
Ammonium meta-vanadate	NH_4VO_3	Extra Pure	Riedel-de Haen	116.98
Aluminum oxide	δ-Al_2O_3	Extra Pure	Alfa Aesar	101.96
Silica gel	SiO_2	Extra Pure	Merck	60.08
Silica Gel Orange	SiO_2	Extra Pure	Sigma-Aldrich	60.08

3.1.2. Gases and Liquids

The H_2, Ar and CO gases used in this study were supplied by Birleşik Oksijen Sanayi (BOS), and He was obtained from HABAŞ Company, Istanbul, Turkey. The applications and specifications of the liquids and gases in this study are listed in the Tables 3.2 and 3.3.

Table 3.2. Applications and specifications of the liquids used.

Liquid	Application	Specification
Water	Aqueous solutions	Deionized

Table 3.3. Applications and specifications of the gases used.

Gas	Application	Specification
Carbon monoxide	Reactant, GC calibration	99.5%
Helium	GC carrier	99.999%
Nitrogen	Reactant (inert), GC calibration	99.998%
Hydrogen	Reactant, Reducing agent, GC calibration	99.99%
Argon	GC carrier	99.999%

3.2. Experimental Systems

The experimental systems used in this work can be classified into three main groups:

(i) Catalyst Preparation System: Catalysts were prepared by sequential or co-impregnation to incipient wetness in this system.

(ii) Micro-reactor Flow System: This system was modified to include mass flow controllers for inlet gases, temperature-controlled heated connecting lines and a fixed bed flow reactor in a vertical furnace whose temperature is controlled by a programmable temperature controller. This system was used for catalytic activity tests.

(iii) Product Analysis System: In this system, the composition of the reactant and product gases is analyzed by using two on-line gas chromatographs.

3.2.1. Catalyst Preparation System

$Rh/\delta\text{-}Al_2O_3$, Rh/SiO_2, $Rh\text{-}La/SiO_2$, $Rh\text{-}La\text{-}V/SiO_2$ catalysts were prepared by sequential or co-impregnation to incipient wetness of silica gel and alumina. The system used for catalyst preparation includes a Retsch UR1 ultrasonic mixer which provides uniform mixing and contact of the solution with the support, a vacuum pump, a Masterflex computerized-drive peristaltic pump which is used for addition of the solution that will be impregnated, a vacuum flask, a beaker and silicone tubing (Figure 3.1).

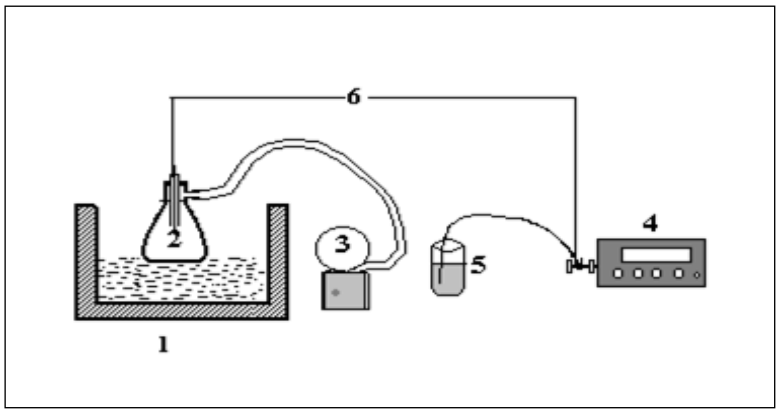

Figure 3.1. The impregnation system: 1.Ultrasonic mixer 2.Vacuum flask 3. Vacuum pump 4.Peristaltic pump 5.Beaker 6.Silicone tubing (Akın, 1996).

3.2.2. Microreactor Flow System

The microreactor flow system used for carbon monoxide hydrogenation reaction was

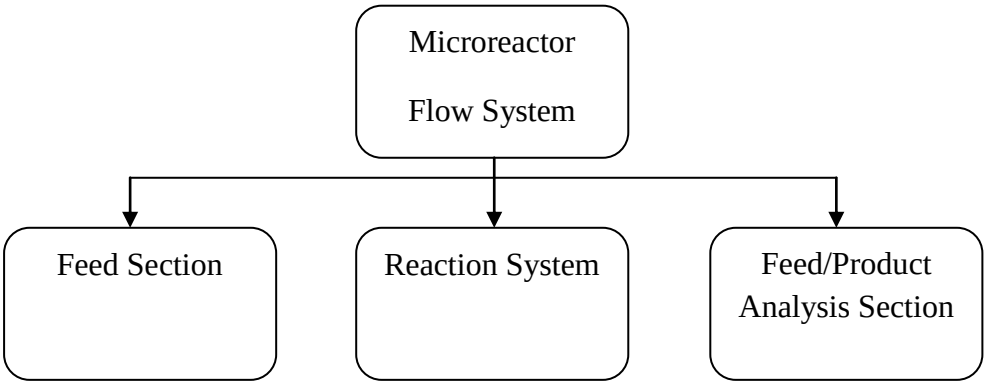

Figure 3.2. Block diagram of the microreactor flow system.

designed in the laboratory. This system includes three main sections as shown in Figure 3.2. Details and the necessary equipment for the system are presented in Section 4.

3.2.3. Product Analysis System

CO, H_2, N_2 gas streams were analyzed using an HP-Agilent 6890N Network temperature-controlled programmable gas chromatograph equipped with a thermal conductivity detector (TCD). A Molecular Sieve 5A packed column was used for detecting the components of the feed and product gases after the reaction and was operated under argon as carrier gas.

CO_2 and CH_4 were analyzed using an HP-Agilent 6850 Network temperature-controlled programmable gas chromatograph equipped with a thermal conductivity detector (TCD). A Porapak Q packed column was used for detecting the components of the feed and product gases after the reaction and was operated under helium as carrier gas.

Reactant and product analysis conditions used in the two gas chromatographs are listed in Table 3.4 and Table 3.5 for HP-Agilent 6890N and HP-Agilent 6850, respectively.

Table 3.4. Reactant and product gas analysis conditions for HP-Agilent 6890N.

Column Type	Packed Column
Detector Type	Thermal Conductivity
Column Oven Temperature	40^oC
Injector Temperature	40^oC
TCD Temperature	150^oC
Carrier Gas	Argon
Carrier Gas Flow Rate	40 $ml.min^{-1}$
Column Packing Material	Molecular Sieve 5A, 60-80 mesh
Column Tubing Material	Stainless Steel
Column ID & Length	1/8" OD x 2 m
Sample Loop	1 ml

Table 3.5. Reactant and product gas analysis conditions for HP-Agilent 6850.

Column Type	Packed Column
Detector Type	Thermal Conductivity
Column Oven Temperature	$40^{o}C$
Injector Temperature	$110^{o}C$
TCD Temperature	$150^{o}C$
Carrier Gas	Helium
Carrier Gas Flow Rate	20 $ml.min^{-1}$
Column Packing Material	Porapak Q, 80-100 mesh
Column Tubing Material	Stainless Steel
Column ID & Length	1/8" OD x 3 m
Sample Loop	1 ml

3.3. Catalyst Preparation

In the experiments Rh/δ-Al_2O_3, Rh/SiO_2, Rh-La/SiO_2, Rh-La-V/SiO_2 catalysts were used. Rh based catalysts supported on silica were prepared twice. Firstly, catalysts were prepared with silica gel, and secondly catalysts with the same precursor weight percentages were prepared using silica gel orange having different physical properties. These catalysts with their percentages can be listed as follows:

(i) 2wt%Rh/δ-Al_2O_3
(ii) 1.5wt%Rh/SiO_2
(iii) 1.5wt%Rh-2.6wt%La/SiO_2
(iv) 1.5wt%Rh-2.6wt%La-1.5wt%V/SiO_2

3.3.1. Preparation of Rh/δ-Al_2O_3 catalyst

Commercial alumina was crushed and sieved into 45-60 mesh size (344-255 μm), and then, as pretreatment, crushed particles were first dried at 150°C for 2 hours followed by calcination at 900°C for 4 hours. For catalyst preparation by the incipient wetness impregnation method, a definite amount of alumina support was put in a vacuum flask and

was kept under vacuum in the first step. The vacuum pump was also kept on during the addition of the precursor solution since the trapped air in the pores of the support could prevent complete penetration of the solution. This treatment provides more uniform distribution of the active component by removing the trapped air. The support material in the vacuum flask was mixed under vacuum with an ultrasonic mixer for 30 minutes before impregnation.

The calculated amount of aqueous solution of $Rh(NO_3)_3$ hydrate was dissolved in deionized water on the basis of 1 g alumina/1.2 ml solution. Aqueous $Rh(NO_3)_3$ hydrate solution was fed to the vacuum flask at a flow rate of 0.5 $ml.min^{-1}$ via a silicone tubing using a Masterflex computerized-drive peristaltic pump. The slurry was mixed ultrasonically during impregnation to maintain uniform distribution of the aqueous $Rh(NO_3)_3$ hydrate solution. After all the solution was fed, the mixing was continued for an additional 90 minutes. The resulting slurry was dried at 120°C overnight before being calcined in air at 500°C for 4 h to obtain the 2wt%Rh/δ-Al_2O_3 catalyst. The preparation steps are given below:

- Sieving support to 45-60 mesh size
- Drying
- Calcination of support
- Evacuation of the support
- Contacting the support with the precursor solution
- Drying
- Calcination

3.3.2. Preparation of SiO_2 supported Rh based catalysts

Catalysts were prepared by sequential or co-impregnation to incipient wetness of silica gel using the system in Figure 3.1 with an aqueous solution of $Rh(NO_3)_3$ hydrate and aqueous solutions of precursors of the promoters (1 g silica gel/2 ml solution), followed by drying at 90^{o}C for 4 h, and then at 120^{o}C overnight before being calcined in air at 500^{o}C for 4 h. These steps are given below:

- Calcination of support
- Sieving support to 45-60 mesh size
- Washing support with boiled distilled water for three times
- Drying the support
- Calcination of support
- Evacuating the support
- Contacting the support with the precursor solution
- Drying
- Calcination

Commercial silica gel support was first calcined in a muffle furnace at 500^{o}C for 4 hours to avoid support from turning into gel form. Then silica gel was crushed and sieved into 45-60 mesh size (344-255 μm), washed 3 times using boiled distilled water to remove possible impurities such as Fe and Na (Mo *et al*., 2009), and then dried in a furnace at 115^{o}C overnight and calcined again in air at 500^{o}C for 4 h before being used as a support.

For the preparation of catalysts by incipient wetness impregnation method, a definite amount of silica gel support was put in a vacuum flask and was kept under vacuum in the first step. The support material in the vacuum flask was mixed under vacuum with an ultrasonic mixer for 30 minutes before impregnation.

The calculated amount of aqueous solution of $Rh(NO_3)_3$ hydrate was dissolved in deionized water on the basis of 1 g silica gel/2 ml solution. Aqueous $Rh(NO_3)_3$ hydrate solution was fed to the vacuum flask at a flow rate of 0.5 ml.min^{-1} via a silicone tubing using a Masterflex computerized-drive peristaltic pump. The slurry was ultrasonically mixed during impregnation to maintain uniform distribution of the aqueous solution of $Rh(NO_3)_3$ hydrate solution. After all the solution was fed, the mixing was continued for an additional 90 minutes. The resulting slurry was dried at 90°C for 4 h, and then at 120°C overnight before being calcined in air at 500°C for 4 h to obtain 1.5wt%Rh/SiO_2 catalyst.

For lanthana promoted Rh catalysts supported on silica, it has been reported that the sequence of impregnation has an effect on catalytic behavior. Thus, co-impregnation of the

La additive with Rh was adopted since well dispersed Rh particles are expected to form without being fully covered by La_2O_3 when this method is used (Borer and Prins, 1993).

La-promoted 1.5wt%Rh-2.6wt%La/SiO_2 catalyst was prepared by co-impregnation to incipient wetness of silica gel with an aqueous solution of $Rh(NO_3)_3$ hydrate and aqueous solution of precursor of the promoter. This time, required amounts of aqueous solution of $Rh(NO_3)_3$ hydrate and $La(NO_3)_3 \cdot 6H_2O$ were dissolved in the same beaker simultaneously in deionized water based on 1 g silica gel/2 ml solution calculation to conduct the co-impregnation method. For feeding solution to support, same procedure described in the first catalyst preparation was followed. After all the solution was fed, the mixing was continued for an additional 90 minutes. The resulting slurry was dried at 90°C for 4 h, and then at 120°C overnight before being calcined in air at 500°C for 4 h to obtain the 1.5wt%Rh-2.6wt%La/SiO_2 catalyst.

Finally, the sequential impregnation method was chosen for vanadium containing catalysts, and doubly promoted 1.5wt%Rh-2.6wt%La-1.5wt%V/SiO_2 was prepared by this method. Firstly, the aqueous solution of NH_4VO_3 was dissolved in deionized water on the basis of 1 g silica gel/2 ml solution and added to the silica gel until incipient wetness. The aqueous solution of NH_4VO_3 was prepared at elevated temperature, approximately 80°C, because of its low solubility at room temperature prior to mixing with other solutions; all the other aqueous solutions were prepared at room temperature (Gao *et al*., 2009a).

After all the solution was fed, the mixing was continued for an additional 90 minutes. The resulting slurry was dried at 90°C for 4 h, and then at 120°C overnight before being calcined in air at 500°C for 4 h to obtain the 1.5wt%V/SiO_2 catalyst. After this step, co-impregnation to incipient wetness of silica gel with an aqueous solution of $Rh(NO_3)_3$ hydrate and $La(NO_3)_3 \cdot 6H_2O$ was carried out. At this time, required amounts of aqueous solution of $Rh(NO_3)_3$ hydrate and $La(NO_3)_3 \cdot 6H_2O$ were dissolved in the same beaker simultaneously in deionized water based on 1 g silica gel/2 ml solution calculation to conduct co-impregnation method and mixture was added on 1.5wt.%V/SiO_2 and after all the solution was fed, the mixing was continued for an additional 90 minutes. The resulting slurry was dried at 90°C for 4 h, and then at 120°C overnight before being calcined in air at 500°C for 4 h to obtain 1.5wt%Rh-2.6wt%La-1.5wt%V/SiO_2 catalyst.

3.4. Catalyst Characterization Systems

3.4.1. Total Surface Area (TSA) Measurements

The total surface area, pore volume and pore size estimations were performed in Boğaziçi University Chemistry Department Photochemistry and Photocatalysis Laboratory. The nitrogen adsorption/desorption isotherm was obtained at liquid nitrogen temperature 77 K by using Quantachrome Nova 2200e automated gas adsorption system. The specific surface areas of reduced 1.5wt%Rh/SiO_2, 1.5wt%Rh-2.6wt%La/SiO_2, and 1.5wt%Rh-2.6wt%La-1.5wt%V/SiO_2 catalysts and of calcined silica supports were determined by using multi-point BET analysis.

In the measurement procedure, firstly two samples were placed and degassed by heating from room temperature to 200°C with the aid of heating jackets under nitrogen gas flow for four and half hours to eliminate the impurities and moisture on the samples. When the nitrogen flows over sample it is discharged from entrance and vented via vacuum pump to the atmosphere. One of the samples that completed its degassing operation is kept under vacuum to avoid contact with air until its measurement is started. The other sample is moved to analysis port of the system and placed between two glass tubes to prevent motion of particles. To start the analysis, liquid nitrogen at temperature of −196°C (77 K) is poured into a dewar flask which is elevated until the catalyst sample in the glass tube is immersed into liquid nitrogen. There is a sensor beside the analysis tube to detect the remaining part of the liquid nitrogen. As liquid nitrogen is used it evaporates and its level decreases. In this case, the sensor detects the liquid nitrogen level and sends a signal to elevate the dewar. The purpose in using liquid nitrogen is to freeze the sample to hinder particle movement, and also to allow physical adsorption of nitrogen gas as it passes through sample; thus, certain number of adsorption-desorption data are taken for BET surface area calculations.

The total surface area calculations were based on adsorption experiments made with N_2 gas by using the following BET equation for determining the monolayer volume V_m:

$$\frac{P}{V(P_0 - P)} = \frac{1}{cV_m} + \left[\frac{c-1}{cV_m}\right]\frac{P}{P_0} \tag{3.1}$$

where

P: the partial pressure (mmHg)

V: volume adsorbed (cm^3)

P_0: saturation or vapor pressure at particular temperature of the system (mmHg)

A plot of $P/V(P_0-P)$ against P/P_0 yields a straight line, from the slope and intercept of which both V_m, the monolayer volume (cm^3) and c, a constant for the particular temperature and gas-solid system, can be calculated. V_m is used in the following equation for calculating the specific surface area (S_t):

$$S_t = \frac{NA_gV_m}{V} \tag{3.2}$$

where

N: Avogadro number ($6.02x10^{23}$ molecules/gmole)

V: Molar volume of the gas at reference conditions (cm^3/gmole)

A_g: Cross sectional area of each adsorbed gas molecule

($16.2x10^{-20}$ m^2/molecule for nitrogen gas)

Barrett, Joyner and Helenda (B.J.H) method allows computation of pore sizes from equilibrium gas pressures. One can therefore generate experimental curves (isotherms) linking adsorbed gas volumes with relative saturation pressures at equilibrium, and convert them into cumulative pores size distributions. In addition to surface area measurements, pore volume and pore size data were also obtained according to BJH method on basis of adsorption data.

3.4.2. X-ray Powder Diffraction

For characterizing the crystallographic structure and revealing chemical composition of the catalysts, X-ray powder diffraction (XRD) technique was used. XRD patterns of

reduced catalysts were recorded on a Rigaku-D/MAX-Ultima diffractometer operating at 40 kV and 40 mA with a fixed Cu anode and symmetric scans with $2\theta = 1.5–70°$.

3.4.3. ESEM Analyses

The microstructure, morphology and composition of freshly reduced catalysts were studied by environmental scanning electron microscopy (ESEM) and energy dispersive X-ray analysis (EDAX). The tests were conducted in a Philips XL 30 ESEM-FEG system, having a maximum resolution of 2 nm. The experiments were performed at the Advanced Technologies Research and Development Center of Boğaziçi University.

3.5. Overview of the Experimental Setup

The microreactor flow system was previously constructed in the laboratory with all necessary tubing and fitting materials and auxiliary units. The details of the system utilized for conducting carbon monoxide hydrogenation experiments are presented in Figures 3.3 and 3.4.

The system consisted of three parts:

- Feed section
- Reaction section
- Feed/Product analysis section

3.5.1. Feed Section

Mass flow controllers, 1/4", 1/8" and 1/16" OD stainless steel and brass tubes and fittings for feeding the reactants to the system are the main parts of the feed section. In this section, the research grades of pure CO, N_2, H_2 gases from pressurized cylinders were passed through brass tubes and fittings. The flow rates of the gases were controlled by Brooks 5850E mass flow controllers. The set point values of the flow controllers were adjusted by four-channel Brooks 0154 control panel. Inlet pressure to the flow controllers was 30 psi for all reaction gases, but flow rate ranges of the flow controllers were different.

These ranges of the mass flow controllers were selected to provide the desired gas flow rates. The specifications of the mass flow controllers used are given in Table 3.6. The mass flow controllers were calibrated *in situ* and their calibration curves are presented in Appendix A. At the inlet and the outlet of the mass flow controllers, 1/4" stainless steel tubes were used until the primary mixing zone. On-off valves were placed after the mass flow controllers. In order to provide homogeneous mixing, the reactant gases were passed through the primary mixing region before entering the reactor. This primary mixing region was designed using 1/8" stainless steel tubes. The gas mixture was mixed in a secondary mixing region.

Table 3.6. Specifications of the mass flow controllers.

Gas Type	**CO**	**N_2**	**H_2**	**CO_2**
Flow Rate Range ($ml.min^{-1}$)	0-20	0-200	0-100	0-50
Upstream Pressure (psi)	30	30	30	30
Maximum Working Pressure (bar)	100	100	100	100
Ambient Temperature Limits (^oC)	5 to 65	5 to 65	5 to 65	5 to 65

This secondary mixing region was made using 1/16" stainless steel tube, after which the diameter of connecting lines was gradually increased to 1/8" and 1/4". Gas flow could be diverted using a three way valve. The flow could be sent to vent line in order to ensure the mixing of the reactant gases to get a steady flow before the reaction or it could be sent to another three way valve. This second valve was used to send the flow to the bypass line, so that feed composition could be analyzed in the gas chromatograph or to the reaction section. An on-off valve was placed at the end of the bypass line. This valve prevented the product gases to fill the bypass line when it was closed.

3.5.2. Reaction Section

The reaction section was connected by 1/4" stainless steel tubes and consisted of a 2.6 cm ID x 46.5 cm tube furnace and 4 mm ID x 60.6 cm stainless steel fixed-bed down-flow microreactor. The reactor was longer than the furnace which facilitated the placement of the reactor in the furnace by the help of stainless steel fittings. The microreactor was located in the furnace controlled to ± 0.5 K sensitivity by a Shimaden FP-21 programmable temperature controller. Silane treated glass wool was used to hold the catalyst bed in fixed position. The catalyst bed was kept in place by plugging the lower end with silane treated glass wool.

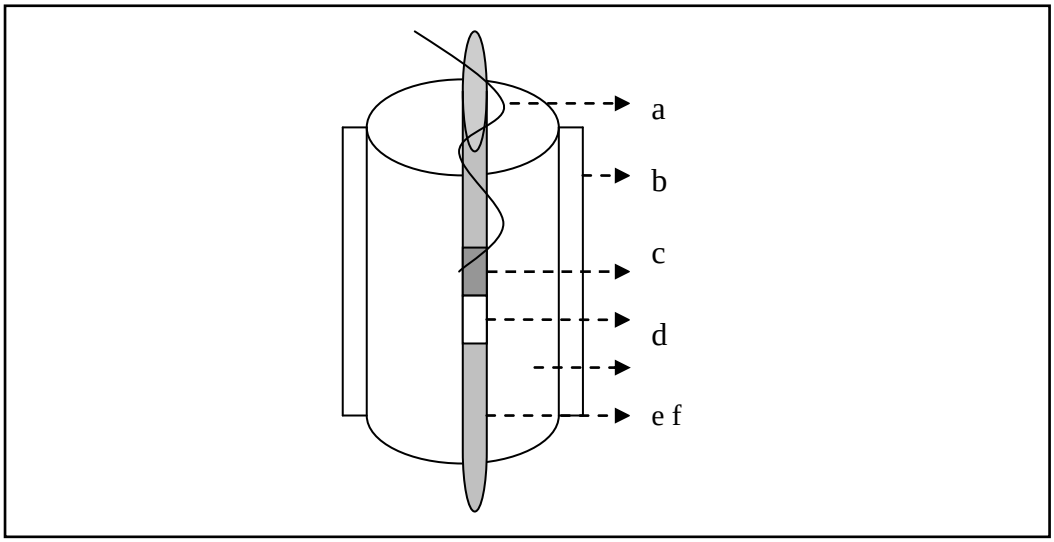

Figure 3.3. Schematic diagram of the reactor and furnace system: a. Thermocouple b. Ceramic wool insulation c. Catalyst d. Catalyst bed e. Furnace f. Reactor.

The catalyst bed was placed in the center of the reactor which was in the constant-temperature region of the furnace. 20-gauge wire K-type sheathed thermocouple was placed near the center of the catalyst bed just outside the microreactor wall and was connected to the temperature controller. The reactor and furnace system is presented in Figure 3.3. The spaces between the inlet of the reactor-furnace and also the outlet of the reactor-furnace were insulated using ceramic wool to prevent heat loss and maintain stable temperature profile. At the end of the reactor an on-off valve was placed and it was kept closed during feed analysis to prevent back flow of the feed mixture into the reactor.

3.5.3. Feed/Product Analysis Section

The product leaving the reactor and the reactant mixtures entering the reactor were analyzed using two online gas chromatographs. It is well known that CO hydrogenation reaction may yield oxygenates. In case of oxygenate production during the reaction the product gas stream leaving the microreactor was separated into two streams.

First stream connected to Gas Chromatography 2 and product gases exiting from reactor passed through an on-off valve and sent to the cold trap in order to condense the remaining water vapor before it was sent to the Gas Chromatograph 2. Cold trap included a box filled with ice and coiled tubing to increase the contact time between the gas flow and cold environment. The product or reactant gas streams were passed through the three way valve which directed the flow to either the soap bubble flowmeter for measuring the flow rate or to the Gas Chromatograph 2 for gas analysis. The gases entered the gas chromatograph through a 1/16" stainless steel tube, therefore, the diameter of the stainless steel connecting lines were decreased gradually from 1/4" to 1/8" and 1/16" after the last three way valve.

On the other hand, since hydrocarbons and oxygenates can be detected in Porapak Q packed column, products entering in the second stream connected to Gas Chromatograph 1. For this manner, product gases exiting from reactor passed through 1/4" stainless steel tubes. By passing through on-off valve, diameter of the line was decreased to 1/8" stainless steel tubes. Before introducing the products into Gas Chromatograph 1 three way valve belonging to Gas Chromatograph 1 was closed and on off valve of line was opened. The gases entered the gas chromatograph through a 1/16" stainless steel tube, therefore, the diameter of the stainless steel connecting line was decreased from 1/8" to 1/16". To avoid from entrance of these liquid products into Gas Chromatograph a 5 m-long heating tape was used to heat the lines and a 16-gauge wire K-type sheathed thermocouple was placed along the heated lines and connected to a temperature controller. The heating tape was

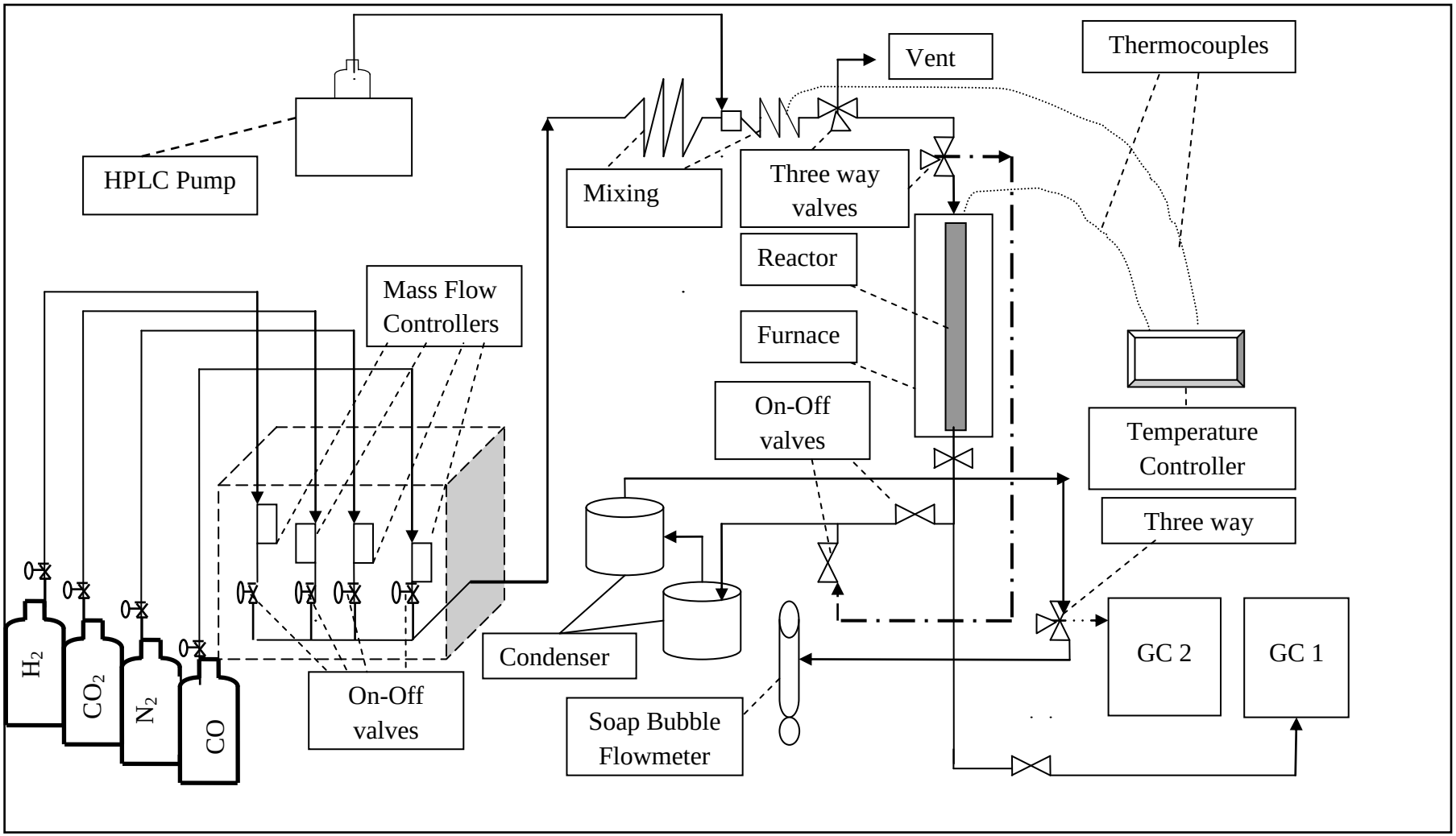

Figure 3.4. Schematic diagram of the microreactor flow system.

covered with ceramic wool insulation to prevent heat losses, and its temperature was controlled by a Dixell single-stage digital temperature controller (XT110C).

3.6. Catalytic Activity Experiments

3.6.1. Preliminary Work

3.6.1.1. Mass Flow Controller Calibration. To start the experiments, firstly calibration of mass flow controllers was performed by sending the gases to the system separately at flow rates between 10-90 set point values and recording the time to cover estimated volume of gas in soap bubble flow meters. Calibration graphs constructed are given in Appendix A.

3.6.1.2. Gas Chromatograph Calibration. Before starting the catalytic activity experiments, gas chromatograph was calibrated by injecting known amounts of each species separately to the chromatographic column under the conditions given in Table 3.4 and Table 3.5, and recording the corresponding retention time and the area under the peak calculated by the integrator software. Using this procedure, micromole versus peak area graphs were constructed for each gas and the constants of the corresponding calibration curves were determined by linear regression. The calibration curves are presented in Appendix B.

3.6.2. Reaction Tests

All catalysts prepared were reduced in situ under H_2 at 500^oC for 2 hours before the reaction and kept under a stream of N_2 until the reaction test was started. The temperature program used for the reductive pretreatment is given in Table 3.7. After reduction, the temperature of the reactor was decreased down to the reaction temperature (230, 270, 290^oC) under inert nitrogen flow and nitrogen was trapped within the reactor until the reaction gases were sent to the reactor. Stainless steel tubular down-flow microreactor was used for determining the catalytic activities of the Rh based silica and alumina supported catalysts. All experiments were performed at atmospheric pressure. The catalytic activity tests for carbon monoxide hydrogenation were conducted with the feed mixture of 10 per cent CO, 20 per cent H_2 and N_2 as balance for all catalysts. Different weights of catalysts (200, 400, 500 mg) were used during experiments to see the effect of W/F_{CO} ratio on CO

conversion. The total flow rate, type of catalyst, reaction temperature, and catalyst weight were changed in order to see the effects of different parameters on the catalyst activity.

Table 3.7. Reduction program for Rh based catalysts.

Segments	**Starting and End Temperatures**	**Segment Gas**
First Segment	Heating from 25^{o}C to reaction temperature at 30 min.	N_2 with flow rate of 15 ml.min^{-1}
Second Segment	Keeping constant at reaction temperature for 15 min.	N_2 with flow rate of 15 ml.min^{-1}
Third Segment	Heating from reaction temperature to 400^{o}C at 15 min.	N_2 with flow rate of 15 ml.min^{-1}
Fourth Segment	Keeping temperature constant at 400^{o}C for 15 min.	N_2 with flow rate of 15 ml.min^{-1}
Fifth Segment	Heating from 400^{o}C to 500^{o}C at 10 min.	N_2 with flow rate of 15 ml.min^{-1}
Sixth Segment	Keeping temperature constant at 500^{o}C for 15 min.	N_2 with flow rate of 15 ml.min^{-1}
Seventh Segment (Reduction)	Keeping temperature constant at 500^{o}C for 2 hours	H_2 with flow rate of 25 ml.min^{-1}
Eighth Segment	Cooling down to reaction temperature	N_2 with flow rate of 10 ml.min^{-1}

The reaction conditions used for δ-Al_2O_3 and SiO_2-based catalysts are summarized in Table 3.8, and the list of the experiments on Rh/δ-Al_2O_3 is given in Table 3.9.

Table 3.8. Reaction conditions for catalytic activity tests.

Parameter	Value
Catalyst Particle Size (mesh size)	45-60 (344-255μm)
Catalyst Amount (mg)	200, 400, 500
Reduction Temperature (^oC)	500
Reaction Temperature (^oC)	230, 270, 290
Reaction Total Flow Rate ($ml.min^{-1}$)	75, 100, 120
W/F_{CO} Ratio ($mg.min.\mu mol^{-1}$)	1.30, 1.22, 0.98, 0.82, 0.49

3.6.2.1. Experiments on Rh based alumina supported catalyst. Three experiments were conducted with 2wt%Rh/δ-Al_2O_3 catalyst.

Table 3.9. List of experiments on 2wt%Rh/δ-Al_2O_3.

Exp. No	Metal Content			Reaction Temperature (^oC)	Catalyst Amount (mg)	Total Flow Rate (ml/min)	Feed Gas Composition in N_2 as balance	
	Rh (wt%)	La (wt%)	V (wt%)				CO (vol%)	H_2 (vol%)
1	2.0	--	--	270	400	120	10	20
2	2.0	--	--	270	400	100	10	20
3	2.0	--	--	270	500	100	10	20

Effects of variation of total inlet flow of gases and weight of catalyst on catalytic activity were observed. The list of experiments performed on this catalyst is given in Table 3.9.

3.6.2.2. Experiments on Rh based silica gel supported catalyst. Nine experiments were performed with Rh/SiO_2, Rh-La/SiO_2, and Rh-La-V/SiO_2. As support, silica gel was used to see effect of different catalyst weights and total inlet flow rates on CO conversion and product distribution. The list of experiments conducted on catalysts with silica gel as support is given in Table 3.10.

Table 3.10. List of experiments on Rh-based silica gel supported catalysts.

Exp. No	Metal Content			Reaction Temperature (^oC)	Catalyst Amount (mg)	Total Flow Rate (ml/min)	Feed Gas Composition in N_2 as balance	
	Rh (wt%)	La (wt%)	V (wt%)				CO (vol%)	H_2 (vol%)
4	1.5	--	--	270	200	100	10	20
5	1.5	--	--	270	400	100	10	20
6	1.5	--	--	270	400	75	10	20
7	1.5	2.6	--	270	200	100	10	20
8	1.5	2.6	--	270	400	100	10	20
9	1.5	2.6	--	270	400	75	10	20
10	1.5	2.6	1.5	270	200	100	10	20
11	1.5	2.6	1.5	270	400	100	10	20
12	1.5	2.6	1.5	270	400	75	10	20

3.6.2.3. Experiments on Rh based silica gel orange supported catalysts. Nine experiments were performed with Rh/SiO_2, $Rh\text{-}La/SiO_2$, and $Rh\text{-}La/V/SiO_2$.

Table 3.11. List of experiments on Rh-based silica gel orange supported catalysts.

Exp. No	Metal Content			Reaction Temperature (^oC)	Catalyst Amount (mg)	Total Flow Rate (ml/min)	Feed Gas Composition in N_2 as balance	
	Rh (wt%)	La (wt%)	V (wt%)				CO (vol%)	H_2 (vol%)
13	1.5	--	--	230	400	100	10	20
14	1.5	--	--	270	400	100	10	20
15	1.5	--	--	290	400	100	10	20
16	1.5	2.6	--	230	400	100	10	20
17	1.5	2.6	--	270	400	100	10	20
18	1.5	2.6	--	290	400	100	10	20
19	1.5	2.6	1.5	230	400	100	10	20
20	1.5	2.6	1.5	270	400	100	10	20
21	1.5	2.6	1.5	290	400	100	10	20

For this case, as support silica gel orange was used to see effect of different temperatures on CO conversion and product distribution. The list of experiments on catalysts with silica gel orange as support is given in Table 3.11.

All catalysts used during the experiments were diluted with inert α-alumina (800 mg) to avoid channeling and hot spots.

4. RESULTS AND DISCUSSION

4.1. Catalyst Characterization

Catalyst characterization involved the use of the following techniques: total surface area accompanied by pore volume and pore size measurements, environmental scanning electron microscopy (ESEM) and energy dispersive X-ray analysis (EDAX), X-ray powder diffraction (XRD).

4.1.1. Total Surface Area Measurements

The total surface area, pore volume and pore size estimations were performed by using a Quantachrome Nova 2200e automated gas adsorption system. Specific surface areas of calcined silica supports (both silica gel and silica gel orange) and freshly reduced 1.5wt%Rh/SiO_2, 1.5wt%Rh-2.6wt%La/SiO_2, 1.5wt%Rh-2.6wt%La-1.5wt%V/SiO_2 were determined using multi-point BET analysis.

Table 4.1. Total surface areas, pore volumes and pore radius of the silica supports, and non-promoted or promoted Rh-based catalysts.

Sample	**BET Surface Area (m^2/g)**	**Pore Volume (cm^3/g)**	**Pore Radius (Angstrom)**
Silica Gel	143.4	0.017	16.50
Silica Gel Orange	224.7	0.120	14.85
1.5wt%Rh/SiO_2	215.9	0.105	14.80
1.5wt%Rh -2.6wt%La/SiO_2	189.2	0.097	14.82
1.5wt%Rh -2.6wt%La-1.5wt%V/SiO_2	180.5	0.091	14.79

In addition to surface area measurements, pore volume and pore size data were obtained according to BJH method on basis of adsorption data. Catalysts were prepared over silica gel orange support. The total surface area, pore volume and pore size of each support or catalyst sample are given in Table 4.1.

Table 4.1 shows that the total surface area of the silica gel orange support decreases as active metal components are impregnated. Silica gel and silica gel orange were calcined at 500°C for 4 h before BET analysis. Moreover, catalysts prepared with the silica gel orange support were freshly reduced at 500°C for 2 h. Total surface areas of silica gel and silica gel orange were estimated as 143.4 and 224.7 m^2/g, respectively, which agrees with literature reports on 30–50 mesh Rh-based catalyst granules with BET surface areas around 250 m^2/g (Mo *et al*., 2009). Firstly, 1.5wt%Rh was loaded onto the silica gel orange support, causing a small decline in total surface area to 215.9 m^2/g.

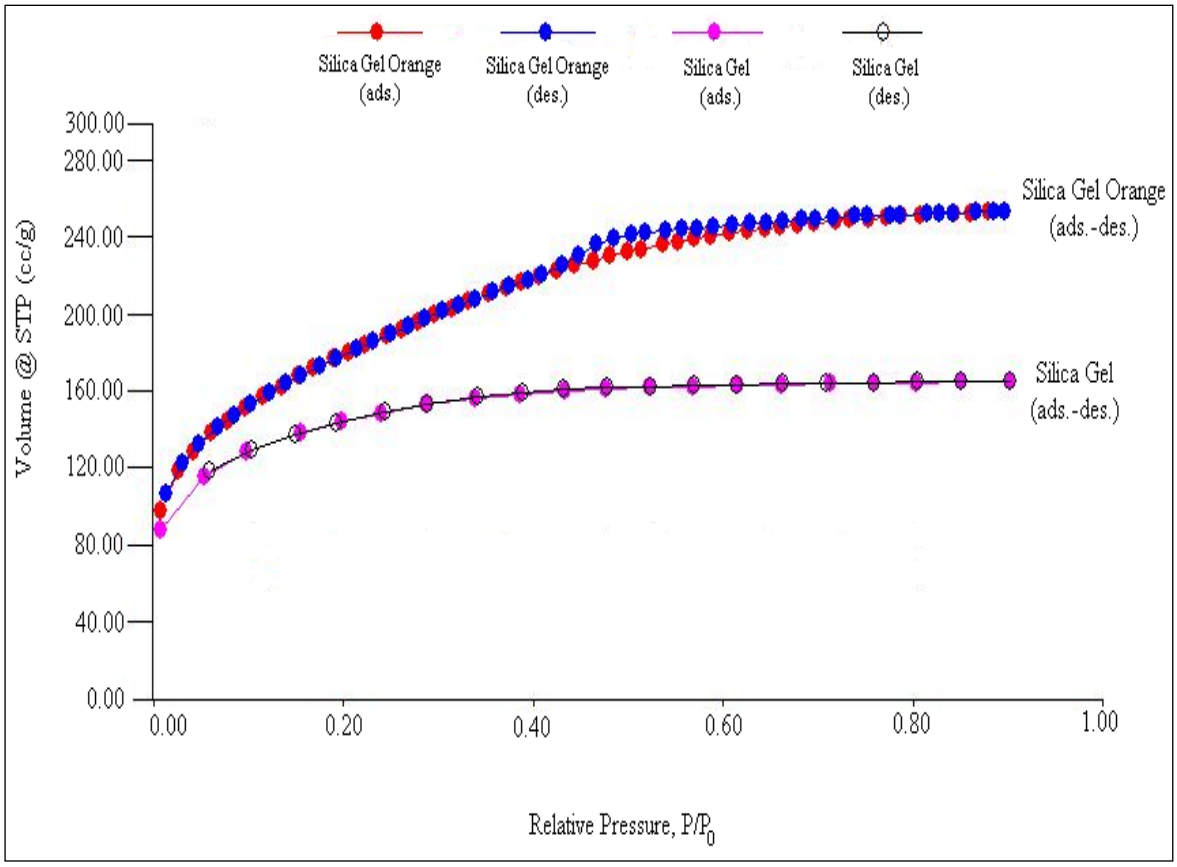

Figure 4.1. Comparison of N_2 adsorption isotherms on silica gel and silica gel orange.

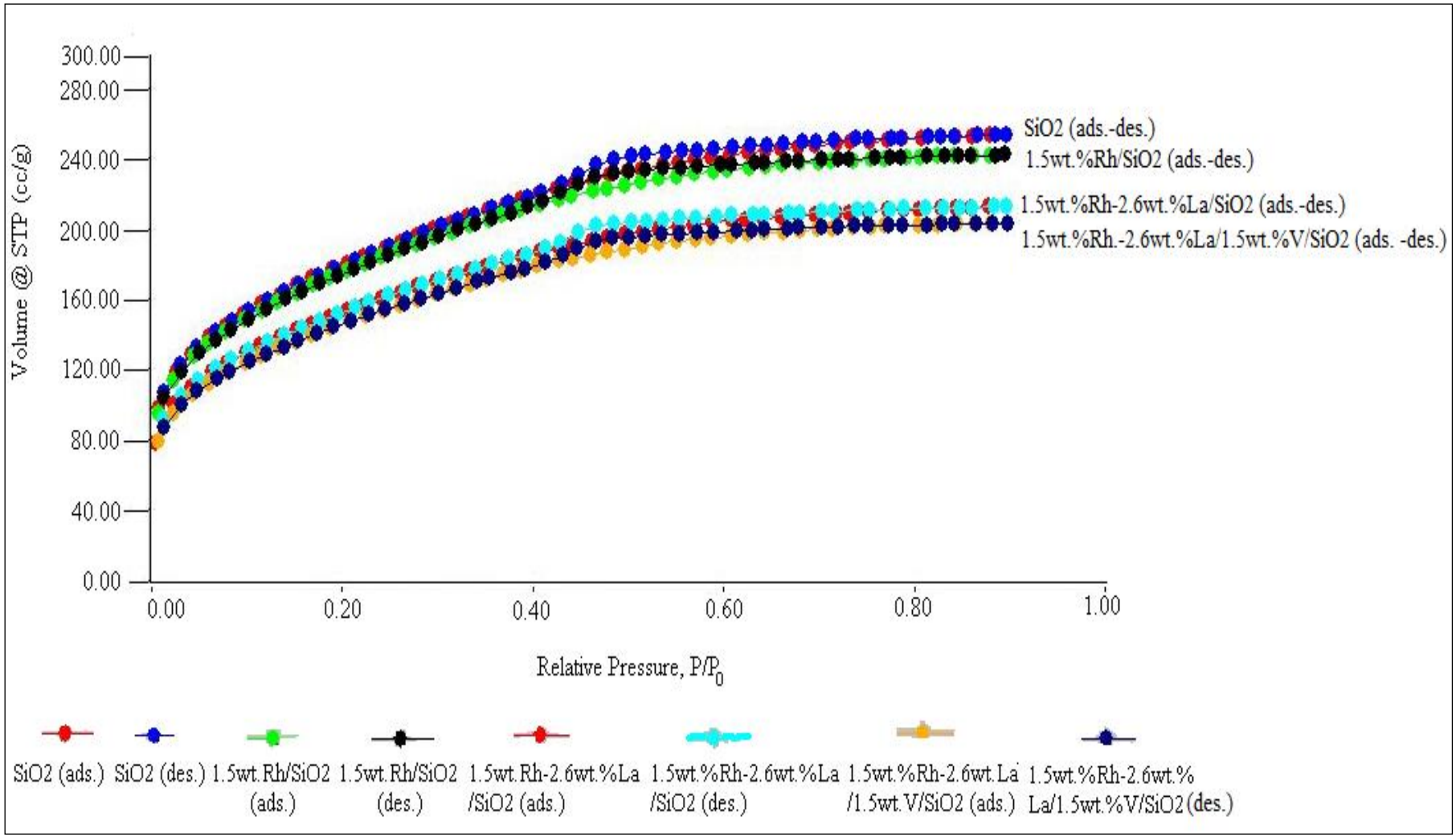

Figure 4.2. Comparison of N_2 adsorption isotherms on silica gel orange support and freshly reduced Rh, Rh-La and Rh-La-V catalysts.

Further addition of other metals in single (La) and double (La + V) promotion resulted in cumulative decreases in both total surface area and pore volume. Nitrogen adsorption/desorption isotherms were measured at liquid N_2 temperature (77 K) for silica supports (Figure 4.1) and also for all catalysts prepared using the silica gel orange support (Figure 4.2).

4.1.2. ESEM Analyses

The microstructure, morphology and composition of freshly reduced catalysts were studied by environmental scanning electron microscopy (ESEM) coupled with energy dispersive X-ray analysis (EDAX). The Philips XL30 ESEM-FEG/EDAX system present in the Advanced Technologies Research Center of Boğaziçi University was used for the analysis and imaging of 1.5wt%Rh/SiO_2, 1.5wt%Rh-2.6wt%La/SiO_2 as well as 1.5wt%Rh-2.6wt%La-1.5wt%V/SiO_2 catalyst samples. The metal dispersion on non-promoted, singly or doubly promoted Rh-based silica supported catalyst samples were also examined.

The ESEM micrographs of the 1.5wt%Rh/SiO_2 catalysts are shown in Figure 4.3 and Figure 4.4 at different magnitude values. In these images, Rh clusters are seen over the silica support as white and shining spots. To understand the catalyst structure better, X-ray mapping of the surface was also conducted (Figure 4.5) which indicates that Rh is well dispersed over the silica support in small particle sizes with some occasional clustering.

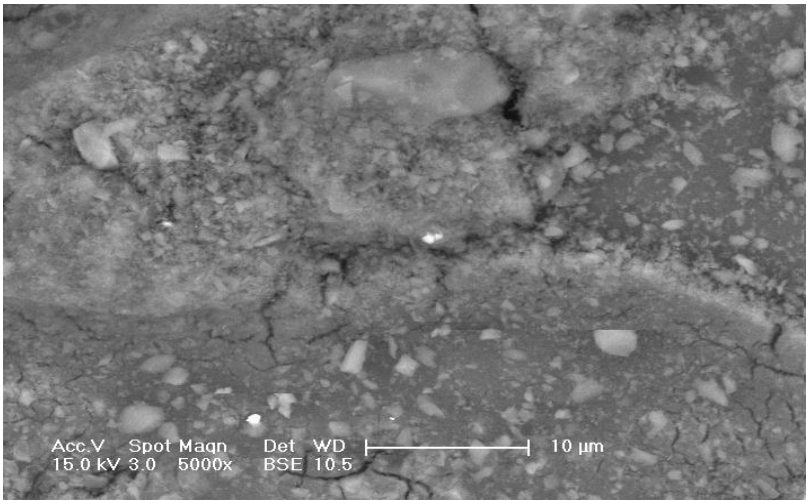

Figure 4.3. SEM image of freshly reduced 1.5wt%Rh/SiO_2 (5000x).

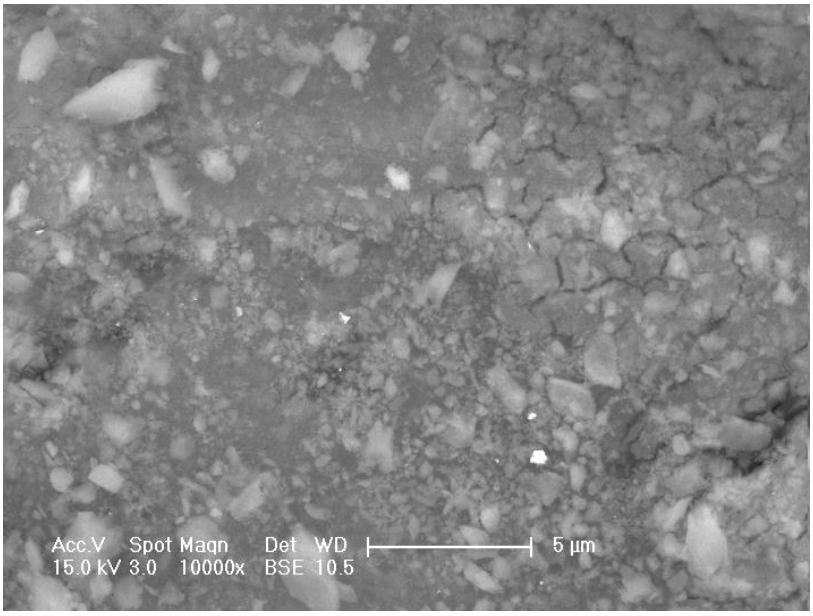

Figure 4.4. SEM image of freshly reduced 1.5wt%Rh/SiO_2 (10000x).

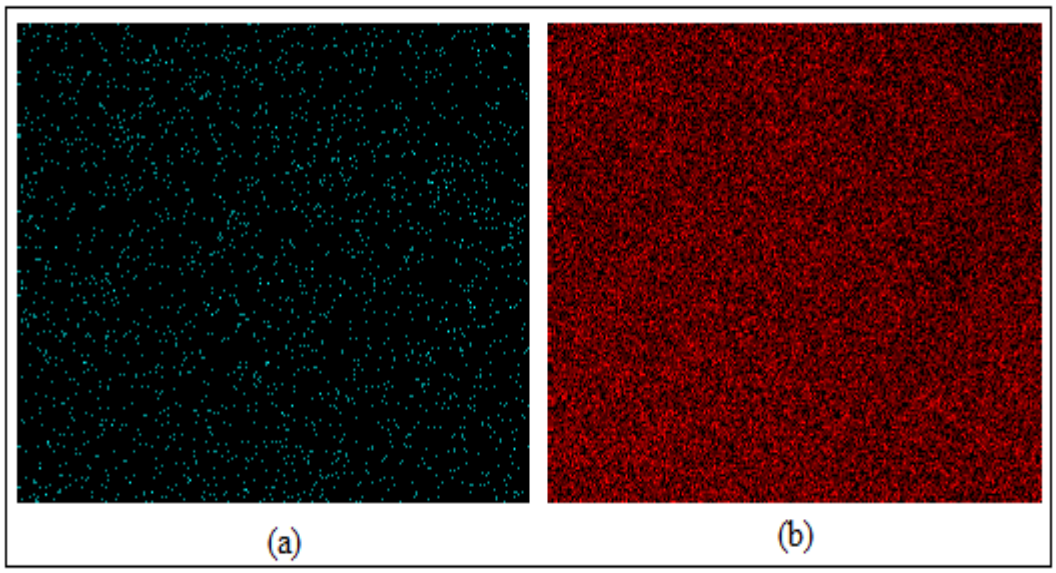

Figure 4.5. X-ray mapping of the 1.5wt%Rh/SiO_2 surface (a) Rh particles, (b) Silica support.

ESEM images of the La promoted Rh/SiO_2 catalyst (Figure 4.6) show that addition of lanthanum slightly enhances the dispersion of Rh particles over silica. Furthermore, on the basis of the X-ray mapping of the 1.5wt%Rh-2.6wt%La/SiO_2 surface in Figure 4.7, it can be concluded that both Rh and La are uniformly dispersed over silica support.

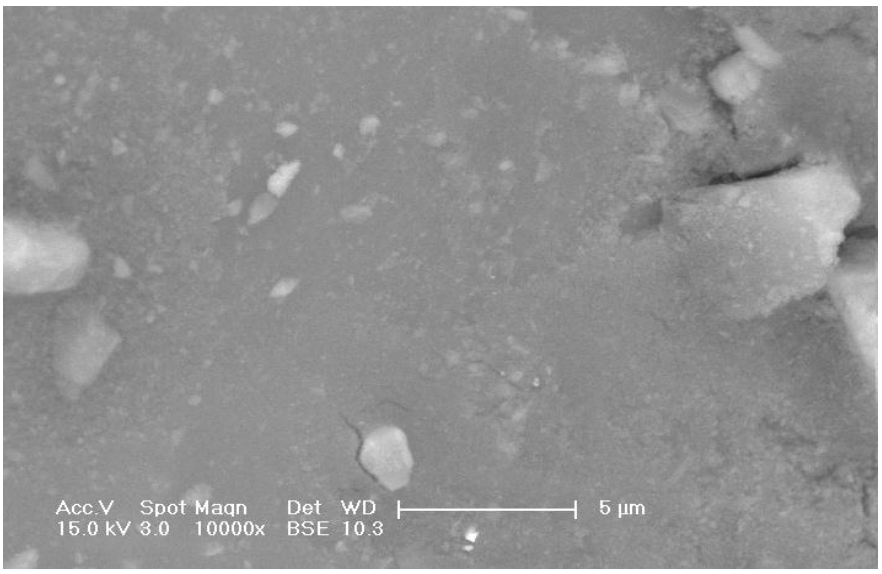

Figure 4.6. SEM image of freshly reduced 1.5wt%Rh-2.6wt%La/SiO_2 (10000x).

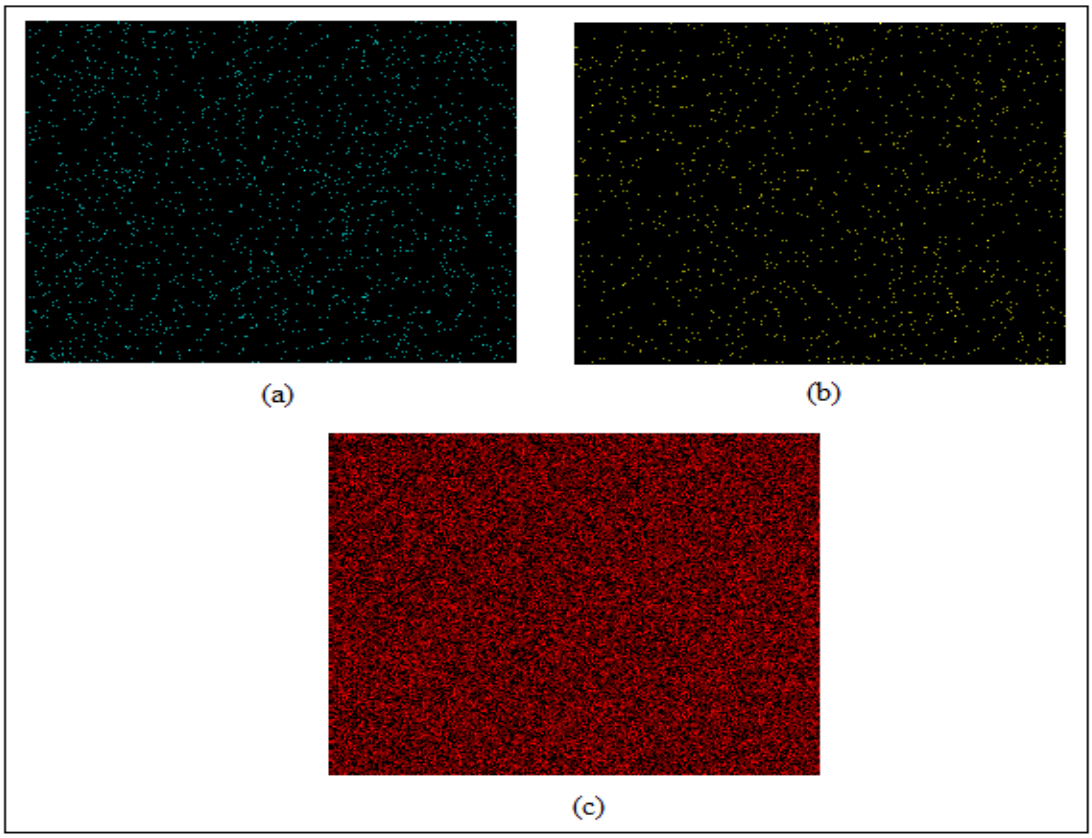

Figure 4.7. X-ray mapping of the 1.5wt%Rh-2.6wt%La/SiO_2 surface (a) Rh particles, (b) La particles, (c) Silica support.

Finally, the ESEM micrographs of 1.5wt%Rh-2.6wt%La-1.5wt%V/SiO_2 catalyst are shown in Figure 4.8 and 4.9. These images and the X-ray mapping presented in Figure 4.10 indicate that the double promotion by lanthanum and vanadium has strong dispersion ability of the Rh clusters on the silica support.

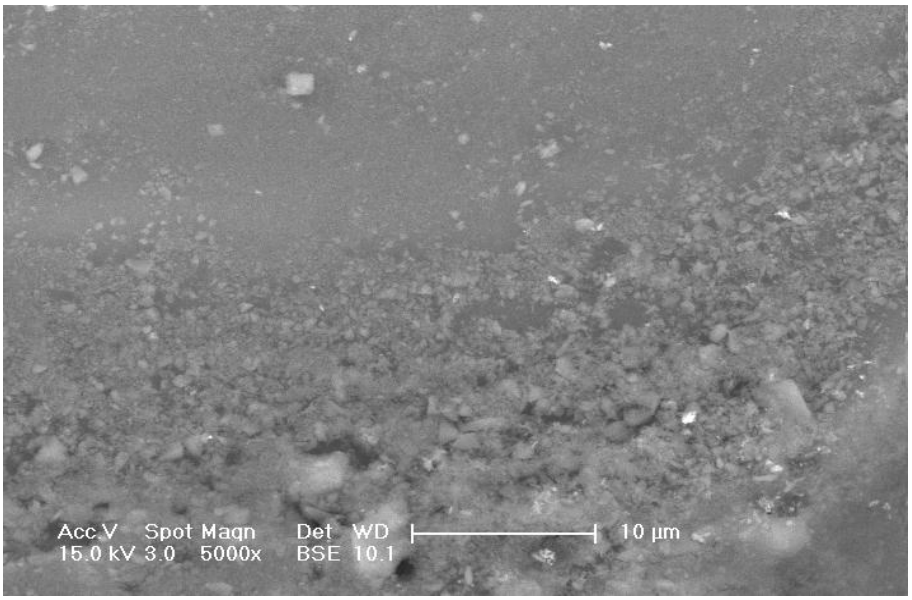

Figure 4.8. SEM image of freshly reduced 1.5wt%Rh-2.6wt%La-1.5wt%V/SiO_2 (5000x).

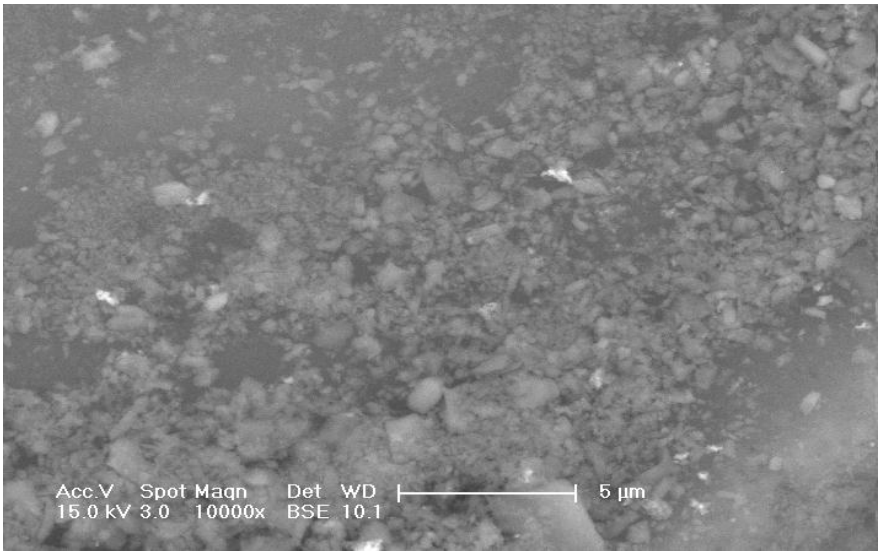

Figure 4.9. SEM image of freshly reduced 1.5wt%Rh-2.6wt%La-1.5wt%V/SiO_2 (10000x).

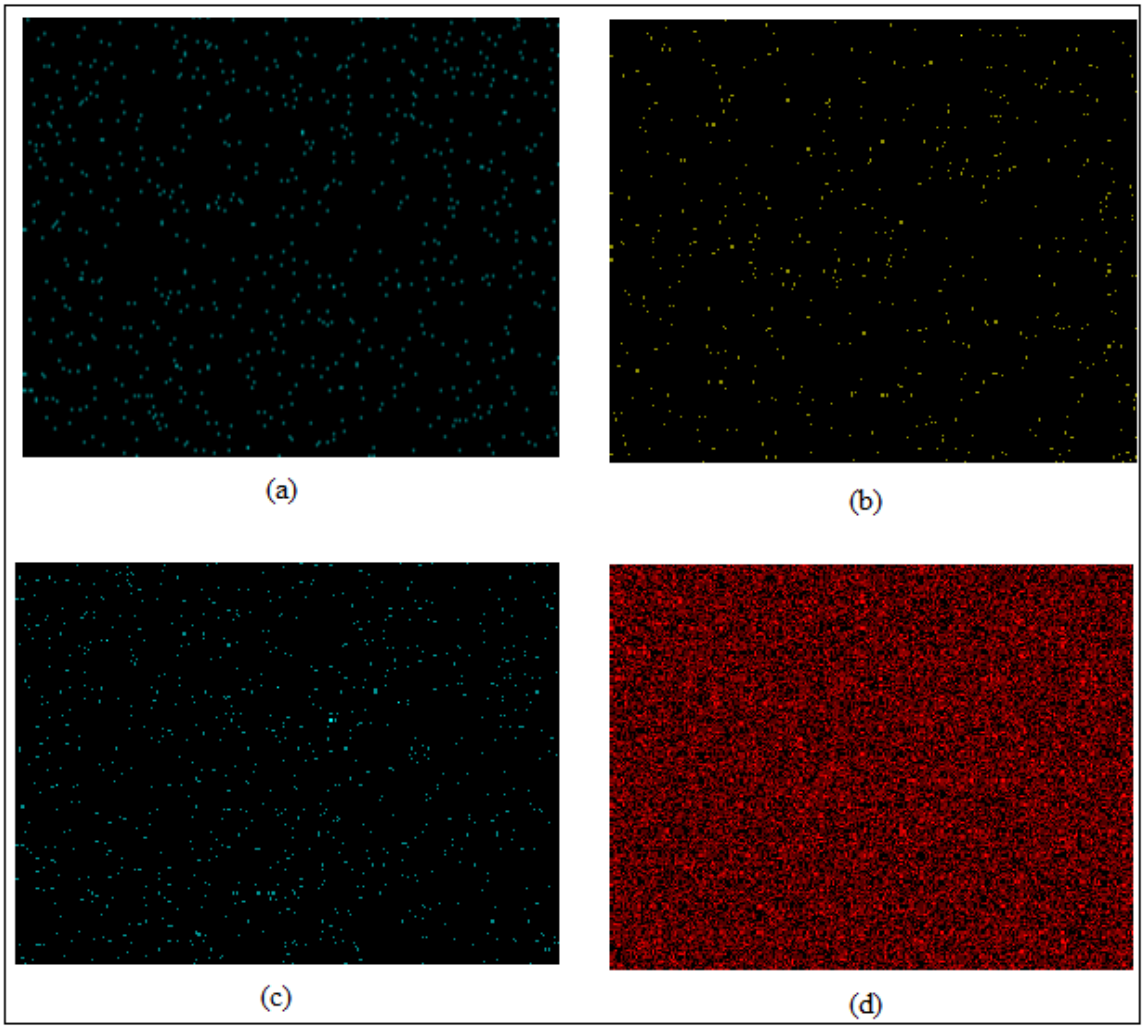

Figure 4.10. X-ray mapping of the 1.5wt%Rh-2.6wt%La-1.5wt%V/SiO_2 surface (a) Rh particles, (b) La particles, (c) V particles, (d) Silica support.

Table 4.2. Targeted and achieved metal loadings by EDX analysis.

Catalyst	**Rh (wt%)**	**La (wt%)**	**V (wt%)**
1.5wt%Rh /SiO_2	3.00	—	—
1.5wt%Rh-2.6wt%La/SiO_2	1.83	3.88	—
1.5wt%Rh-2.6wt%La-1.5wt%V/SiO_2	1. 25	2.81	1.21

ESEM coupled with EDX was used for quantitative analysis and X-ray mapping of each freshly reduced sample, and of several regions on each sample, to determine average metal loadings. Targeted and achieved metal loadings are presented in Table 4.2.

4.1.3. X-ray Powder Diffraction

X-ray diffraction (XRD) patterns of all three catalysts, 1.5wt%Rh/SiO_2, 1.5wt%Rh -2.6wt%La/SiO_2, and 1.5wt%Rh-2.6wt%La-1.5wt%V/SiO_2 reduced at 500°C showed no distinguishable metal peaks (Figure 4.11-4.13) which indicates that Rh, La, and V metal laodings are quite low and are finely dispersed over silica, which agrees with EDX and ESEM results.

Similar results were also obtained in other studies. Rh, La and V containing catalysts showed no crystalline phases, indicating that Rh, La and V were all highly dispersed (Gao *et al*., 2009b). In another study, it was found that XRD patterns of Rh/SiO_2, Rh-La/SiO_2, Rh-La-V/SiO_2 catalysts reduced at 500°C were identical, with no distinct peaks in the 2θ range of 5–65°, suggesting that Rh and promoters were highly dispersed after preparation and pretreatment (Mo *et al*., 2009).

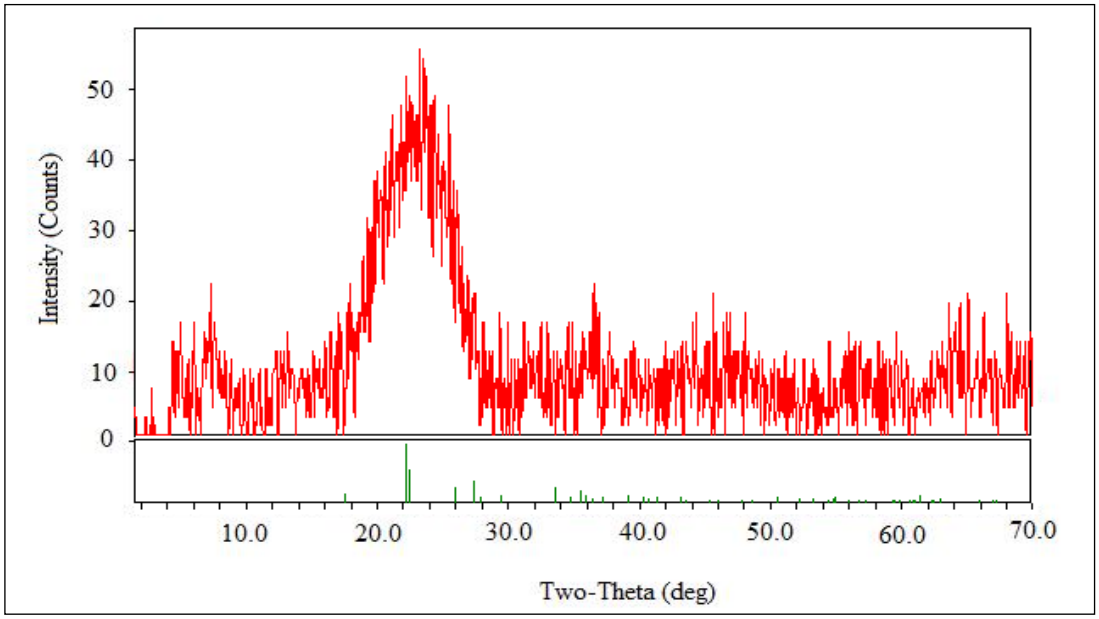

Figure 4.11. XRD pattern of 1.5wt%Rh/SiO_2 catalyst.

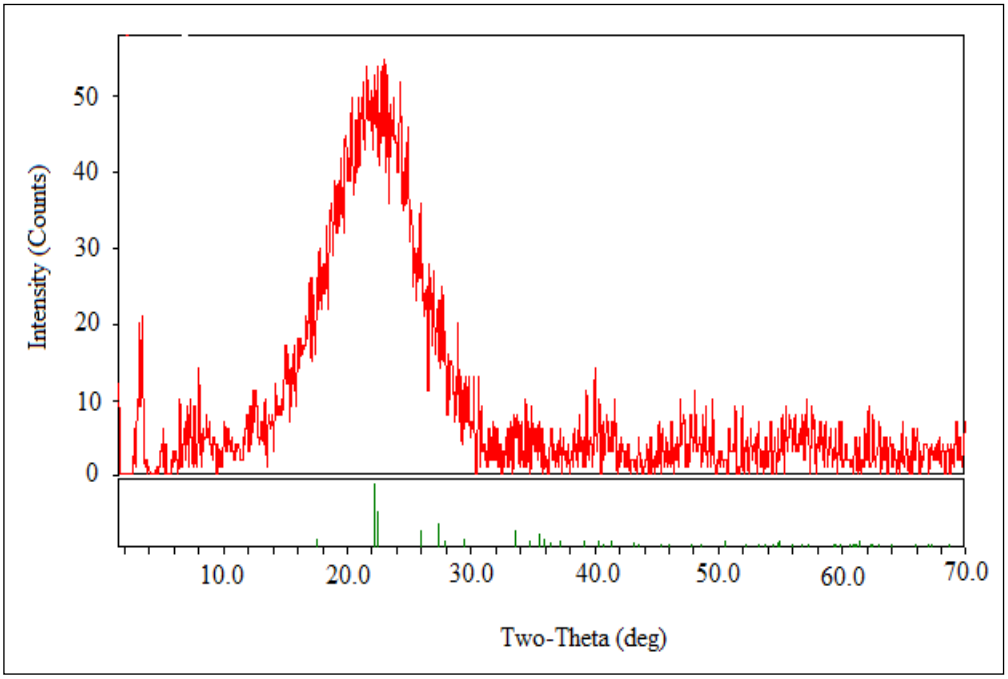

Figure 4.12. XRD pattern of 1.5wt%Rh-2.6wt%La/SiO_2.

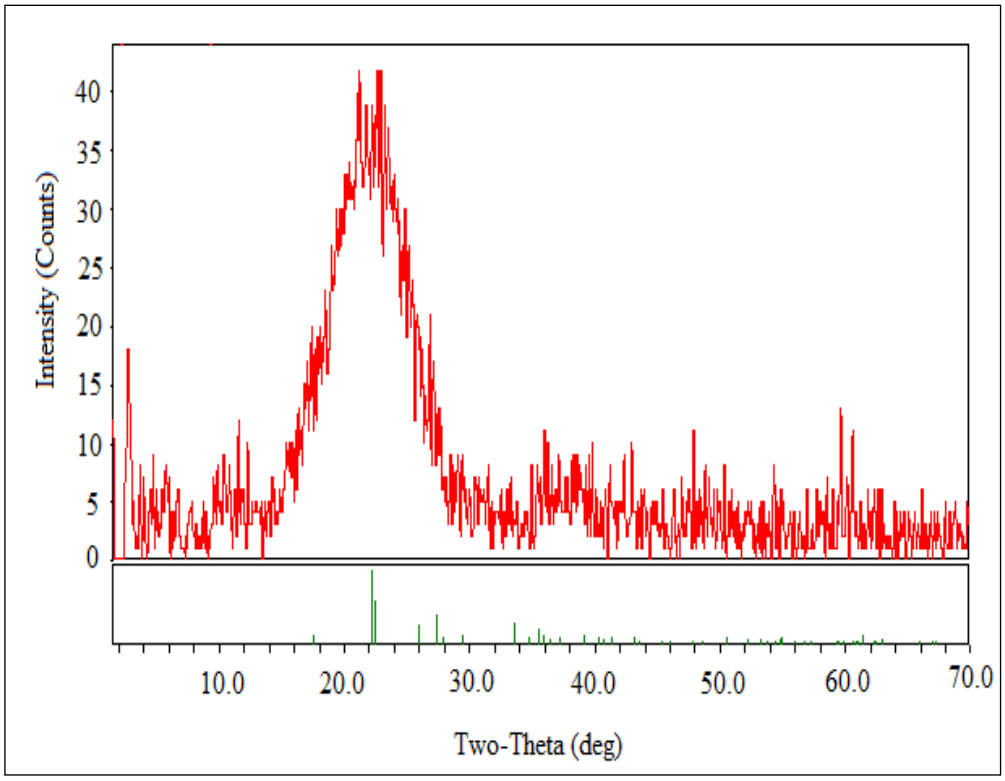

Figure 4.13. XRD pattern of 1.5wt%Rh-2.6wt%La-1.5wt%V/SiO_2.

4.2. Carbon Monoxide Hydrogenation Reaction Experiments

The aim of this work was the development and testing of supported rhodium catalysts for hydrocarbon production by CO hydrogenation. Four different catalysts were prepared by sequential or co-impregnation to incipient wetness of δ-Al_2O_3 and SiO_2 supports, namely 2wt%Rh/δ-Al_2O_3 and 1.5wt%Rh/SiO_2 in addition to La and V promoted catalysts, 1.5wt%Rh-2.6wt%La/SiO_2 and 1.5wt%Rh-2.6wt%La-1.5wt%V/SiO_2.

A parametric study was conducted to determine the effects of reaction temperature and contact time (W/F_{CO}) as well as support material and promoters on CO conversion. The reaction system described in the Section 3.2 consisted of mass flow controllers for gases, a down-flow micro-reactor located in a temperature-controlled furnace, traps, heated stainless steel connecting lines and two on-line gas chromatographs for feed and product analysis. Parametric studies were first conducted on 2wt%Rh/δ-Al_2O_3 and 1.5wt%Rh/SiO_2 using a fixed inlet composition of 10 mol% CO, 20 mol% H_2 and balance N_2 for W/F_{CO} ratios of 0.49-1.30 mg.min.μmol^{-1} at 230^{o}C and atmospheric pressure. Subsequent experiments were performed at 230-290^{o}C using various W/F_{CO} ratios in the same range over both non-promoted and singly or doubly-promoted Rh/SiO_2.

By far the most widely studied catalysts for CO hydrogenation to oxygenates are based on Rh. Supported Rh has been known for decades to have the ability to produce C_2^+ oxygenates such as ethanol, acetaldehyde and acetic acid selectively from syngas (Bhasin *et al*., 1978). Rhodium occupies an interesting position in the periodic table because it lies between metals that easily dissociate CO to form higher hydrocarbons (e.g., Fe and Co) and those which do not dissociate CO and hence produce methanol (e.g., Pd, Pt, and Ir) (Forzatti, *et al*., 1991; Poutsma *et al*., 1978). Rh can form methane, alcohols, or other oxygenates, by CO hydrogenation depending on the catalyst support, promoter(s), and the reaction conditions used (Ichikawa *et al*., 1982).

Catalyst particle size, gas space velocity and contact time are important factors which influence internal and external mass transfer resistances in a heterogeneous system. In previous studies and reactor systems, catalyst particles 250-344 μm in size were found to be sufficiently small to avoid internal mass transport effects arising from pore diffusion

under the reaction conditions and in the reaction system used in this work (Akın and Önsan, 1997). Therefore, the catalyst particle size range was selected as 255-344 μm.

The composition of the reactor outlet stream was measured at 30-minute intervals for 270 minutes and these data were used for CO conversion calculations. In all experiments, steady state was reached approximately after approximately 210 minutes, as indicated by the CO conversions obtained. CO conversion was defined and calculated as follows:

$$\text{CO conversion (\%)} = \frac{[CO]_{in} - [CO]_{out}}{[CO]_{in}} \times 100 \qquad (4.1)$$

4.2.1. Effect of W/F_{CO} Ratio

4.2.1.1. Alumina supported Rhodium based catalyst. The first step in the study was to investigate the effect of residence time on the CO conversion. The reactions were carried out at 270°C using a feed gas mixture of 10 per cent CO, 20 per cent H_2 by mole or volume and N_2 as balance. All gas flow rates were calculated at NTP (25°C and 1 atm). The catalyst used in the experiments conducted at different residence times was 2wt%Rh/δ-Al_2O_3. Total surface area of the δ-Al_2O_3 support prepared by heat treatment of γ-Al_2O_3 was 82 m^2/g (Avcı *et al*., 2004). The reduction time was 2 hours at 500°C. The weight of the catalyst was 400 and 500 mg but total flow rates which directly affected contact time were changed between 100 and 120 $ml.min^{-1}$. CO conversions reached at different W/F_{CO} ratios are presented in Table 4.3 and Figure 4.14.

As expected, in the experiments, using 500 mg catalyst with 100 ml total inlet flow rate yielded highest carbon monoxide conversion compared to other W/F_{CO} ratios at 270°C and 270 minutes time-on-stream. At 0.82 $mg.min.\mu mol^{-1}$ residence time, the catalyst exhibited CO conversion approximately 5% at steady state conditions. When the W/F_{CO} ratio was increased to 1.22 $mg.min.\mu mol^{-1}$, CO conversion was doubled and reached approximately 11%.

Regarding product distribution, methane and carbon dioxide formations were also detected during these three experiments and are presented in Tables 4.4 and 4.5. As shown

in Figure 4.15 when the residence time is increased from 0.82 mg.min.μmol^{-1} to 0.98 mg.min.μmol^{-1} methane production is almost doubled. Further increase in residence time to 1.30 mg.min.μmol^{-1} does not increase methane formation. Similar to CH_4 formation, the CO_2 production also doubles when residence time is increased from 0.82 mg.min.μmol^{-1} to 0.98 mg.min.μmol^{-1} (Figure 4.16). There is no dramatic change in carbon dioxide production between 0.98 mg.min.μmol^{-1} and 1.30 mg.min.μmol^{-1}. Produced amount of methane and carbon dioxide is so low that they are multiplied with 1000.

Table 4.3. Effect of W/F_{CO} ratio on CO conversion over 2wt%Rh/δ-Al_2O_3 at 270^{o}C.

Time (min)	**W/F_{CO} (mg.min.μmol^{-1})**		
	1.22	**0.98**	**0.82**
	CO conversion (%)		
30	8.1	6.2	11.2
60	11.4	9.8	9.5
90	12.4	9.8	6.3
120	12.2	10.6	6.3
150	12.6	10.0	6.1
180	11.8	9.6	5.1
210	11.5	9.6	3.9
240	10.4	9.4	4.7
270	10.8	9.8	4.9

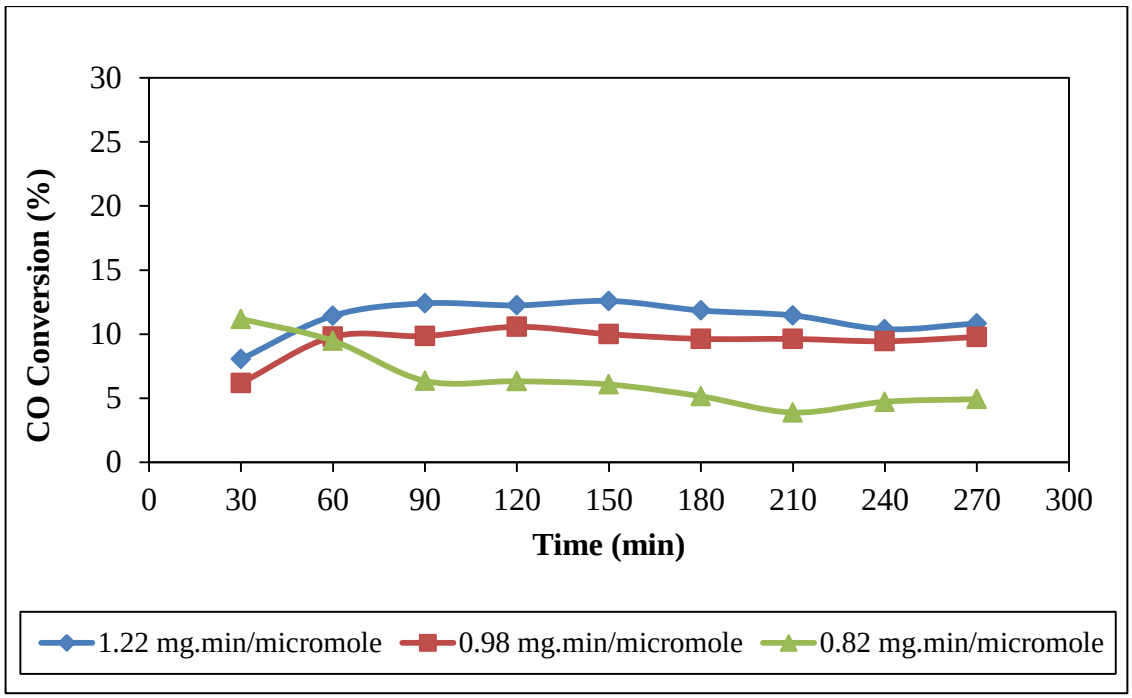

Figure 4.14. Effect of W/F_{CO} ratio on CO conversion over 2wt%Rh/δ-Al_2O_3 at 270°C.

Table 4.4. Effect of W/F_{CO} ratio on CH_4 production over 2wt%Rh/δ-Al_2O_3 at 270°C.

Time (min)	**W/F_{CO} (mg.min.µmol^{-1})**		
	1.22	**0.98**	**0.82**
	CH_4 Production (micromole/gcat/sec)x1000		
30	8.3	8.7	10.0
60	9.7	10.8	8.0
90	10.6	11.4	6.4
120	11.2	11.7	5.7
150	10.7	11.6	5.2
180	10.3	11.5	5.2
210	10.1	11.0	4.8
240	9.9	10.5	4.8
270	9.3	10.1	4.7

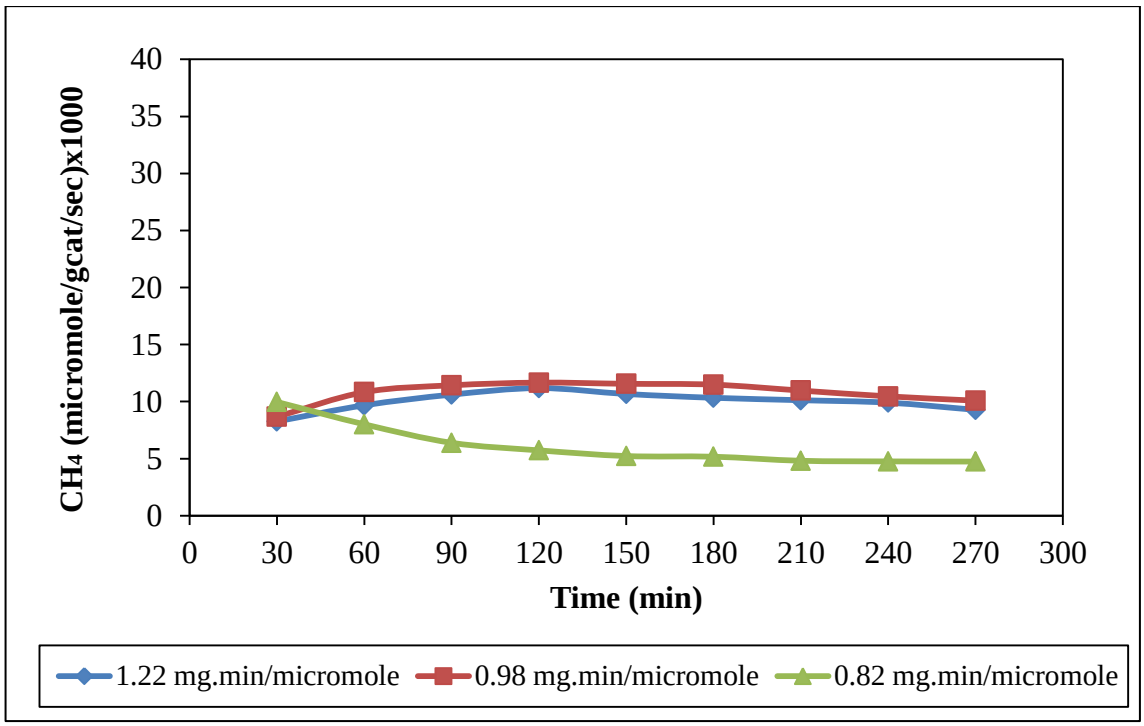

Figure 4.15. Effect of W/F_{CO} ratio on CH_4 production over 2wt%Rh/δ-Al_2O_3 at 270°C.

Table 4.5. Effect of W/F_{CO} ratio on CO_2 production over 2wt%Rh/δ-Al_2O_3 at 270°C.

Time (min)	**W/F_{CO} (mg.min.µmol^{-1})**		
	1.22	**0.98**	0.82
	CO_2 Production (micromole/gcat/sec)x1000		
30	0.345	0.330	0.312
60	0.379	0.382	0.180
90	0.365	0.303	0.168
120	0.335	0.227	0.137
150	0.329	0.337	0.117
180	0.312	0.303	0.102
210	0.295	0.243	0.097
240	0.284	0.192	0.095
270	0.209	0.148	0.090

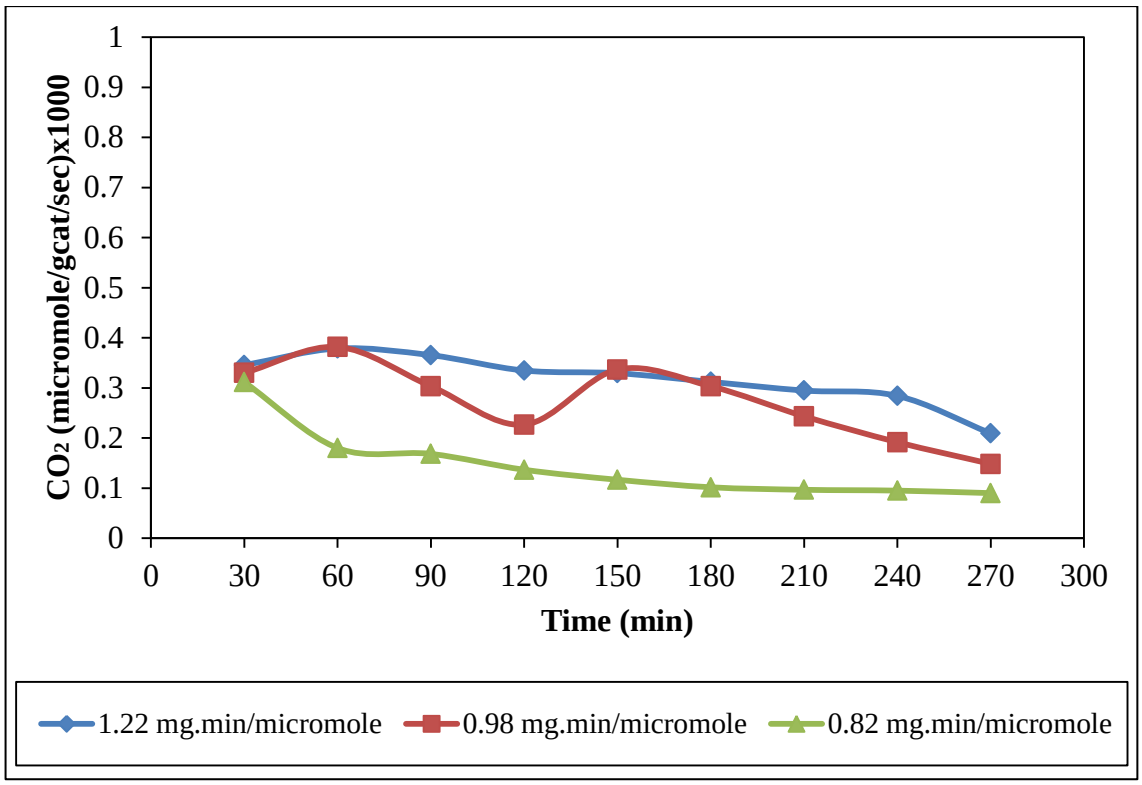

Figure 4.16. Effect of W/F_{CO} ratio on CO_2 production over 2wt%Rh/δ-Al_2O_3 at 270°C.

4.2.1.2. Silica supported Rhodium based catalysts. In CO hydrogenation, SiO_2 has been frequently used as support material for Rh based catalysts. Most Rh based SiO_2-supported catalysts have shown moderate activity and also good selectivity towards C_2^+ oxygenates during CO hydrogenation at high pressures (Chuang *et al.*, 2005). Therefore, in the second part of the experimental work, the effect of residence time on CO conversion was studied over the 1.5wt%Rh/SiO_2 catalyst. The reactions were carried out again at 270°C using a feed gas mixture of 10 per cent CO, 20 per cent H_2 and N_2 as balance. The weight of the catalyst was varied as 200 and 400 mg and total flow rates directly affecting contact time were changed as 75 and 100 ml.min^{-1}. CO conversions for different W/F_{CO} ratios are presented in Table 4.6 and Figure 4.17.

At the lower residence time selected as 0.49 mg.min.µmol^{-1}, CO conversion was very low and it was around 2.5%. When residence time was increased to 0.98 mg.min.µmol^{-1}; an appreciable change was not observed. Finally, residence time was further increased to 1.30 mg.min.µmol^{-1} which resulted in an observable increment in CO conversion; and at steady state conditions, 5% CO conversion was obtained.

As for the product scale, it is evident in Table 4.6 that at residence times of 0.49 mg.min.µmol^{-1} and 0.98 mg.min.µmol^{-1} CO conversion values are quite low and they do not produce any product. However, at a residence time to 1.30 mg.min.µmol^{-1}, a small amount of carbon dioxide is generated as indicated in Table 4.7 and Figure 4.18.

Table 4.6. Effect of W/F_{CO} ratio on CO conversion over 1.5wt%Rh/SiO_2 at 270°C.

Time (min)	**W/F_{CO} (mg.min.µmol^{-1})**		
	1.30	**0.98**	**0.49**
	CO conversion (%)		
30	2.4	3.8	3.5
60	3.9	1.9	3.3
90	4.9	2.4	2.4
120	4.1	3.3	2.5
150	4.4	2.7	2.3
180	3.6	2.5	2.9
210	4.4	3.2	2.4
240	4.1	2.2	3.1
270	4.9	2.7	2.2

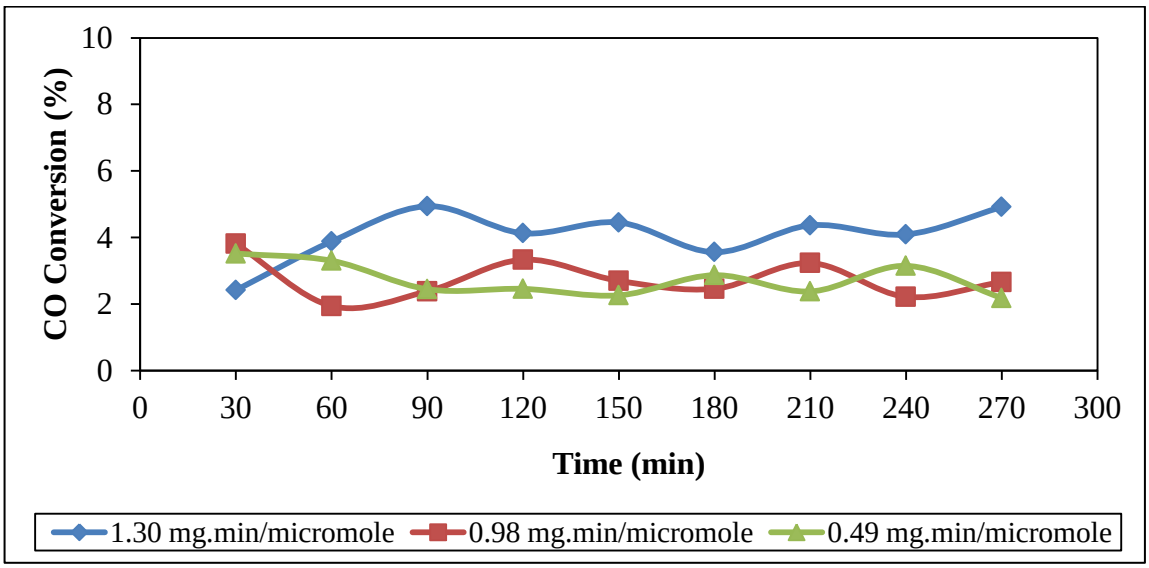

Figure 4.17. Effect of W/F_{CO} ratio on CO conversion over 1.5wt%Rh/SiO_2 at 270°C.

Table 4.7. Effect of W/F_{CO} ratio on CO_2 production over 1.5wt%Rh/SiO_2 at 270°C.

Time (min)	**W/F_{CO} (mg.min.µmol^{-1})**
	1.30
	CO_2 Production (micromole/gcat/sec)x1000
30	0.368
60	0.35
90	0.337
120	0.322
150	0.317
180	0.303
210	0.302
240	0.298
270	0.297

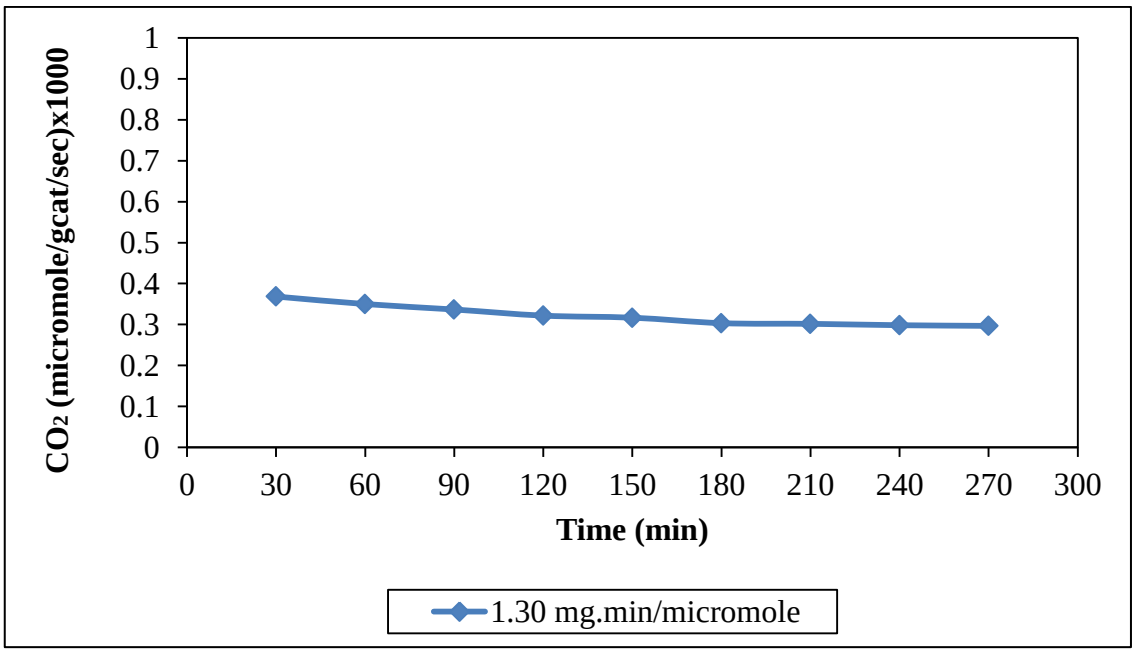

Figure 4.18. Effect of W/F_{CO} ratio on CO_2 production over 1.5wt%Rh/SiO_2 at 270°C.

It was found that the singly promoted catalyst, Rh–La/SiO_2, showed improved reactivity (3×) compared to non-promoted Rh/SiO_2 (Gao *et al*., 2009a). Besides this effect, in another study it was established that the higher catalytic activity observed on La-promoted Rh/SiO_2 catalyst may primarily be caused by an increase in the concentration of the adsorbed CO species in the presence of H_2, possibly because of the formation of new active sites at the LaO_x-Rh interface (Mo *et al*., 2009). Therefore, as a next step, the effect of loading lanthana onto Rh/SiO_2 was investigated. Rh content was fixed and lanthana was added to prepare the 1.5wt%Rh-2.6wt%La/SiO_2 catalyst.

The reactions were carried out again at 270^oC using a feed gas mixture of 10% CO, 20% H_2 and N_2 as balance. The weight of the catalyst was varied as 200 and 400 mg and total inlet flow rate was changed as 75 and 100 ml.min^{-1}.

Table 4.8. Effect of W/F_{CO} ratio on CO conversion over 1.5wt%Rh-2.6wt%La/SiO_2 at 270^oC.

Time (min)	**W/F_{CO} (mg.min.µmol^{-1})**		
	1.30	**0.98**	**0.49**
	CO conversion (%)		
30	10.8	8.5	1.4
60	9.6	6.6	1.6
90	8.0	7.0	2.0
120	5.3	6.3	1.1
150	6.6	6.0	1.6
180	7.5	6.1	1.1
210	7.2	5.2	1.8
240	6.0	5.3	1.1
270	7.6	5.6	1.4

Same residence time values used during experiments for unpromoted Rh based silica supported catalyst were used and CO conversions obtained at different W/F_{CO} ratios are presented in Table 4.8 and Figure 4.19 at 1.30 mg.min.µmol^{-1} and 0.98 mg.min.µmol^{-1}

residence times, at steady state conditions CO conversion is around 7.5 and 5.5, respectively. At 0.49 mg.min.µmol^{-1} residence time, a very low CO conversion around 1.5% was obtained.

Methane production is not observable at a contact time of 0.49 mg.min.µmol^{-1}, and as the contact time is increased from 0.98 mg.min.µmol^{-1} to 1.30 mg.min.µmol^{-1}, methane production increases from 0.0033 µmol/gcat/sec to 0.0044 µmol/gcat/sec at steady state conditions (Table 4.9 and Figure 4.20).

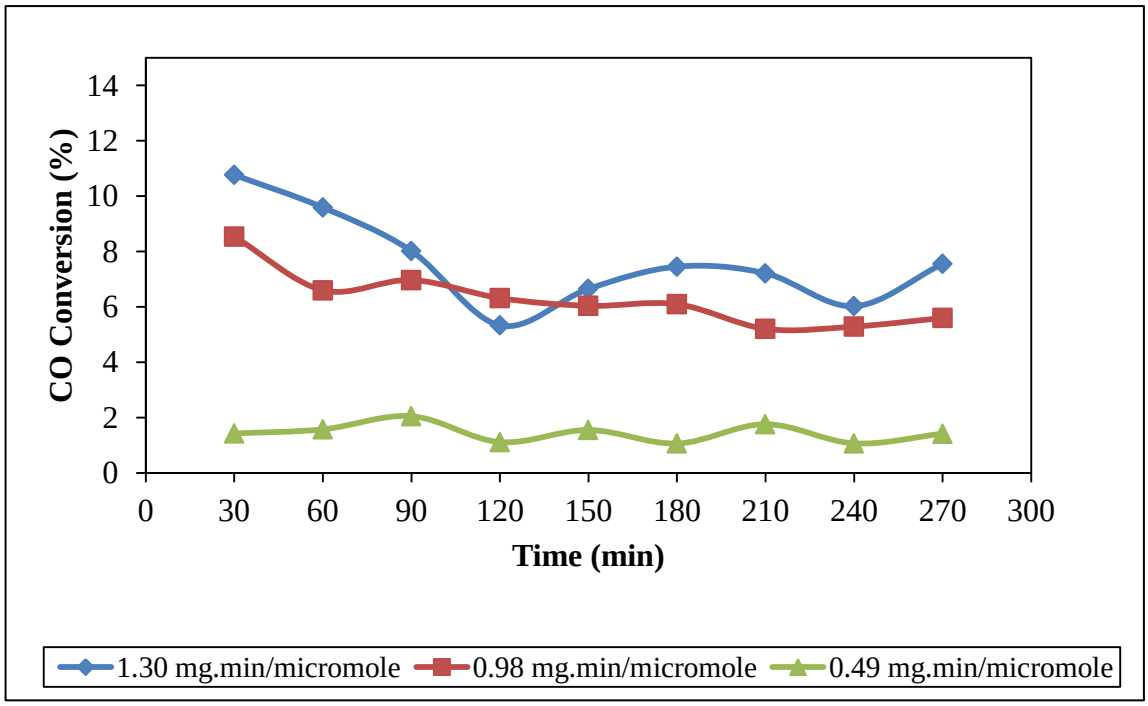

Figure 4.19. Effect of W/F_{CO} ratio on CO conversion over 1.5wt%Rh-2.6wt%La/SiO_2 at 270^{o}C.

Although CO hydrogenation conducted at 0.49 mg.min.µmol^{-1} does not produce any methane, it generates some amount of carbon dioxide as a result of water gas shift reaction. Moreover, as shown in Table 4.10 and Figure 4.21 at elevated residence times, carbon dioxide formation increases 4 times compared to that at 0.49 mg.min.µmol^{-1}.

Table 4.9. Effect of W/F_{CO} ratio on CH_4 production over 1.5wt%Rh-2.6wt%La/SiO_2 at 270°C.

Time (min)	**W/F_{CO} (mg.min.µmol^{-1})**	
	1.30	**0.98**
	CH_4 Production (micromole/gcat/sec)x1000	
30	6.26	5.88
60	5.99	4.98
90	5.76	4.26
120	5.41	4.00
150	5.16	3.64
180	4.62	3.53
210	4.54	3.37
240	4.71	3.33
270	4.43	3.33

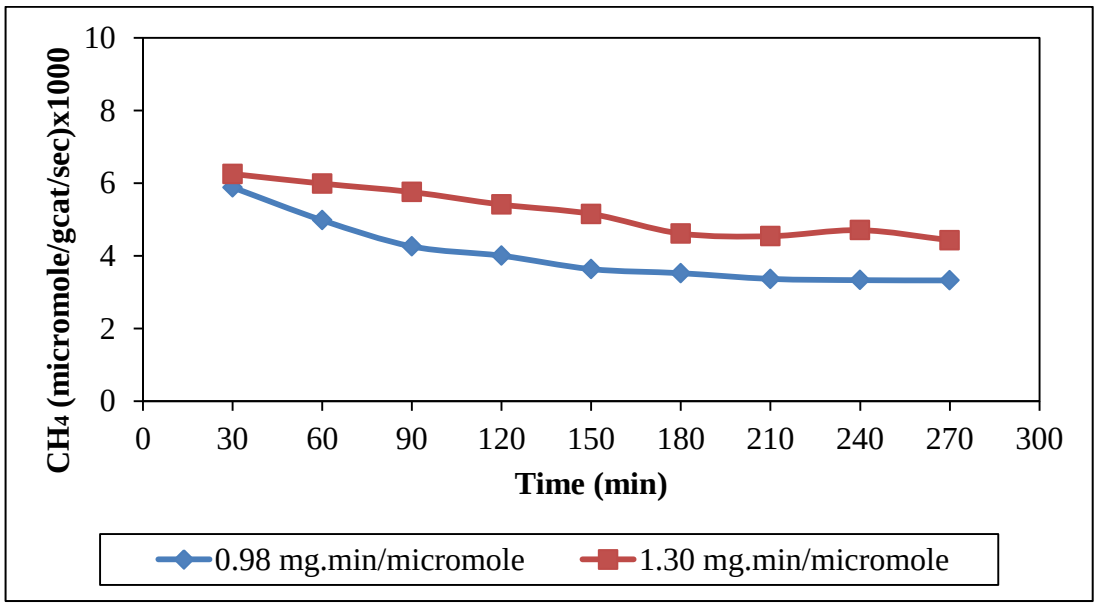

Figure 4.20. Effect of W/F_{CO} ratio on CH_4 production over 1.5wt%Rh-2.6wt%La/SiO_2 at 270°C.

It is reported that the molar selectivity to methanol and methane is expected to be relatively high at high space velocities since these products are formed initially in the reaction network by hydrogenation of (i) associatively adsorbed CO (forming methanol) and (ii) dissociatively adsorbed CO (forming CH_4). Moreover, as the space velocity decreases, an increase in CO conversion is expected at the same operating conditions. The rate of CO conversion increases with pressure, the selectivity to undesired methane is greater at 40 bar compared to 14 bar, oxygenates selectivity decreases at 40 bar (Subramanian *et al*., 2010).

Table 4.10. Effect of W/F_{CO} ratio on CO_2 production over 1.5wt%Rh-2.6wt%La/SiO_2 at 270^{o}C.

Time (min)	**W/F_{CO} (mg.min.µmol^{-1})**		
	1.30	**0.98**	**0.49**
	CO_2 Production (micromole/gcat/sec)x1000		
30	2.628	2.823	0.623
60	2.450	2.241	0.393
90	2.262	2.150	0.340
120	2.128	1.822	0.347
150	1.913	1.840	0.357
180	2.005	1.778	0.363
210	1.955	1.687	0.380
240	1.912	1.619	0.343
270	1.857	1.567	0.397

To compare experimental results with literature, 1.5wt.%Rh/SiO_2 and 1.5wt.%Rh-2.6wt.%La/SiO_2 catalysts are taken as basis with conditions of 270°C and H_2/CO=2. The results are clearly expressed in Table 4.11 and it can be inferred that although compared to literature study, lower space velocity value is used in this thesis that has better impact on CO conversion.

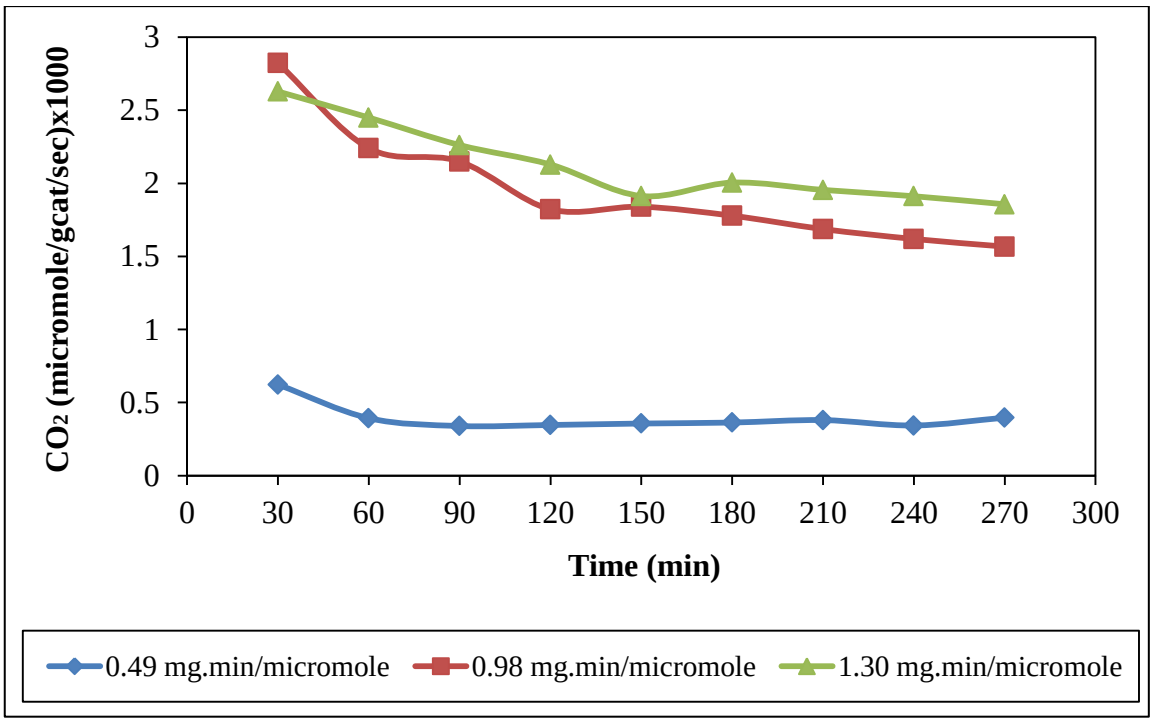

Figure 4.21. Effect of W/F_{CO} ratio on CO_2 production over 1.5wt%Rh-2.6wt%La/SiO_2 at 270^{o}C.

Table 4.11. Comparison of CO hydrogenation performance of 1.5wt%Rh/SiO_2 and 1.5wt%Rh-2.6wt%La/SiO_2 at 270°C and H_2/CO=2 at different pressures.

Catalyst	**P (atm)**	**Space Velocity (ml/h/gcat)**	**Rate of CO conversion (µmoles/gcat/s)**	**CH_4 Production (µmoles/gcat/s) (x1000)**	**CO_2 Production (µmoles/gcat/s) (x1000)**
Rh(1.5)/SiO_2	20	18000	0.12	55	4
Rh(1.5)-La(2.6)/SiO_2	20	18000	0.59	140	12
Rh(1.5)/SiO_2	1	15000	0.007	0	0.36
Rh(1.5)-La(2.6)/SiO_2	1	15000	0.01	3.3	1.6

The literature study yielded higher CO conversion accompanied by much higher methane and carbon dioxide production due to its elevated operating pressure of 20 atm (Subramanian *et al*., 2010).

It is reported that doubly promoted Rh–La–V/SiO_2 catalysts exhibit much higher activity (9×) compared to non-promoted Rh/SiO_2 (Gao *et al*., 2009b). The better performance of Rh–La–V/SiO_2 catalysts appears to be due to a synergistic promoting effect of the combined lanthana and vanadia additions through intimate contact with Rh. Use of just one promoter by itself was not able to produce enhanced catalytic performance (Gao *et al*., 2009). The La and V doubly promoted catalyst showed both new adsorbed CO species and increased desorption rate/reactivity of the adsorbed species during CO hydrogenation due to a synergistic promoting effect of La and V (Mo *et al*., 2009).

CO hydrogenation over the doubly promoted Rh–La-V/SiO_2 catalyst was conducted at 270^oC using a feed gas mixture of 10 per cent CO, 20 per cent H_2 and N_2 as balance. The weight of the catalyst was varied as 200 and 400 mg and total inlet flow rate was changed as 75 and 100 ml.min^{-1} at the same residence times used previously in testing of Rh/SiO_2 and Rh-La/SiO_2 catalysts, and, similarly, highest CO conversions were obtained with 1.30 mg.min.µmol^{-1} residence time (Table 4.12 and Figure 4.22). When W/F_{CO} ratio was increased from 0.49 mg.min.µmol^{-1} to 0.98 mg.min.µmol^{-1} CO conversion increased twice, while further increase in residence time to 1.30 mg.min.µmol^{-1} altered CO conversion only slightly. Product distributions are presented in and Figures 4.23 and 4.24. Residence time of 0.98 mg.min.µmol^{-1} and 1.30 mg.min.µmol^{-1} produces almost same amount of carbon dioxide and methane (Tables 4.13 and 4.14) and, when residence time is decreased to 0.49 mg.min.µmol^{-1}, amounts of reaction products drop considerably.

Table 4.12. Effect of W/F_{CO} ratio on CO conversion over 1.5wt%Rh-2.6wt%La-1.5wt%V/SiO_2 at 270°C.

Time (min)	**W/F_{CO} (mg.min.µmol^{-1})**		
	1.30	**0.98**	**0.49**
	CO conversion (%)		
30	30.3	27.0	9.5
60	22.4	24.3	8.1
90	22.1	22.6	7.8
120	20.7	23.1	7.3
150	20.3	18.5	6.6
180	19.9	18.2	6.9
210	17.9	17.2	6.8
240	16.9	15.8	6.3
270	17.3	15.4	6.8

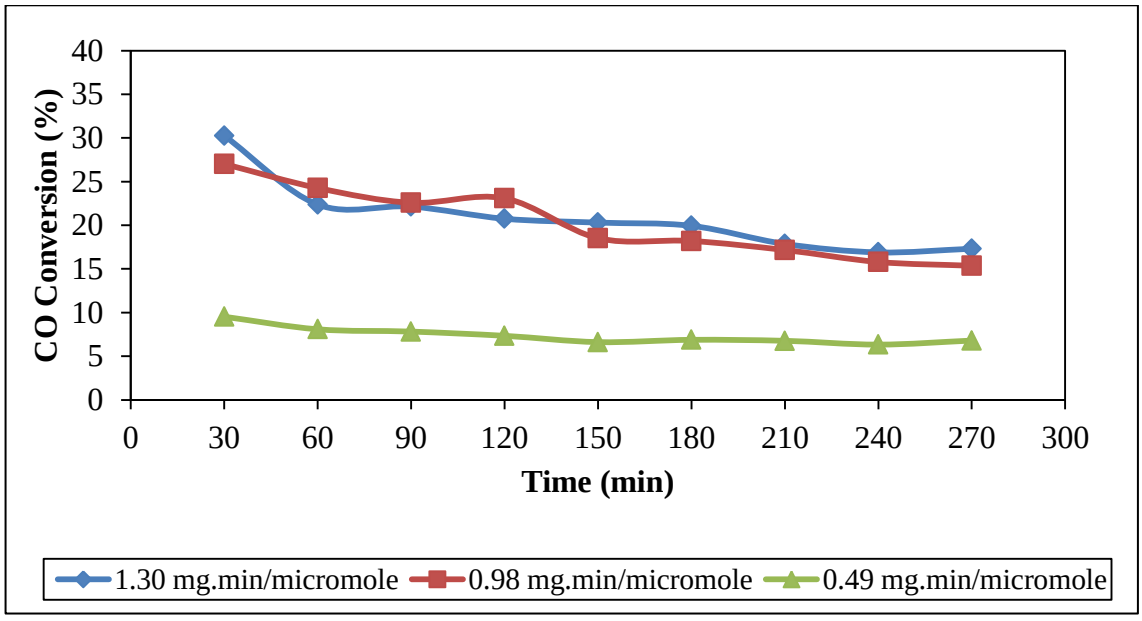

Figure 4.22. Effect of W/F_{CO} ratio on CO conversion over 1.5wt%Rh-2.6wt%La-1.5wt%V/SiO_2 at 270°C.

Table 4.13. Effect of W/F_{CO} ratio on CH_4 production over 1.5wt%Rh-2.6wt%La-1.5wt%V/SiO_2 at 270°C.

Time (min)	W/F_{CO} (mg.min.µmol^{-1})		
	1.30	0.98	0.49
	CH_4 Production (micromole/gcat/sec)x1000		
30	44.85	37.72	20.99
60	36.47	32.71	16.45
90	29.65	29.45	12.66
120	25.30	26.28	11.01
150	22.30	23.52	8.85
180	19.28	21.56	7.85
210	16.99	19.87	7.10
240	15.36	18.43	6.51
270	13.72	17.16	5.98

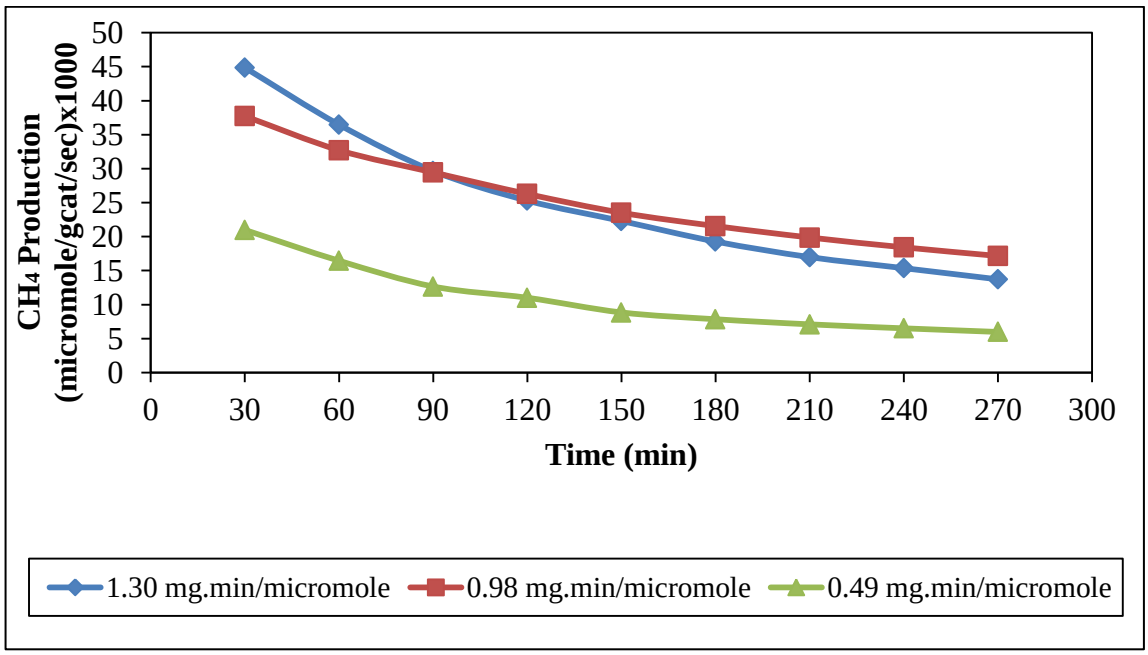

Figure 4.23. Effect of W/F_{CO} ratio on CH_4 production over 1.5wt%Rh-2.6wt%La-1.5wt%V/SiO_2 at 270°C.

Table 4.14. Effect of W/F_{CO} ratio on CO_2 production over 1.5wt%Rh-2.6wt%La-1.5wt%V/SiO_2 at 270°C.

Time (min)	W/F_{CO} (mg.min.µmol^{-1})		
	1.30	**0.98**	**0.49**
	CO_2 Production (micromole/gcat/sec)x1000		
30	8.21	6.46	3.28
60	7.53	5.90	3.20
90	6.88	5.51	2.76
120	6.50	5.04	2.51
150	5.96	4.86	2.68
180	5.79	4.65	2.59
210	5.60	4.51	2.23
240	5.50	4.48	2.26
270	5.24	4.33	2.23

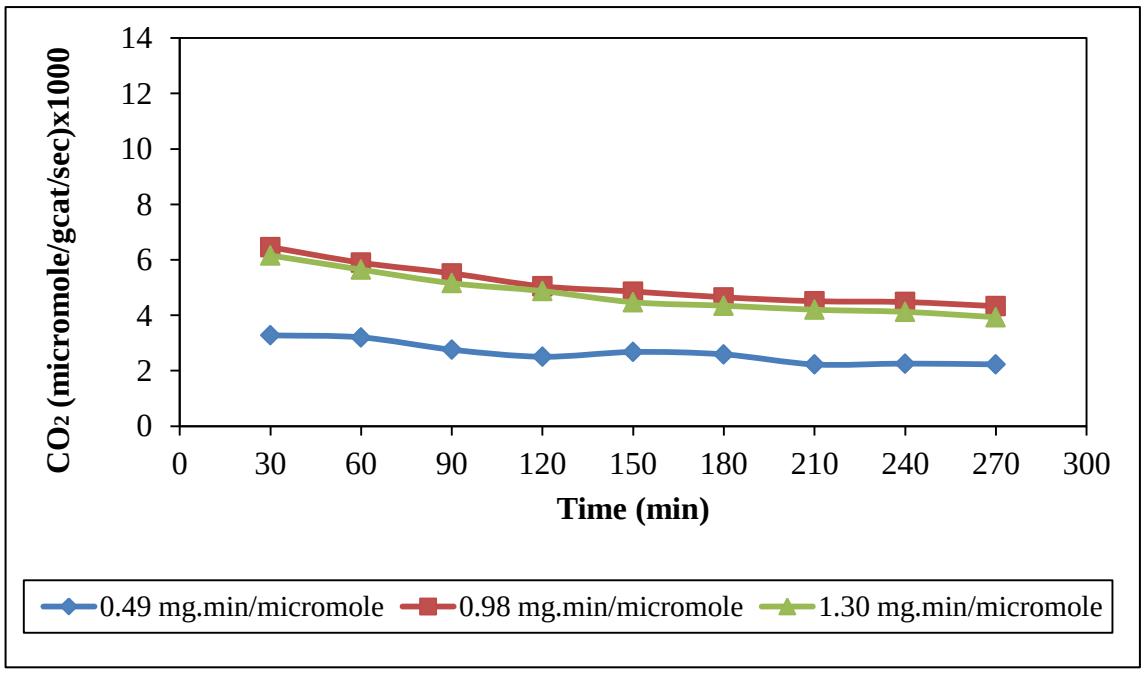

Figure 4.24. Effect of W/F_{CO} ratio on CO_2 production over 1.5wt%Rh-2.6wt%La-1.5wt%V/SiO_2 at 270°C.

Considering Table 4.15, similar literature studies conducted at elevated pressures over 1.5wt%Rh-2.6wt%La-1.5wt%V/SiO_2, show that higher CO conversions can be obtained (Subramanian *et al*., 2010). CO hydrogenation explored at an operating pressure of 20 atm and temperature of 270°C with 18000 ml/h/gcat space velocity gives 0.69 µmoles/gcat/s CO consumption, and also at 14 atm pressure with 36000 ml/h/gcat space velocity, CO consumption decreases to 0.43 µmoles/gcat/s at steady state conditions. Normally, increase in space velocity raises methane production as it is the initial product during CO hydrogenation reaction. Besides this, raising the pressure has a strong influence on CO conversion. At lower space velocity and atmospheric pressure, a CO conversion rate less than one tenth of that at 14 atm was obtained in the present work, methane and CO_2 productions are accordingly lower.

Finally, the catalytic activities of 2wt%Rh/Al_2O_3, 1.5wt%Rh/SiO_2, 1.5wt%Rh-2.6wt%La/SiO_2, 1.5wt%Rh-2.6wt%La-1.5wt%V/SiO_2 catalysts prepared in this work are compared at conditions of 0.98 mg.min.µmol^{-1} residence time, 270^{o}C temperature and with feed of 10% CO, 20% H_2 and N_2 as balance component in 100ml/min inlet flow rate and results are presented in Table 4.17 and Figure 4.24. It is evident that under these conditions 1.5wt%Rh-2.6wt%La-1.5wt%V/SiO_2 provides the highest CO conversion with 15% at steady state, 2wt%Rh/Al_2O_3 yields 10% CO conversion which is greater than the CO conversion achieved with 1.5wt%Rh-2.6wt%La/SiO_2.

At atmospheric pressure, the effect of V loading on 1.5wt%Rh-2.6wt%La/SiO_2 and 5wt%Ni/Al_2O_3 catalysts are compared as regards their hydrocarbon and carbon dioxide productions. Both studies were carried out around 270°C and results are shown in Table 4.16. Clearly, when V is added to 5wt%Ni/Al_2O_3 catalyst, at W/Q ratio of 2.7 mg.min/ml hydrocarbon production rises from 1.37 µmoles/gcat/s to 1.63 µmoles/gcat/s (Karaselçuk *et al*., 2000). Moreover, in the Rh-La catalyst at W/Q ratio of 4.0 mg.min/ml addition of vanadium also increases hydrocarbon production from 0.008 µmoles/gcat/s to 0.027 µmoles/gcat/s at steady state conditions.

Table 4.15. Comparison of CO hydrogenation performance of 1.5wt%Rh-2.6wt%La-1.5wt%V/SiO_2 at 270°C and H_2/CO=2 at different pressures.

Catalyst	**P (atm)**	**Space Velocity (ml/h/gcat)**	**Rate of CO conversion (µmoles/gcat/s)**	**CH_4 Production (µmoles/gcat/s) (x1000)**	**CO_2 Production (µmoles/gcat/s) (x1000)**
Rh(1.5)-La(2.6)/V(1.5) over silica support	20	18000	0.69	70	48
Rh(1.5)-La(2.6)/V(1.5) over silica support	14	36000	0.43	114.8	19.4
Rh(1.5)-La(2.6)/V(1.5) over silica support	1	15000	0.03	17.2	4.4

Table 4.16. Effect of V addition on hydrocarbon production with H_2/CO=2 and 10 vol% CO in feed.

Catalyst	**T (°C)**	**Total Hydrocarbon Production (µmoles/gcat/s)(x1000)**	**CO_2 Production (µmoles/gcat/s) (x1000)**
Rh(1.5)-La(2.6)/SiO_2	270	8	4
Rh(1.5)-La(2.6)/V(1.5)/SiO_2	270	20.7	6
Ni(5)/Al_2O_3	275	1370	160
Ni(5)-V(1)/Al_2O_3	275	1630	150

Table 4.17. Comparison of CO conversions over Rh-based catalysts with different supports and promoters at 270°C and H_2/CO=2 and W/F_{CO}= 0.98 mg.min.µmol^{-1}.

Time (min)	CO conversion (%)			
	2wt%Rh/Al_2O_3	1.5wt%Rh/SiO_2	1.5wt%Rh-2.6wt%La/SiO_2	1.5wt%Rh-2.6wt%La/1.5wt%V/SiO_2
30	6.2	3.8	8.5	27.0
60	9.8	1.9	6.6	24.3
90	9.8	2.4	7.0	22.6
120	10.6	3.3	6.3	23.1
150	10.0	2.7	6.0	18.5
180	9.6	2.5	6.1	18.2
210	9.6	3.2	5.2	17.2
240	9.4	2.2	5.3	15.8
270	9.8	2.7	5.6	15.4

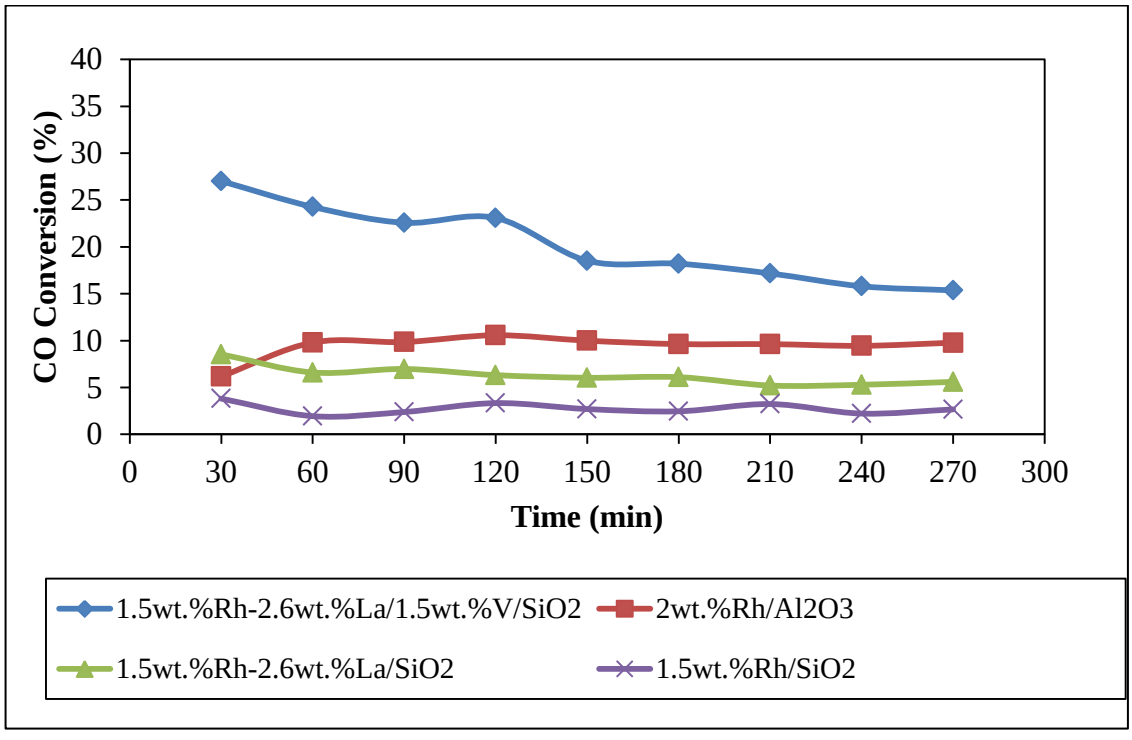

Figure 4.25. Comparison of CO conversions over Rh-based catalysts with different supports and promoters at 270°C and H_2/CO=2 and W/F_{CO}= 0.98 mg.min.µmol^{-1}.

On the other hand, at elevated pressures the combined La and V addition reduces methane selectivity and increases C_2^+ oxygenates selectivity compared to the singly promoted catalysts, by increasing the rate of CO insertion (Subramanian *et al*., 2010).

4.2.2. Effect of Reaction Temperature

4.2.2.1. Unpromoted Rhodium catalyst. The dependence of CO conversion on the reaction temperature was studied over all three catalysts reduced at 500^{o}C for 2 hours. The composition of the feed gas mixture was 10 per cent CO, 20 per cent H_2 and N_2 as balance in 100 ml/min inlet flow rate. Reactions were carried out at 230^{o}C, 270^{o}C and 290^{o}C and atmospheric pressure. Since it was seen that increasing the contact time from 0.98 mg.min.µmol^{-1} to 1.30 mg.min.µmol^{-1} did not change CO conversion significantly, contact time of 0.98 mg.min.µmol^{-1} was selected to observe the influence of reaction temperature on activity of catalysts. The results obtained at 30 minute intervals are given in Tables 4.18-4.20 and Figure 4.26-4.28. Evidently, increase of temperature from 230^{o}C to 290^{o}C increases CO conversion from 0.5% to ca. 6% at steady state conditions.

Table 4.18. Effect of temperature on CO conversion over 1.5wt%Rh/SiO_2 with H_2/CO=2 and W/F_{CO}= 0.98 mg.min.µmol^{-1}.

Time (min)	**CO conversion (%)**		
	290^{o}C	**270^{o}C**	**230^{o}C**
30	6.1	6.0	0.7
60	4.7	3.2	0.3
90	9.4	3.8	1.0
120	6.9	2.8	0.6
150	6.5	3.2	0.6
180	6.4	3.9	0.3
210	6.3	3.2	1.3
240	6.6	4.2	1.0
270	5.7	3.4	0.6

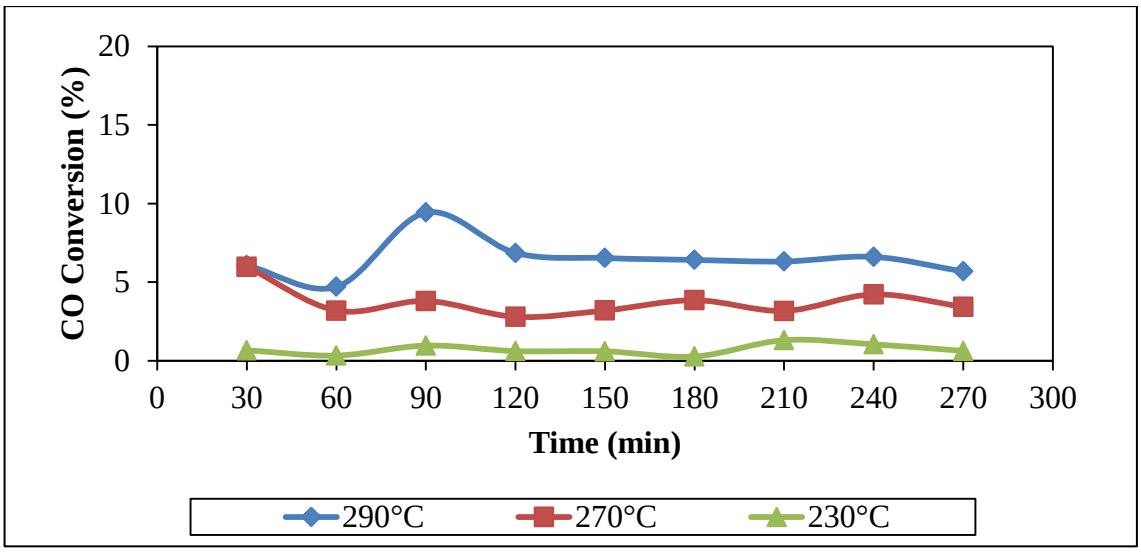

Figure 4.26. Effect of temperature on CO conversion over 1.5wt%Rh/SiO_2 with H_2/CO=2 and W/F_{CO}= 0.98 mg.min.µmol^{-1}.

Table 4.19. Effect of temperature on CH_4 production over 1.5wt%Rh/SiO_2 with H_2/CO=2 and W/F_{CO}= 0.98 mg.min.µmol^{-1} at 290°C.

Time (min)	**CH_4 Production (micromole/gcat/sec)x1000**
30	5.84
60	5.00
90	4.74
120	4.26
150	3.87
180	3.76
210	3.64
240	3.69
270	3.30

However, associated with its low CO conversion, reaction conducted at 230°C does not produce any product. Moreover, when 270°C is used, a slight amount of carbon dioxide is observed over 1.5wt%Rh/SiO_2 as seen in Table 4.20 and Figure 4.28. Since elevated temperature provides better catalytic activity and produces carbon dioxide, further increment of temperature was applied on reaction system. For this purpose, next experiment was conducted at 290°C and this temperature displays higher CO conversion with 0.0033 micromole/gcat/sec CH_4 and 0.0017 micromole/gcat/sec CO_2 production at steady state conditions as shown in Figures 4.27 and 4.28.

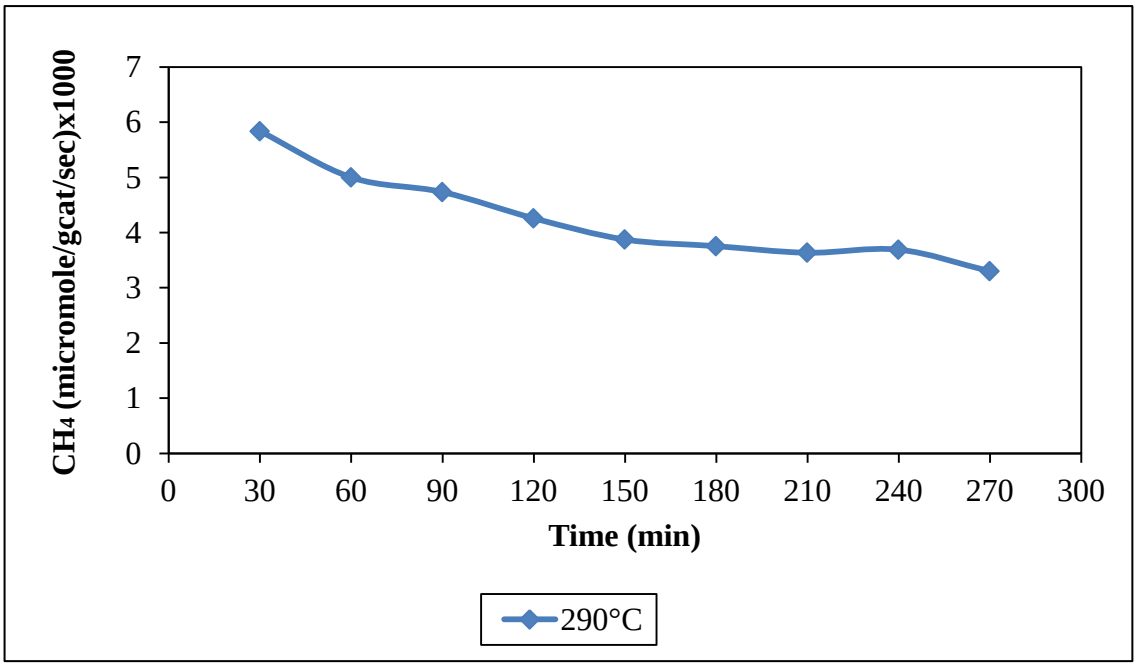

Figure 4.27. CH_4 production over 1.5wt%Rh/SiO_2 at 290°C with H_2/CO=2 and W/F_{CO}= 0.98 mg.min.µmol^{-1}.

Table 4.20. Effect of temperature on CO_2 production over 1.5wt%Rh/SiO_2 with H_2/CO=2 and W/F_{CO}= 0.98 mg.min.µmol^{-1}.

Time (min)	CO_2 Production (micromole/gcat/sec)x1000	
	290°C	270°C
30	2.35	0.61
60	2.12	0.48
90	1.96	0.46
120	1.9	0.41
150	1.87	0.43
180	1.79	0.39
210	1.73	0.39
240	1.8	0.29
270	1.69	0.36

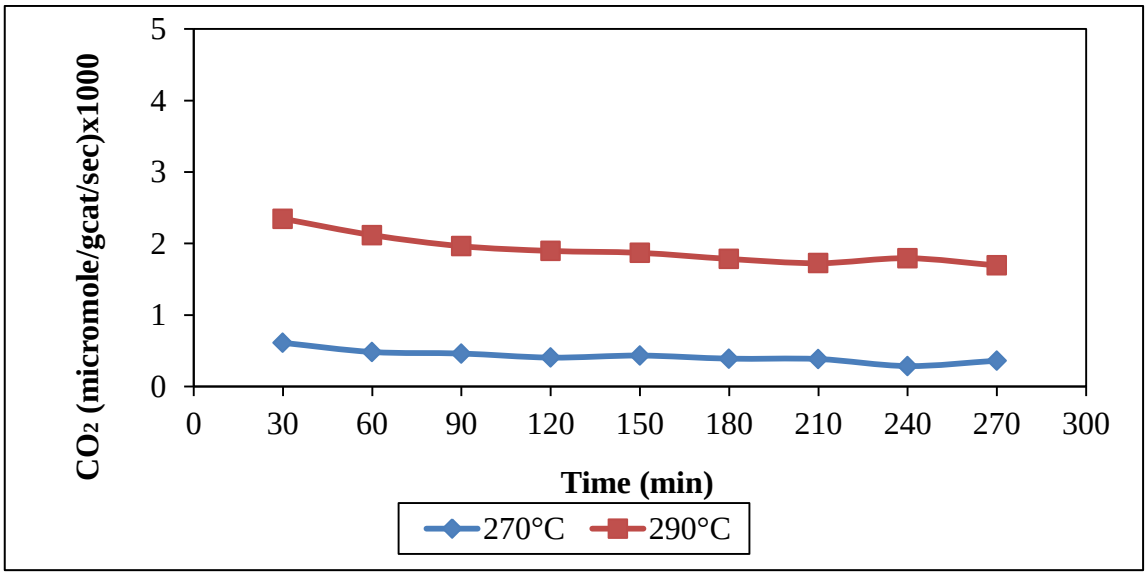

Figure 4.28. Effect of temperature on CO_2 production over 1.5wt%Rh/SiO_2 with H_2/CO=2 and W/F_{CO}= 0.98 mg.min.µmol^{-1}.

4.2.2.2. Effect of Lanthanum promotion. Similar to non-promoted Rh/SiO_2, the dependence of CO conversion on the reaction temperature was studied over lanthana promoted Rhodium based silica supported catalysts reduced at 500°C for 2 hours. The catalyst is 1.5wt.%Rh-2.6wt.%La/SiO_2 and the composition of the feed gas mixture was 10 per cent CO, 20 per cent H_2 and N_2 as balance in 100 ml/min inlet flow rate. Reactions were carried out at 230°C, 270°C and 290°C and atmospheric pressure with residence time of 0.98 mg.min.µmol^{-1}. Compared to non-promoted Rh/SiO_2 CO conversions at steady state conditions increased at all temperatures. Similar to non-promoted case, again in lanthana promoted catalyst showed very low CO conversion. In addition to this, as performed in Table 4.21 and Figure 4.29 CO conversion increases from 1.6% to 10.2% at steady state conditions as the temperature rises from 230°C to 290°C.

Table 4.21. Effect of temperature on CO conversion over 1.5wt%Rh-2.6wt%La/SiO_2 with $H_2/CO=2$ and $W/F_{CO}=0.98$ mg.min.µmol^{-1}.

Time (min)	**CO conversion (%)**		
	290°C	**270°C**	**230°C**
30	12.4	11.3	0.8
60	12.5	8.0	1.2
90	5.7	8.7	1.6
120	6.5	7.5	0.7
150	10.5	7.8	1.2
180	10.6	6.6	1.2
210	10.8	6.6	1.5
240	9.7	6.6	0.4
270	10.2	6.5	1.6

Methane production over 1.5wt%Rh-2.6wt%La/SiO_2 catalyst is also recorded and the results are performed in Table 4.22 and Figure 4.30. Similar to non-promoted Rh case, operating condition of 230°C does not yield any CH_4 over 1.5wt.%Rh-2.6wt.%La/SiO_2.

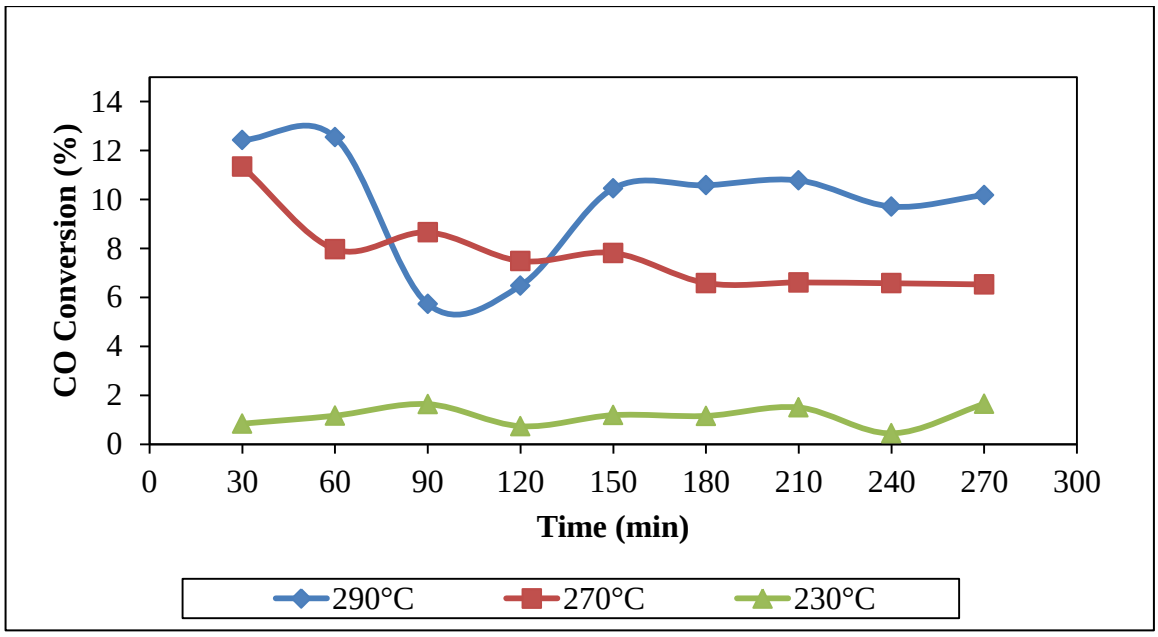

Figure 4.29. Effect of temperature on CO conversion over 1.5wt%Rh-2.6wt%La/SiO_2 with H_2/CO=2 and W/F_{CO}=0.98 mg.min.µmol^{-1}.

Table 4.22. Effect of temperature on CH_4 production over 1.5wt%Rh-2.6wt%La/SiO_2 with H_2/CO=2 and W/F_{CO}=0.98 mg.min.µmol^{-1}.

Time (min)	**CH_4 Production (micromole/gcat/sec)x1000**	
	290°C	**270°C**
30	10.29	7.93
60	9.92	6.5
90	9.67	5.48
120	8.75	5.95
150	8.44	5.4
180	8.07	5.15
210	7.86	5.11
240	7.89	4.86
270	7.72	4.69

However, when temperature of reaction is risen to 270°C and 290°C at steady state conditions 0.0047 and 0.0077 micromole/gcat/sec methane is produced, respectively.

During the reaction conducted at 230°C carbon dioxide production is observed just at the end of the 30 minutes and 60 minutes with quite low amounts. As time temperature is increased from 270°C to 290°C, CO_2 formations seen at steady state are approximately 0.0029 and 0.004 micromole/gcat/sec carbon dioxide is produced, respectively (Table 4.23 and Figure 4.31).

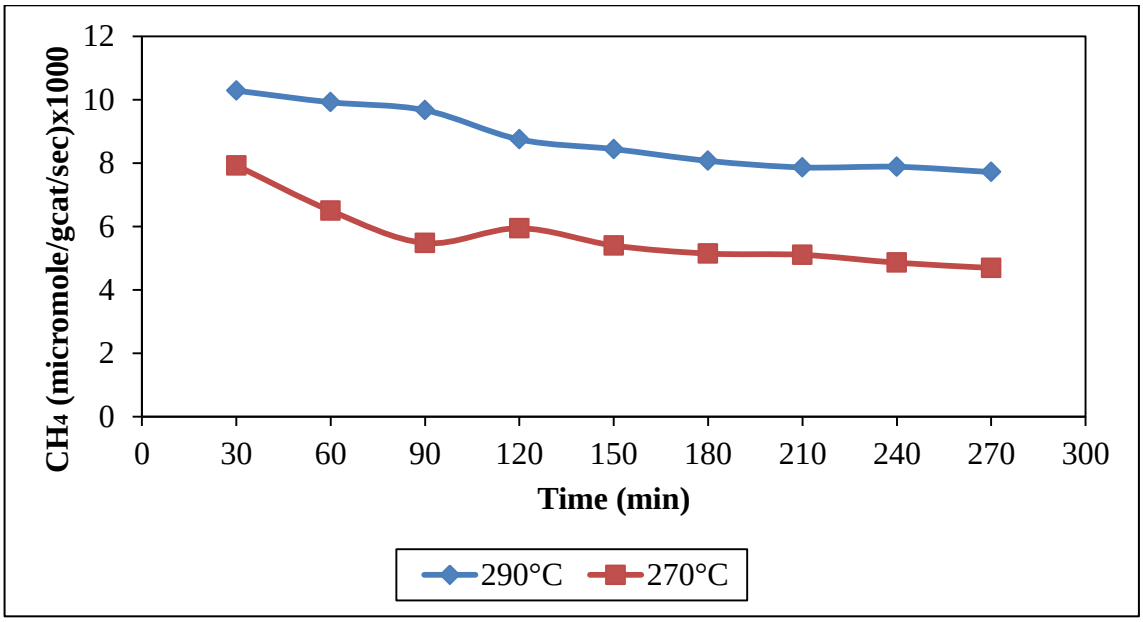

Figure 4.30. Effect of temperature on CH_4 production over 1.5wt%Rh-2.6wt%La/SiO_2 with $H_2/CO=2$ and W/F_{CO}= 0.98 mg.min.µmol^{-1}.

Table 4.23. Effect of temperature on CO_2 production over 1.5wt%Rh-2.6wt%La/SiO_2 with $H_2/CO=2$ and $W/F_{CO}=0.98$ mg.min.µmol^{-1}.

Time (min)	CO_2 Production (micromole/gcat/sec)x1000		
	290°C	270°C	230°C
30	4.70	4.68	0.04
60	4.71	3.81	0.05
90	4.72	3.27	--
120	4.38	3.57	--
150	4.28	3.30	--
180	4.17	3.19	--
210	4.10	2.95	--
240	4.09	2.90	--
270	3.96	2.87	--

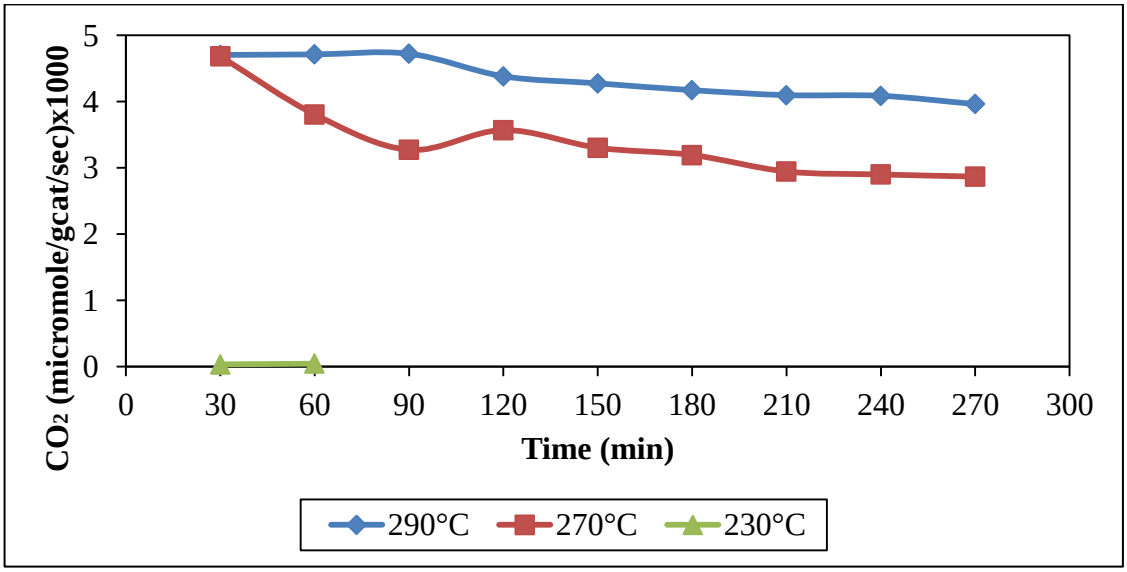

Figure 4.31. Effect of temperature on CO_2 production over 1.5wt%Rh-2.6wt%La/SiO_2 with $H_2/CO=2$ and $W/F_{CO}=0.98$ mg.min.µmol^{-1}.

In Table 4.24, the 1.5wt%Rh-2.6wt%La/SiO_2 catalyst is also compared with co-precipitated 36wt%Co/Al_2O_3 catalyst. At similar reaction conditions 36wt%Co/Al_2O_3 catalyst yields 0.83 μmoles/gcat/s CH_4 and 0.36 μmoles/gcat/s CO_2 (Akın and Önsan, 1997). These rates are much higher than those obtained on 1.5wt%Rh-2.6wt%La/SiO_2.

In Table 4.25, production values of 1.5wt%Rh-2.6wt%La/SiO_2 catalyst are compared to Ni(5)-V(1)-K(0.5)/Al_2O_3 catalyst; at similar reaction conditions, the Ni-V-K catalyst Ni(5)-V(1)-K(0.5)/Al_2O_3 yields 1.972 μmoles/gcat/s CH_4 and 0.41 μmoles/gcat/s CO_2 (Karaselçuk *et al.*, 2000). These rates are much higher than the product values obtained with 1.5wt%Rh-2.6wt%La/SiO_2 catalyst.

Table 4.24. Comparison of product distributions of 1.5wt%Rh-2.6wt%La/SiO_2 and 36wt%Co/Al_2O_3 catalysts.

Catalyst	**T (°C)**	**CO Conversion (%)**	**CH_4 Production (μmoles/gcat/s) (x1000)**	**CO_2 Production (μmoles/gcat/s) (x1000)**	**CO in feed (%)**
1.5wt.%Rh-2.6wt.%La/SiO_2	290	10	7.8	4	10
Coprecipitated 36wt.% Co/Al_2O_3	290	9	833.3	366.6	20

Table 4.25. Comparison of product distributions of Rh(1.5)-La(2.6)/SiO_2 and Ni(5)-V(1)-K(0.5)/Al_2O_3 catalysts.

Catalyst	**T (°C)**	**CO Conversion (%)**	**CH_4 Production (μmoles/gcat/s) (x1000)**	**CO_2 Production (μmoles/gcat/s) (x1000)**
Rh(1.5)-La(2.6)/SiO_2	290	10	7.80	4
Ni(5)-V(1)-K(0.5)/Al_2O_3	300	9	1972	410

4.2.2.3. Effect of combined Lanthanum and Vanadium promotion. Finally, the dependence of CO conversion on the reaction temperature was investigated on doubly promoted Rh-La-V/SiO_2 catalyst. The catalyst was reduced at 500^oC for 2 hours.

Table 4.26. Effect of temperature on CO conversion over 1.5wt%Rh-2.6wt%La-1.5wt%V/SiO_2 with $H_2/CO=2$ and $W/F_{CO}=0.98$ mg.min.µmol^{-1}.

Time (min)	**CO conversion (%)**		
	290^{o}C	**270^{o}C**	**230^{o}C**
30	33.6	27.7	3.3
60	31.9	24.4	2.6
90	30.1	23.3	2.3
120	26.7	23.0	2.2
150	25.6	19.8	2.9
180	25.0	19.5	3.1
210	24.0	18.2	2.8
240	23.8	17.0	2.9
270	24.5	17.3	2.5

The catalyst is 1.5wt%Rh-2.6wt%La-1.5wt%V/SiO_2 and the composition of the feed gas mixture was 10 per cent CO, 20 per cent H_2 and N_2 as balance in 100 ml/min inlet flow rate. Reactions were carried out at 230^{o}C, 270^{o}C and 290^{o}C and atmospheric pressure with residence time of 0.98 mg.min.µmol^{-1}.

Compared to the unpromoted and La promoted Rh/SiO_2 , CO conversion was again very low at 230^{o}C, but the V loading increased CO conversion at 270^{o}C and 290^{o}C to 17% and 24% at steady state as performed shown in Table 4.26 and Figure 4.32.

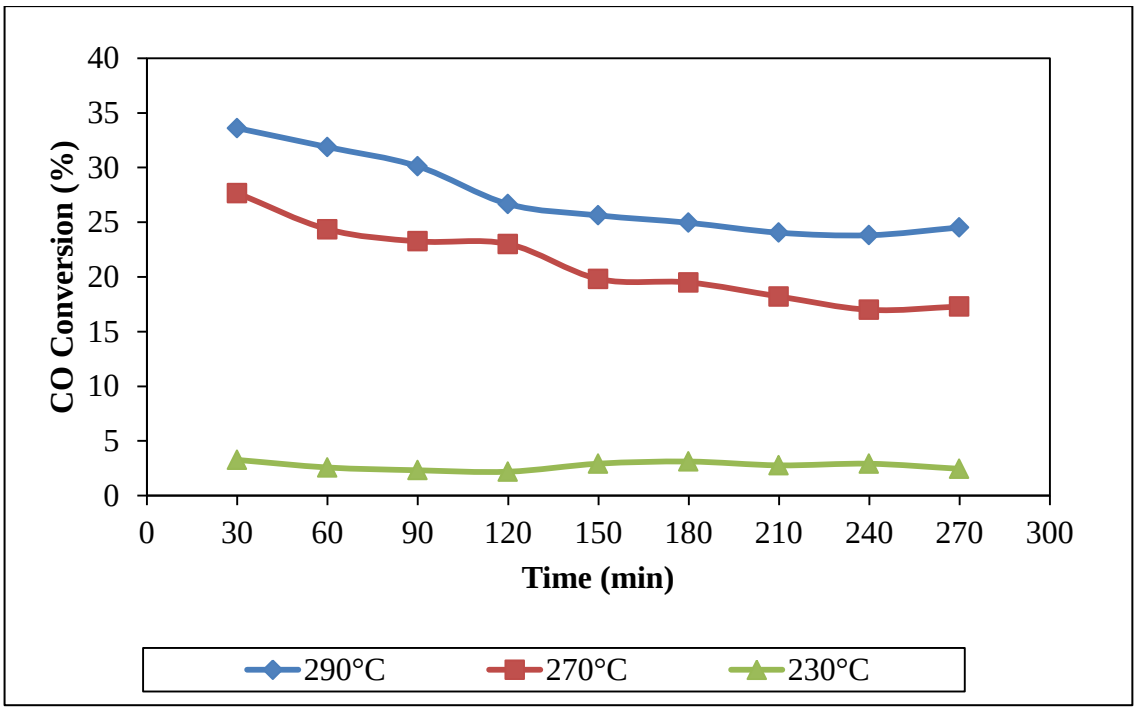

Figure 4.32. Effect of temperature on CO conversion over 1.5wt%Rh-2.6wt%La-1.5wt%V/SiO_2 with H_2/CO=2 and W/F_{CO}=0.98 mg.min.µmol^{-1}.

According to peaks obtained in Gas Chromatographs methane and carbon dioxide productions are also calculated for different temperatures and the results are shown in Table 4.27 and Table 4.28. According to these tables, to provide better vision production amounts are plotted in Figure 4.33 and Figure 4.34. Although reaction carried out at 230°C does not produce any methane gas, it produces slight amount of carbon dioxide. Enhancement of temperature to 270°C and 290°C with same reaction conditions improves methane and carbon dioxide production significantly. As can be seen in Table 4.27, at 270°C and 290°C temperatures, methane production rises up to 0.021 and 0.027 micromole/gcat/sec, respectively. In addition to that, as shown in Table 4.28, at steady state conditions 0.006 micromole/gcat/sec and 0.001 micromole/gcat/sec carbon dioxide is produced at 270°C and 290°C temperatures, respectively.

Table 4.27. Effect of temperature on CH_4 production over 1.5wt%Rh-2.6wt%La-1.5wt%V/SiO_2 with $H_2/CO=2$ and $W/F_{CO}=0.98$ mg.min.µmol^{-1}.

Time (min)	CH_4 Production (micromole/gcat/sec)x1000	
	290°C	270°C
30	54.06	41.80
60	44.70	35.63
90	40.74	33.39
120	37.03	30.32
150	34.10	27.31
180	29.17	24.76
210	27.99	22.88
240	27.72	21.48
270	27.58	20.70

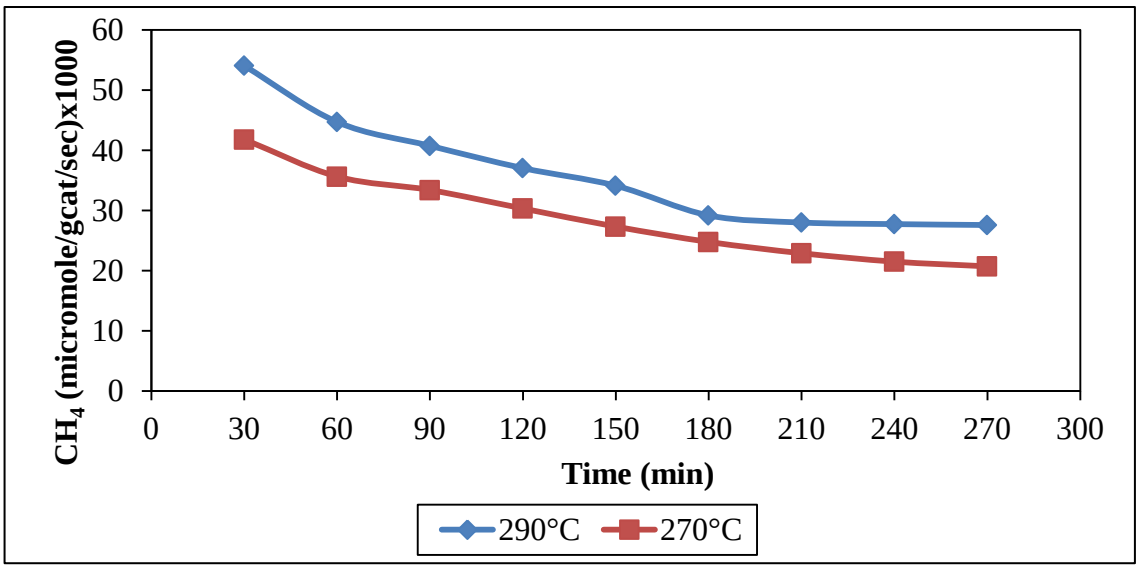

Figure 4.33. Effect of temperature on CH_4 production over 1.5wt%Rh-2.6wt%La-1.5wt%V/SiO_2 with $H_2/CO=2$ and $W/F_{CO}=0.98$ mg.min.µmol^{-1}.

Table 4.28. Effect of temperature on CO_2 production over 1.5wt%Rh-2.6wt%La-1.5wt%V/SiO_2 with $H_2/CO=2$ and $W/F_{CO}=0.98$ mg.min.µmol^{-1}.

Time (min)	**CO_2 Production (micromole/gcat/sec)x1000**		
	290°C	**270°C**	**230°C**
30	12.76	9.79	1.64
60	11.43	8.06	1.40
90	10.97	7.08	1.25
120	10.79	6.60	1.16
150	10.59	6.40	1.05
180	10.49	6.20	0.98
210	10.40	6.09	0.93
240	10.37	6.00	0.85
270	10.34	5.95	0.82

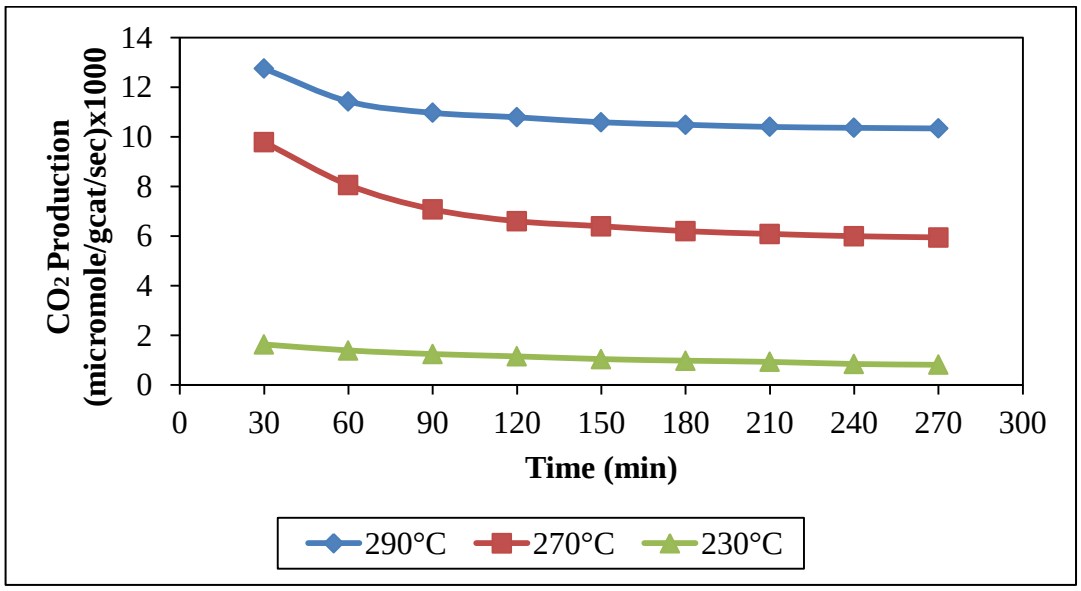

Figure 4.34. Effect of temperature on CO_2 production over 1.5wt%Rh-2.6wt%La-1.5wt%V/SiO_2 with $H_2/CO=2$ and $W/F_{CO}=0.98$ mg.min.µmol^{-1}.

From Table 4.29 it is seen that as the temperature rises from 230°C to 270°C in 1.5wt.%Rh/SiO_2, 1.5wt.%Rh-2.6wt.%La/SiO_2, 1.5wt.%Rh-2.6wt.%La/1.5wt.%V/SiO_2 catalysts rate of CO conversion increases significantly. Obviously, although CO hydrogenation reaction is carried out with space velocity close to literature value, in this thesis much lower rate of CO conversions were achieved. It is evident that literature study was performed at 20 bar and this results in obtaining much higher rate of CO conversion compared to reaction performed at atmospheric pressure (Subramanian *et al*., 2010).

Table 4.29. Comparison of non-promoted, singly or doubly promoted Rh based silica supported catalysts with literature at 270°C and H_2/CO=2.

Catalyst	**Rate of CO conversion (µmoles/gcat/s)**		**Pressure (bar)**	**S.V. (ml/h/gcat)**
	230°C	**270°C**		
Rh(1.5)/SiO_2	0.03	0.12	20	18000
Rh(1.5)-La(2.6)/SiO_2	0.29	0.59	20	18000
Rh(1.5)-La(2.6)/V(1.5)/SiO_2	0.13	0.69	20	18000
Rh(1.5)/SiO_2	0.002	0.007	1	15000
Rh(1.5)-La(2.6)/SiO_2	0.003	0.01	1	15000
Rh(1.5)-La(2.6)/V(1.5)/SiO_2	0.005	0.03	1	15000

5. CONCLUSIONS AND RECOMMENDATIONS

5.1. Conclusions

The aim of this study is to test and develop supported solid catalysts for hydrocarbon production by CO hydrogenation. An existing micro-reactor flow system modifed for CO hydrogenation reaction was used for testing four different catalysts. These catalysts were 2wt%Rh/δ-Al_2O_3, 1.5wt%Rh/SiO_2, 1.5wt%Rh-2.6wt%La/SiO_2, 1.5wt%Rh-2.6wt%La-1.5wt%V/SiO_2 prepared by sequential or co-impregnation to incipient wetness of silica or alumina supports. The experimental work involved a parametric study of CO hydrogenation reaction as a function of temperature, contact time (W/F_{CO}), promoter loading (La, V) on Rh catalysts supported over δ-Al_2O_3 and SiO_2.

The major conclusions obtained in this study can be summarized as follows:

- Over 2wt%Rh/δ-Al_2O_3, CO conversion increases with increasing residence time, as indicated by the results at 270^{o}C for W/F_{CO} ratios between 0.82-1.22 mg.min.μmol^{-1}.

- Scanning electron microscopy and X-ray Diffraction results indicate uniform dispersion of Rh over silica support with occasional formation of Rh clusters.

- On non-promoted, La or La and V promoted Rh/SiO_2 catalysts, CO conversion increases with increasing residence time, as indicated by the results at 270^{o}C for W/F_{CO} ratios between 0.49-1.30 mg.min.μmol^{-1}.

- Addition of La or combined La and V promoters improves catalytic activity of Rh/SiO_2 catalysts significantly at the same reaction temperature.

- The reaction temperature has considerable effect on CO conversion for all Rh based silica supported catalysts studied. CO conversion increases as reaction temperature is increased from 230 to 290^{o}C.

5.2. Recommendations

Under the light of the results of the present work, the following studies are recommended:

- As indicated by the results of this study, methane and carbon dioxide are the main products of this reaction under these operating conditions. By elevating pressure on the system different product distributions may be obtained.

- Different techniques of catalyst preparation may be applied.

- Kinetic studies can be performed over non-promoted, singly or doubly promoted Rh/SiO_2 catalysts.

- The percent weight of Rh, La and V may be changed to search for better catalytic activity.

APPENDIX A: CALIBRATION CURVES OF THE MASS FLOW CONTROLLERS

Calibration curves of the mass flow controllers used in the experiments are illustrated below.

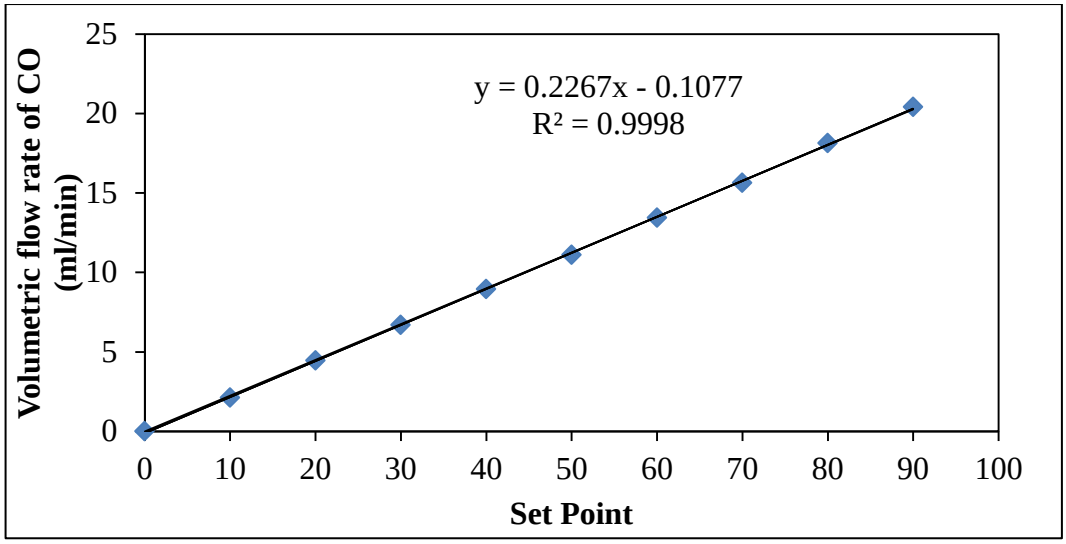

Figure A.1. Calibration curve of the carbon monoxide mass flow controller.

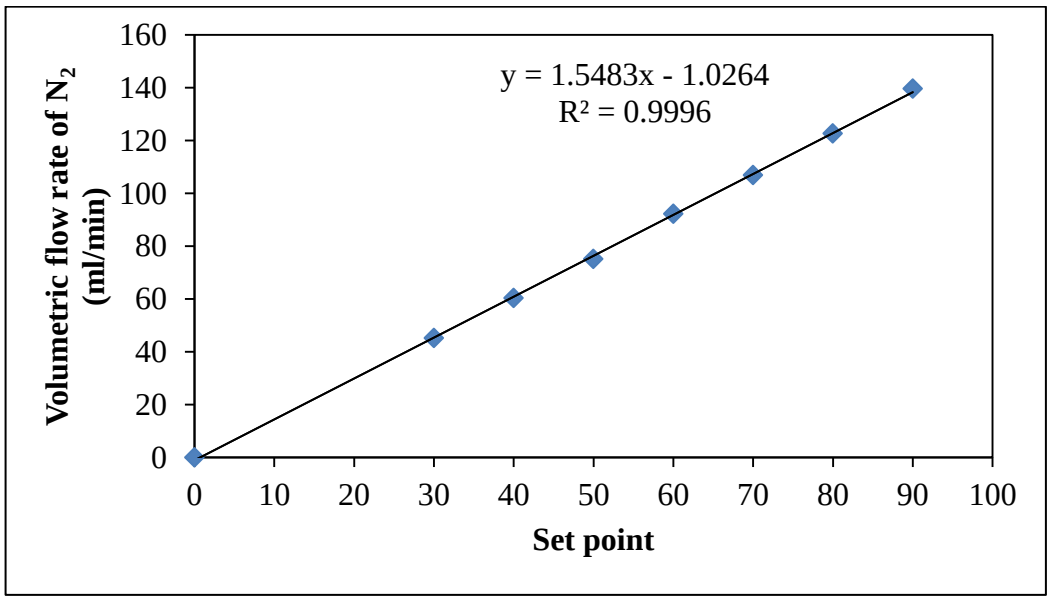

Figure A.2. Calibration curve of the nitrogen mass flow controller.

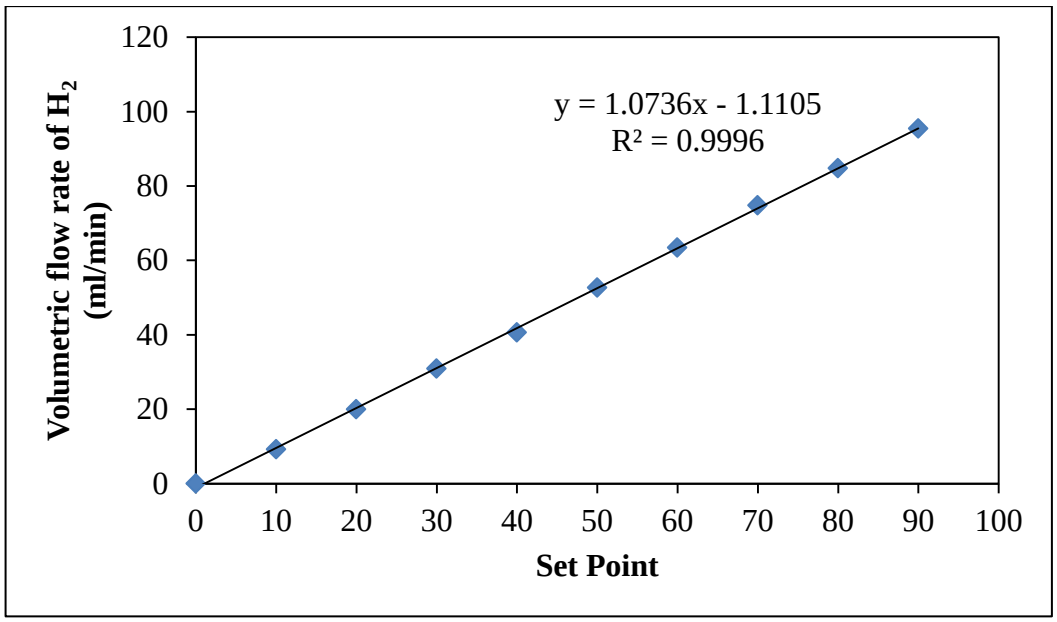

Figure A.3. Calibration curve of the hydrogen mass flow controller.

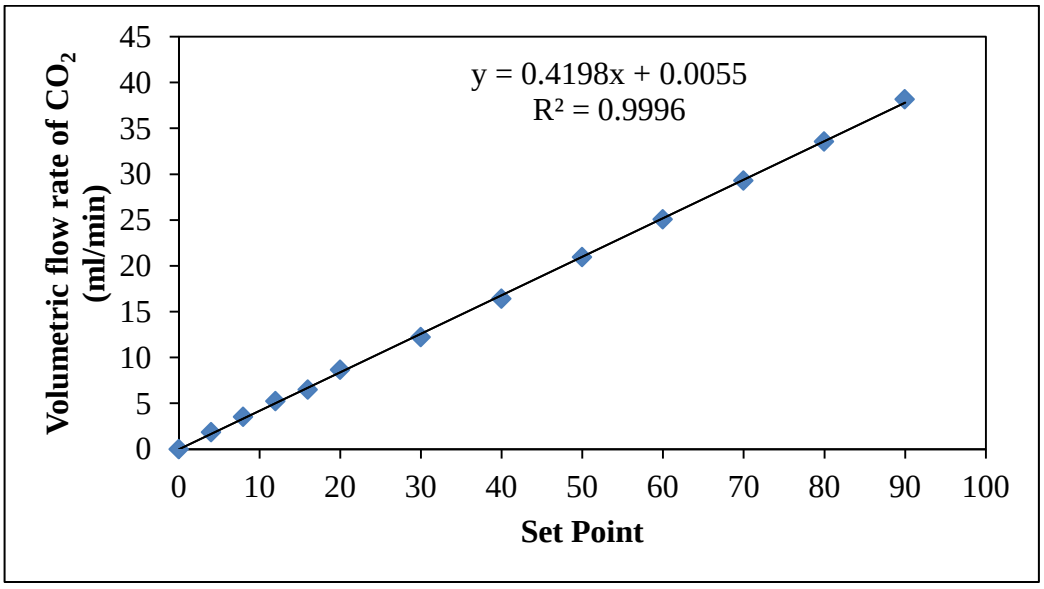

Figure A.4. Calibration curve of the carbon dioxide mass flow controller.

APPENDIX B: CALIBRATION CURVES OF THE GAS CHROMATOGRAPHS

Calibration curves of the gas chromatographs used in the experiments are given below.

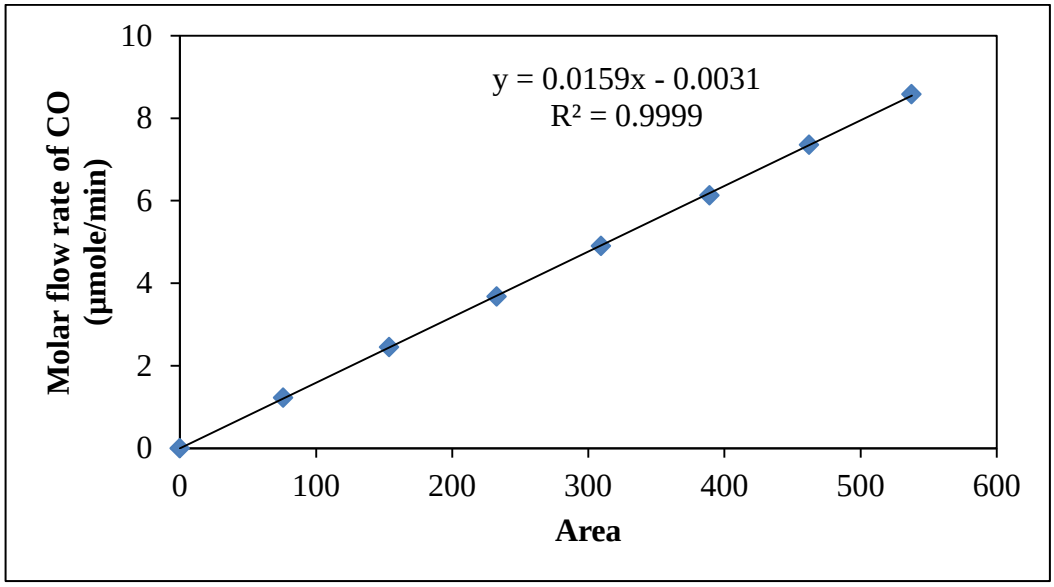

Figure B.1. GC calibration curve of carbon monoxide.

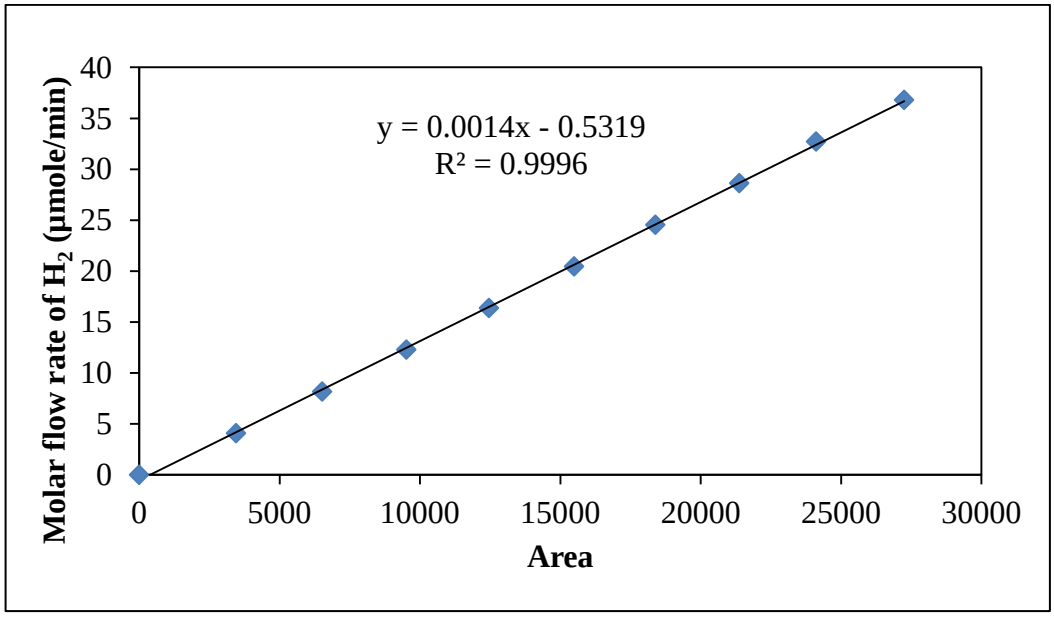

Figure B.2. GC calibration curve of hydrogen.

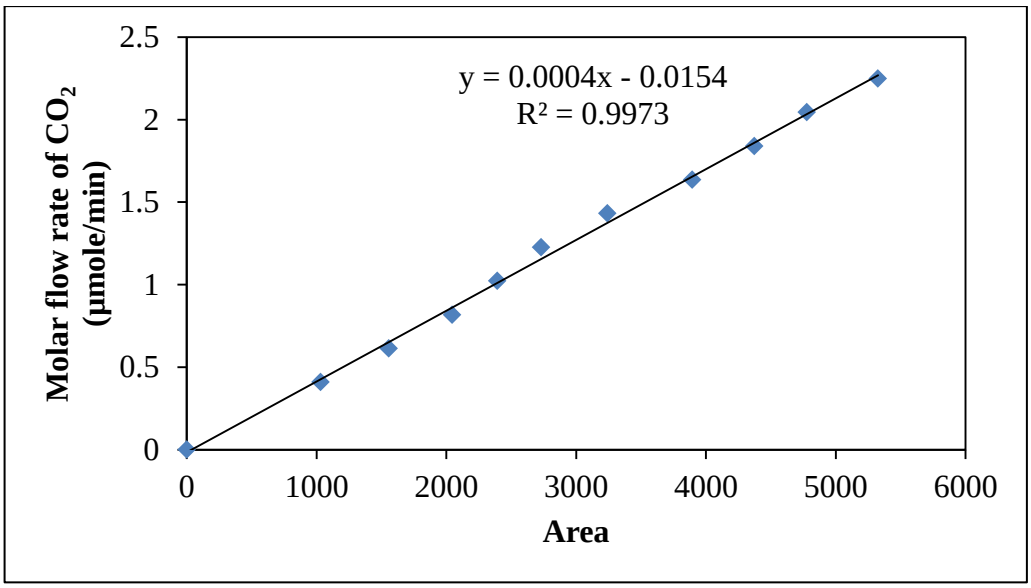

Figure B.3. GC calibration curve of carbon dioxide.

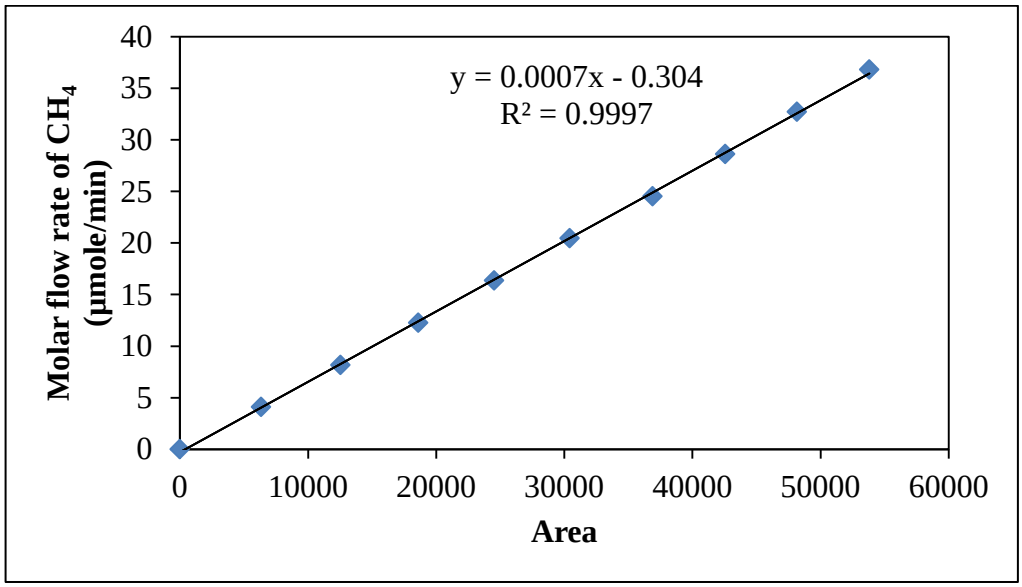

Figure B.4. GC calibration curve of methane.

REFERENCES

Adesina, A. A., 1996, "Hydrocarbon Synthesis via Fischer-Tropsch Reaction: Travails and Triumphs", *Applied Catalysis A: General*, Vol. 138, pp. 345-367.

Akın, A. N. and Z. İ. Önsan, 2000, "CO Hydrogenation by K-promoted Coprecipitated Co/Al_2O_3", *Reaction Kinetics and Catalysis Letters*, Vol. 70, pp. 275-280.

Aksoylu, A. E. and Z. İ. Önsan, 1998, "Interaction between Nickel and Molybdenum in $Ni\text{-}Mo/Al_2O_3$ Catalysts: II CO Hydrogenation", *Applied Catalysis A: General*, Vol. 168, pp. 399-407.

Anderson, J. R., M. Boudart, 1981, *Catalysis Science and Technology*, Springer, Berlin.

Anderson, R. B., 1956, "Catalysts for the Fischer-Tropsch Synthesis", *Catalysis*, Vol. 4, pp. 29-255.

Anderson, R. B., 1984, "The Fischer-Tropsch Synthesis", Academic Press, New York.

Anderson, R. B., H. H. Storch and N. Golumbic, 1951, "The Fischer-Tropsch and Related Synthesis", Vol. 4, pp. 345-367, Wiley, New York.

Avcı, A. K., D. L. Trimm, A. E. Aksoylu and Z. İ. Önsan, 2004, "Hydrogen production by steam reforming of n-butane over supported Ni and Pt-Ni catalysts", *Applied Catalysis A: General*, Vol. 258, pp. 235-240.

Bahome, M. C., 2007, *Synthesis and Use of Carbon Nanotubes as a Support for the Fischer-Tropsch Synthesis*, Ph. D. Thesis, University of the Witwatersrand, Johannesburg.

Basini, L. and L. Piovesan, 1998, "Reduction on Synthesis Gas Costs by Decrease of Steam/Carbon and Oxygen/Carbon Ratios in the Feedstock", *Ind. Eng. Chem. Res.,* Vol. 37, pp. 258–266.

Bhasin, M. M., W. J. Bartley, P. C. Ellgen and T. P. Wilson, 1978, "Synthesis Gas Conversion over Supported Rhodium and Rhodium-Iron Catalysts", *Journal of Catalysis*, Vol. 54, pp. 120-128.

Borer, A. L. and R. Prins, 1993, "Temperature Programmed Reduction and CO Hydrogenation of La_2O_3 Promoted Rh/SiO_2 Catalysts", *Journal of Catalysis,* Vol. 144, pp. 439-451.

Botes, F. G., 2005, "The Effect of a Higher Operating Temperature on the Fischer–Tropsch/HZSM-5 Bifunctional Process", *Applied Catalysis A: General,* Vol. 284, pp. 21–29.

Botes, F. G., 2008, *Kinetic and Selectivity Modelling of the Iron-Based Low-Temperature Fischer-Tropsch Synthesis*, Ph. D. Dissertation, Eindhoven University of Technology.

Bukur, D. B., S. A. Patel and X. Lang, 1990, "Fixed Bed and Slurry Reactor Studies of Fischer-Tropsch Synthesis on Precipitated Iron Catalyst", *Applied Catalysis A: General*, Vol. 61, pp. 329–349.

Castner, D. G., R. L. Blackadar and G. A. Somorjai, 1980, "CO Hydrogenation over Clean and Oxidized Rhodium Foil and Single Crystal Catalysts. Correlations of Catalyst Activity, Selectivity and Surface Composition", *Journal of Catalysis*, Vol. 66, pp. 257-266.

Chaumette, P., P. Courty, A. Kiennemann and B. Ernst, 1995, "Higher Alcohol and Paraffin Synthesis on Cobalt Based Catalysts: Comparison of Mechanistic Aspects", *Topics in Catalysis*, Vol. 2, pp. 117–126.

Chen, G., C. Guo, Z. Huang and Z. Yuan, 2011, "Synthesis of Ethanol from Syngas over Iron-promoted Rh Immobilized on Modified SBA-15 Molecular Sieve: Effect of Iron Loading", *Chemical Engineering Research and Design*, Vol. 89, pp. 249-253.

Choi, G. N., S. J. Kramer, S. T. Tam, J. M. Fox, N. L. Carr and G. R. Wilson, 1997, "Design/economics of a Once-through Natural Gas Based Fischer-Tropsch Plant with Power Co-production", *Coal Liquefaction and Solid Fuels*, Pittsburgh.

Choi, G. N., S. J. Kramer, S. T. Tam, J. M. Fox, 1996, "Design/economics of a natural gas based Fischer-Tropsch plant, *Spring National Meeting*, American Institute of Chemical Engineers, Houston.

Chuang, S. S. C., R. W. Stevens and R. Khatri, 2005, "Mechanism of C_2^+ Oxygenate Synthesis on Rh Catalysts", *Topics in Catalysis*, Vol. 32, p. 225.

Cybulski, A., R. Edvinsson, S. Irandoust and B. Andersson, 1993, **"**Liquid-phase Methanol Synthesis: Modelling of a Monolithic Reactor", *Chemical Engineering Science*, Vol. 48, pp. 3463–3478.

Das, P. C., N. C. Pradhan, A. K. Dalai and N. N. Bakhshi, 2004, "Carbon Monoxide Hydrogenation over Various Titania-supported Ru–Ni Bimetallic Catalysts", *Fuel Processing Technology*, Vol. 85, pp. 1487– 1501.

Dictor, R. A. and A. T. Bell, 1986, "Fischer-Tropsch Synthesis over Reduced and Unreduced Iron Oxide Catalysts", *Journal of Catalysis*, Vol. 97, pp. 121–136.

Donnelly, T. J. and C. N. Satterfield, 1989, "Product Distributions of the Fischer-Tropsch Synthesis on Precipitated Iron Catalysts", *Applied Catalysis A: General*, Vol. 52, pp. 93–114.

Dry, M. E., 1981, "The Fischer-Tropsch Synthesis", *Catalysis Science and Technology*, Vol. 1, pp. 160–255.

Dry, M. E., 1983, “The Sasol Fischer-Tropsch Process”, Vol. 2, Chap. 5, Academic Press Inc.

Dry, M.E., 1996, “Practical and Theoretical Aspects of the Catalytic Fischer-Tropsch process”, *Applied Catalysis A: General*, Vol. 138, pp. 319-344.

Dry, M. E., 2002, “The Fischer–Tropsch Process: 1950–2000”, *Catalysis Today*, Vol. 71, pp. 227-241.

Dry. M. E. and A. Steynberg, 2004, “Commercial FT Process Applications”, in A. Steynberg and M. Dry (eds.), *Fischer Tropsch Technology, Studies in Surface Science and Catalysis 152*, pp. 406-481, Elsevier.

Everson, R.C. and H. Mulder, 1993, “Fischer-Tropsch Reaction Studies with Supported Ruthenium Catalysts”, *Journal Catalysis*, Vol. 143, pp.166-174.

Fischer, F. and H. Tropsch, 1923, “Uber die Herstellung Synthetischer Olgemische (Synthol) durch Aufbau aus Kohlenoxyd und Wasserstoff”, *Brennst. Chem.*, 4, 276–285.

Forzatti, P., E. Tronconi and I. Pasquon, 1991, “Higher Alcohol Synthesis”, *Catalysis Reviews*, Vol. 33, pp. 109-168.

Gao, J., X. Mo and J. G. Goodwin, 2009a, “La, V, and Fe Promotion of Rh/SiO_2 for CO Hydrogenation: Detailed Analysis of Kinetics and Mechanism”, *Journal of Catalysis*, Vol. 268, pp. 142–149.

Gao, J., X. Mo, A. C. Chien, W. Torres and J. G. Goodwin, 2009b, “CO Hydrogenation on Lanthana and Vanadia Doubly Promoted Rh/SiO_2 Catalysts”, *Journal of Catalysis*, Vol. 262, pp. 119–126.

Habazaki, H., M. Yamasaki, B. Zhang, A. Kawashima, S. Khono, T. Takia and K. Hashimoto, 1998, "Co-methanation of Carbon Monoxide and Carbon Dioxide on Supported Nickel and Cobalt Catalysts Prepared from Amorphous Alloys", *Applied Catalysis*, Vol. 172, p. 131.

Haider, M., M. Gogate and R. Davis, 2009, "Fe-promotion of Supported Rh Catalysts for Direct Conversion of Syngas to Ethanol", *Journal of Catalysis*, Vol. 261, pp. 9–16.

Hayakawa, H., H. Tanaka and K. Fujimoto, 2007, "Studies on Catalytic Performance of Precipitated Iron/Silica Catalysts for Fischer–Tropsch Synthesis", *Applied Catalysis A: General*, Vol. 328, pp. 117–123.

Hinchiranana, S., Y. Zhanga, S. Nagamoria, T. Vitidsantb, N. Tsubakia, 2008, "TiO_2 Promoted Co/SiO_2 Catalysts for Fischer–Tropsch Synthesis", *Fuel Processing Technology*, Vol. 89, pp. 455-459.

Hong, J., P. A. Chernavskii, A. Y. Khodakov and W. Chu, 2009, "Effect of Promotion with Ruthenium on the Structure and Catalytic Performance of Mesoporous Silica (Smaller and Larger Pore) Supported Cobalt Fischer–Tropsch Catalysts", *Catalysis Today*, Vol. 140, pp. 135–141.

Ichikawa, M., 1982, "Cluster-derived Supported Catalysts and Their Use", *Chemtech*, Vol. 12, pp. 674-680.

Iglesia, E., S. C. Reyes and R. J. Madon, 1991, "Transport-enhanced -olefin Readsorption Pathways Ru-catalyzed Hydrocarbon Synthesis", *Journal of Catalysis*, Vol. 129, pp. 238–256.

Iglesia, E., S. L. Soled and R. A. Fiato, 1992, "Fischer-Tropsch Synthesis on Cobalt and Ruthenium. Metal Dispersion and Support Effects on Reaction Rate and Selectivity", *Journal of Catalysis*, Vol. 137, pp. 212-224.

Ito, S., S. Ishiguro and K. Kunimori, 1998, "CO Hydrogenation over a Rhodium Vanadate Catalyst: Reduction and Regeneration of $RhVO_4$ on SiO_2", *Catalysis Today,* Vol. 44, pp. 145-149.

Jacobs, G., M. C. Ribeiro, W. Maa, Y. Ji and S. Khalid, 2009, "Group 11 (Cu, Ag, Au) Promotion of 15%Co/Al_2O_3 Fischer–Tropsch Synthesis Catalysts", *Applied Catalysis A: General,* Vol. 361, pp. 137–151.

Jager, B. and R. Espinoza, 1995, "Advances in Low-Temperature Fischer-Tropsch Synthesis", *Catalysis Today,* Vol. 23, pp. 17–28.

Jalama, K., N. J. Coville, D. Hildebrandt, D. Glasser and L. L. Jewell, 2007, "Fischer–Tropsch Synthesis over Co/TiO_2: Effect of Ethanol Addition", *Fuel,* Vol. 86, pp. 73–80.

Jenewein, B., S. Penner and K. Hayek, 2006, "Structure–Activity Correlation in Thin Film Model Catalysts: CO Hydrogenation on Rh/VO_x Part II. Catalytic Activity as a Function of Oxidation and Reduction", *Applied Catalysis A: General,* Vol. 308, pp. 43–49.

Jongsomjit, B., C. Sakdamnuson and P. Praserthdam, 2005, "Dependence of Crystalline Phases in Titania on Catalytic Properties during CO Hydrogenation of Co/TiO_2 Catalysts", *Materials Chemistry and Physics,* Vol. 89, pp. 395-401.

Karaselçuk, R., A. İ. İşli, A. E. Aksoylu and Z. İ. Önsan, 2000, "CO Hydrogenation over Bimetallic Nickel–Vanadium Catalysts", *Applied Catalysis A: General,* Vol. 192, pp. 263–271.

Khodakov, A. Y., A. Griboval-Constant, R. Bechara and V. L. Zholobenko, 2002, "Pore Size Effects in Fischer-Tropsch Synthesis over Cobalt-Supported Mesoporous Silicas", *Journal of Catalysis,* Vol. 206, pp. 230-241.

Kim, W., T. Hanaoka, M. Kishida and K. Wakabayashi, 1997, "Hydrogenation of Carbon Monoxide over Zirconia-Supported Palladium Catalysts Prepared Using Water-In-Oil Microemulsion", *Applied Catalysis A: General*, Vol. 155, pp. 283-289.

Kolbel, H. and M. Ralek, 1980, "The Fischer-Tropsch Synthesis in the Liquid Phase", *Catalysis Reviews, Science and Engineering*, Vol. 21, pp. 225–274.

Kuipers, E.W., C. Scheper, J. H. Wilson and H. Oosterbeek, 1996, "Non-ASF Product Distributions due to Secondary Reactions during Fischer-Tropsch Synthesis", *Journal of Catalysis*, Vol. 158, pp. 288–300.

Lahtine, J. and G.A. Somorjai, 1998, "The effects of Promoters in Carbon Monoxide Hydrogenation on Cobalt Foil Model Catalysts", *Journal of Molecular Catalysis A: Chemical*, Vol. 130, pp. 255–260.

Lihong, H., C. Wei, H. Jingping and L. Shizhong, 2006, "Effect of Carbon Nanotubes on Activity of Rh-Ce-Mn/SiO_2 Catalyst for CO Hydrogenation to Oxygenates", *Chinese Journal of Catalysis*, Vol. 27, pp. 596–600.

Lili, Z., L. Guangrong and L. Jinlin, 2009, "Effect of La_2O_3 on a Precipitated Iron Catalyst for Fischer-Tropsch Synthesis", *Chinese Journal of Catalysis*, Vol. 30, pp. 637–642.

Liu, Y., B. Teng, X Guoa, Y. Li, J. Changa, L. Tian, X. Haoa, Y. Wanga, H. Xiang, Y. Xua and Y. Li, 2007, "Effect of Reaction Conditions on the Catalytic Performance of Fe-Mn Catalyst for Fischer-Tropsch Synthesis", *Journal of Molecular Catalysis A: Chemical*, Vol. 272, pp. 182–190.

Liu, Y., T. Hanaoka, T. Miyazawa, K. Murata, K. Okabe and K. Sakanishi, 2009, "Fischer–Tropsch Synthesis in Slurry-phase Reactors over Mn- and Zr-modified Co/SiO_2 Catalysts", *Fuel Processing Technology*, Vol. 90, pp. 901–908.

Liua, Y., C. Zhanga, Y. Wanga, Y. Li, X. Haoa, L. Baia, H. Xianga, Y. Xua, B. Zhonga and Y. Lia, 2008, "Effect of Co-feeding Carbon Dioxide on Fischer–Tropsch Synthesis over an Iron–Manganese Catalyst in a Spinning Basket Reactor", *Fuel Processing Technology*, Vol. 89, pp. 234-241.

Louis, C., Z. Cheng and M. Che, 1993, "Characterization of Nickel/Silica Catalysts during Impregnation and Further Thermal Activation Treatment Leading to Metal Particles", *Journal of Physical Chemistry*, Vol. 97, pp. 5703–5712.

Marura, A. E., 2002, *Influence of the Preparation Techniques on the Fischer-Tropsch Performance of Supported Cobalt Catalysts*, Ph.D. Thesis, University of Cape Town.

Mei, D., R. Rousseau, S. Kathmann, M. Engelhard, W. Jiang, C. Wang, M. Gerber, J. White and D. Stevens, 2010, "Ethanol Synthesis from Syngas over Rh-based/SiO_2 Catalysts: A Combined Experimental and Theoretical Modeling Study", *Journal of Catalysis*, Vol. 271, pp. 325–342.

Mo, X., J. Gao and J. G. Goodwin, 2009, "Role of Promoters on Rh/SiO_2 in CO Hydrogenation: A Comparison Using DRIFTS", *Catalysis Today*, Vol. 147, pp. 139–149.

Pour, A. N., Y. Zamani, A. Tavasoli, S. M. K. Shahri and S. A. Taheri, 2008, "Study on Products Distribution of Iron and Iron–Zeolite Catalysts in Fischer–Tropsch Synthesis", *Fuel*, Vol. 87, pp. 2004–2012.

Poutsma, M. L., L. F. Elek, P. A. Ibarbia, A. P. Risch and J. A. Rabo, 1978, "Selective Formation of Methanol from Synthesis Gas over Palladium Catalysts", *Journal of Catal*ysis, Vol. 52, pp. 157-168.

Price, J. G., 1994, *An Investigation into novel bimetallic catalysts for use in the Fischer-Tropsch reaction*, Ph. D. Thesis, University of the Witwatersrand.

Rao, V. U. S., G. J. Stiegel, G. J. Cinquegrane and R. D. Srivastave, 1992, “Iron-based Catalysts for Slurry-phase Fischer-Tropsch Process: Technology Review”, *Fuel Processing Technology*, Vol. 30, pp. 83–107.

Reuel, R. C. and C. H. Bartholomew, 1984, "Effects of Support and Dispersion on the CO Hydrogenation Activity/Selectivity Properties of Cobalt”, *Journal of Catalysis*, Vol. 85, pp. 78-88.

Roper, M., 1983, Fischer-Tropsch synthesis, in W. Keim, ed., Catalysis in C_1 chemistry, D. Reidel, Dordrecht, The Netherlands, pp. 41–88.

Schulz, H., 1999, “Short History and Present Trends of Fischer-Tropsch Synthesis”, *Applied Catalysis A: General*, Vol. 186, pp. 3-12.

Subramanian, N.D., J. Gao, X. Mo, J. Goodwin, W. Torres and J. J. Spivey, 2010, “La and/or V Oxide Promoted Rh/SiO_2 Catalysts: Effect of Temperature, H_2/CO Ratio, Space Velocity and Pressure on Ethanol Selectivity from Syngas”, *Journal of Catalysis*, Vol. 272, pp. 204–209.

Takeishia, K., Y. Yamashitab and K. Aika, 1998, “Comparison of Carbon Dioxide and Carbon Monoxide with Respects to Hydrogenation on Raney Ruthenium Catalysts under 1.1 and 2.1 MPa”, *Applied Catalysis A: General*, Vol. 168, pp. 345-351.

Tau, L., H. A. Dabbagh and B. H. Davis, 1991, “Fischer-Tropsch Synthesis: Comparison of ^{14}C distributions when Labelled Alcohol is Added to the Synthesis Gas”, *Energy & Fuels*, Vol. 5, p. 174.

Tien-Thao, N., M. H. Zahedi-Niaki, H. Alamdari and S. Kaliaguine, 2007, “Conversion of Syngas to Higher Alcohols over Nanosized $LaCo_{0.7}Cu_{0.3}O_3$ Perovskite Precursors”, *Applied Catalysis A: General*, Vol. 326, pp. 152–163

Trepanie, M., A. Tavasoli, A. K. Dalai and N. Abatzoglou, 2009, "Co, Ru and K Loadings Effects on the Activity and Selectivity of Carbon Nanotubes Supported Cobalt Catalyst in Fischer–Tropsch Synthesis", *Applied Catalysis A: General*, Vol. 353, pp. 193–202.

Tristantini, D., S. Lögdberg, B. Gevert, Ø. Borg and A. Holmen, 2007, "The Effect of Synthesis Gas Composition on the Fischer–Tropsch Synthesis over Co/γ-Al_2O_3 and Co–Re/γ-Al_2O_3 Catalysts", *Fuel Processing Technology*, Vol. 88, pp. 643–649.

Van der Laan, G.P., 1999, *Kinetics, Selectivity and Scale Up of the Fischer-Tropsch Synthesis*, Ph. D. Thesis, Rijksuniversiteit Groningen.

Van der Laan, G. P. and A. A. C. M. Beenackers, 1999, "Kinetics and Selectivity of the Fischer-Tropsch Synthesis: A Literature Review", *Catalysis Reviews, Science and Engineering*, Vol. 41, p. 255.

Vannice, M. A., 1975, "The Catalytic Synthesis of Hydrocarbons from H_2/CO Mixtures over the Group VIII Metals. II. The Kinetics of the Methanation Reaction over Supported Metals", *Journal of Catalysis*, Vol. 37, pp. 462–473.

Wan, H., B. Wu, C. Zhang, B. Teng, Z. Tao, Y. Yang, Y. Zhu, H. Xiang and Y. Li, 2006, "Effect of Al_2O_3/SiO_2 Ratio on Iron-based Catalysts for Fischer–Tropsch Synthesis", *Fuel*, Vol. 85, pp. 1371–1377.

Wan, H., B. Wu, Z. Tao, T. Li, X. Ana, H. Xiang and Y. Li, 2006, "Study of an Iron-based Fischer–Tropsch Synthesis Catalyst Incorporated with SiO_2", *Journal of Molecular Catalysis A: Chemical*, Vol. 260, pp. 255–263.

Wang, T., Y. Ding, Y. Lu, H. Zhu and L. Lin, 2008, "Influence of Lanthanum on the Performance of Zr-Co/activated Carbon Catalysts in Fischer-Tropsch Synthesis", *Journal of Natural Gas Chemistry*, Vol. 17, pp.153–158.

Wu, B., L. Bai, H. Xiang, Y. Li, Z. Zhang and B. Zhong, 2004, "An Active Iron Catalyst Containing Sulfur for Fischer–Tropsch Synthesis", *Fuel*, Vol. 83, pp. 205–212.

Xiang, M., D. Li, W. Li, B. Zhong and Y. Sun, 2007, "K/Fe/β-Mo_2C: A Novel Catalyst for Mixed Alcohols Synthesis from Carbon Monoxide Hydrogenation", *Catalysis Communications*, Vol. 8, pp. 88–90.

Yana, Z., B. B. Dragomir and D. W. Goodmana, 2011, "Silica-supported Rhodium-Cobalt Catalysts for Fischer–Tropsch Synthesis", *Catalysis Today*, Vol. 160, pp. 39-43.

Yong, Y., W. Yangdong, L. Su, S. Qingying, X. Zaiku and G. Zi, 2007, "Mo–Co–K Sulfide-based Catalysts Promoted by Rare Earth Salts for Selective Synthesis of Ethanol and Mixed Alcohols from Syngas", *Chinese Journal of Catal*ysis, Vol. 28, pp. 1028–1030.

Zhang, Y., H. Xiong, K. Liew and J. Li, 2005, "Effect of Magnesia on Alumina-supported Cobalt Fischer–Tropsch Synthesis Catalysts", *Journal of Molecular Catalysis A: Chemical*, Vol. 237, pp. 172–181.

Zhoua, W., Z. Maa, K. Fangb, J. Chenb and Y. Sunb, 2008, "Effects of Methanol Co-feeding in F–T Synthesis on Silica Supported Co-catalyst", *Fuel Processing Technology*, Vol. 89, pp. 1113–1120.